COASTAL POPULATION VULNERABILITY TO SEA LEVEL RISE AND TROPICAL CYCLONE INTENSIFICATION UNDER GLOBAL WARMING

CELESTE C. BARNES
B.Sc. University of Saskatchewan, 1988

A Thesis
Submitted to the School of Graduate Studies
of the University of Lethbridge
in Partial Fulfillment of the
Requirements for the Degree

MASTERS OF SCIENCE

Department of Geography
University of Lethbridge
LETHBRIDGE, ALBERTA, CANADA

Abstract

This research focuses on developing a framework for first order estimates of locations at risk to Tropical Cyclones (TC) and elevated water levels in coastal regions. The International Best Track Archive for Climate Stewardship (IBTrACS) 64 knot wind radii data identifies locations in the North Atlantic (NA) basin hit by hurricane strength storms. Geographic Information System (GIS) temporal and spatial analysis of IBTrACS data identifies impact zone locations where multiple TCs have occurred. Aster 30 m elevation data identifies locations within 5 and 10 m of sea level that may become inundated by TC storm surges. Population density and land cover data maps are created to identify urban and food production areas. Overlay maps are created of the coastal inundations, population, land cover, and hurricane track impact zones. Mapping results show the Bahamas and Cuba are most susceptible to the effects of tropical cyclone and storm surge inundation.

Table of Contents

List of Figures

List of Tables

List of Abbreviations

3D	Three Dimensional
AI	Artificial Intelligence
CCOIL	Climate Change Ocean Inundation Level
CO_2	Carbon Dioxide
CPU	Central Processing Unit
DEM	Digital Elevation Model
DSM	Digital Surface Model
DTM	Digital Terrain Model
ECWMF	European Center for Medium-range Weather Forecasts
EMR	Electromagnetic Radiation
EQ	Equation
FAO	Food and Agriculture Organization of the United Nations
GIS	Geographical Information System
GPU	Graphics Processing Unit
IBTrACS	International Best Track Archive for Climate Stewardship
KM	Kilometer
KT	Knot
LGEM	Logistic Growth Equation Model
M	Meter
MB	millibar
METI	Ministry of Economy, Trade and Industry of Japan
MLR	Multiple Linear Regression
NA	North Atlantic (hurricane basin)
NE	North East
NI	North Indian (hurricane basin)
NM	International Nautical Miles
NOAA	National Oceanic and Atmospheric Administration
NASA	National Aeronautics and Space Administration
P.P.M.V.	Parts Per Million by Volume
RMSE	Root Mean Square Error
SHIPS	Statistical Hurricane Intensity Prediction Scheme
SLR	Sea Level Rise
SSHWS	Saffir-Simpson Hurricane Wind Scale
SST	Sea Surface Temperature
TC	Tropical Cyclone
TIN	Triangular Irregular Network
UE3	Unreal Engine 3 (Epic Corporation)
UTC	Universal Time Coordinate
WP	Western Pacific (hurricane basin)

List of Variables

Season	Year of Hurricane
Name	Hurricane Name
ISO_time (UTC)	ISO Date/Time stamp (6 hr intervals)
wmo_wind (kt)	Wind Speed (kt)
wmo_pres (mb)	Pressure (mb)
ATC_w64_r1 (nm)	64 Knot Rad 1 – NE Quadrant – hurricane force winds
ATC_w64_r2 (nm)	64 Knot Rad 2 – SE Quadrant
ATC_w64_r3 (nm)	64 Knot Rad 3 – SW Quadrant
ATC_w64_r4 (nm)	64 Knot Rad 4 – NW Quadrant
year	Year
month	Month
day	Day
hour	Hour
min	Minute
HURR_DATE	Date format of hurricane observation DD-MMM-YYYY HH:MM (change in SPSS to this format)
HURRLINEID	Hurricane Line Segment ID – data interchange value between ArcGIS and excel
X_START	Longitude Start Point
X_END	Longitude End Point
Y_START	Latitude Start Point
Y_END	Latitude End Point
X_LONG_DIR	Longitude Direction
Y_LAT_DIR	Latitude Direction
Y_START_ROUND	Y_START - Latitude variable rounded to the nearest 0.00 (2 decimal places)
X_QUAD	X Quadrant
Y_QUAD	Y Quadrant
QUAD	Line Segment Direction Quadrant
INTM	Formula – Intermediary angle used by arctan to convert to degrees
NORTH_0_360	Hurricane 360 degree direction of travel 0/360 points North at 0° mark on compass
HURR_OBSER	Observation number within each hurricane. Numbered starting at 1 to the last observation.
HURR_FCAT_OBSER	Observation number within each hurricane once the hurricane hits category 1 Numbered starting at 1 to the last observation.
SSHWS_CATEGORY	Classification the Line segment is in the Saffir-Simpson Hurricane Wind Scale
SSHWS_MAX	Maximum SSHWS the individual hurricane reached – used to separate out storms not reaching hurricane strength
Max_64	Maximum Value of the Rad 1, 2, 3, 4 distances
RIGHT_DIMENSION	ATC_w64 value one quadrant to the right of the hurricane trajectory quadrant - right side of the ellipse based on hurricane trajectory
LEFT_DIMENSION	ATC_w64 value one quadrant to the left of the hurricane trajectory quadrant left side (opposite side) of the ellipse based on hurricane trajectory
HR_VEL_KT_fine	Hurricane Velocity – kt – rounded to the nearest 5 knots with 1-5 broken down

1 Overview

1.1 Introduction

This is a multidisciplinary thesis that combines research in Geography, Sociology, and New Media. The objective of this research is to create a framework for scientific and social science data relating to the impacts of Tropical Cyclones (TC) and rising sea levels in coastal regions. Tropical cyclones (TC) have the potential to inflict significant wind and storm surge damage in coastal regions (K. Emanuel, 2011). Warming sea surface temperatures increase the frequency of TCs as well as intensify circular wind speeds (K. A. Emanuel, 2013). Higher TC storm surges are produced from global warming induced rising sea levels (Claudia, Benjamin, & Chris, 2012). TC wave heights are directly related to the TC circular wind speed intensity (Komar & Allan, 2008). Extreme TC weather events and rising seas have the potential to increase vulnerabilities to coastal populations and infrastructure (Rygel, O'sullivan, & Yarnal, 2006), increase economic losses (Tracy, Trumbull, & Loh, 2007), and impact food production (Krishnamurthy, Fisher, & Johnson, 2011).

The development of a framework is based on GIS analysis methods to generate maps identifying regions with land elevations close to sea level and the frequency at which tropical cyclones hit any given location. Standardized population densities will be calculated using official country census data to locate concentrations of people. A further refinement to identify population concentrations and food production regions is required. The United Nations Food and Agriculture (FAO) land cover/land use (Nachtergaele, 2008) will provide data to locate urban and agriculture & grazing regions. Raster analysis of Aster GDEM Version 2 (Tachikawa, Hato, Kaku, & Iwasaki, 2011a) digital elevation models will obtain a first order estimation of potential coastal regions susceptible to higher water levels and storm surge inundation. Historical International Best Track Archive for Climate Stewardship (IBTrACS) data (Knapp, Kruk, Levinson, Diamond, & Neumann, 2010) is available for all global hurricane basins. GIS overlays will be produced to identify historical hurricane paths located in coastal regions in the North Atlantic (NA), North Indian (NI), and Western Pacific (WP) basins. In the Caribbean, TC impact paths will be investigated to find regions hit by repeated hurricane activity. A temporal analysis of hurricane strength storm activity will be

completed for the North Atlantic hurricane basin to identify convergence pattern trends and possible locations of future vulnerabilities to TC activity.

1.2 Research Question

The countries selected for this research are located in less developed regions of the world. Outsider access to any detailed datasets is limited or non-existent. There are dataset collections available from the FAO, National Oceanic and Atmospheric Administration (NOAA), and Ministry of Economy, Trade and Industry of Japan (METI). These datasets are generally at a course resolution and may contain significant missing or anomalous data for locations being evaluated. Given the issues of global warming, tropical cyclone intensification, and rising sea levels, there is still a need to identify at a homogeneous global level, a method to identify a first order level of risk to coastal populations. The question is:

> "How can existing datasets be better utilized to create a visually accurate and effective framework for identifying potential disruptions to populations and food production regions caused by global oceanic change?"

1.3 Milestones

To achieve the objective of identifying populations and food production regions vulnerable to the effects of intensifying tropical cyclones, increased water levels and storm surge, the following milestones were completed.

Phase 1: An investigation and identification of populations in the Caribbean, Philippines, Bangladesh, Jakarta, parts of China, and the east coast of India with low coastal and inland elevations and a high frequency of historical hurricane tracks.

- Utilize the Aster GDEM dataset to identify a first order approximation of locations close to sea level.
- Utilize the IBTrACS NA, NI, WP historical dataset to identify hurricane tracks.
- Utilize official country census data to calculate standardized population densities.

- GIS overlays of locations close to sea level, hurricane tracks, and population densities
- Select a local study area for further investigation.
- Research and test current and next-generation data visualization technology and methods to assess suitability, practicality and efficacy.

Phase 2: An investigation and identification of hurricane frequency hit counts in the Caribbean, specifically, the Bahamas, Cuba, Dominican Republic, Haiti, Jamaica, and Puerto Rico.

- Utilize the 2004-2011 IBTrACS NA basin dataset to derive a 64 kt impact path around each storm track using GIS overlay analysis. A minimum TC circular wind speed of 64 kt is required to categorize a storm track observation as hurricane strength.
- Extend the impact path analysis to 1979 – 2011 using Multiple Linear Regression (MLR) analysis of 2004 – 2011 impact path data as 64 kt wind radii data is not available before 2004.
- Use MLR relationship to create 64 kt impact paths for all storms 1979 – 2003; thus providing a time series 1979-2011.
- GIS overlay analysis of historical hurricane tracks (1979 – 2011) observed and derived impact paths over the study area. This overlay analysis provides occurrence(s) for 64 kt impacts for all geographic regions.
- Land cover/land use defines population centers and food production areas. This overlay analysis identifies locations impacted by the 64 kt storm paths, including frequency counts.
- Identify locations close to sea level related to population densities: potential inundation zones due to TC precipitation, runoff, storm surge, and rising sea levels - 5 & 10 m.
    - Komar and Allan (2008) conducted a study using NOAA buoys located in deep water. Three were located along the US Atlantic coast and one was in the Gulf of Mexico. The research showed wave heights above 3 meters were attributable to TCs. As well, decrease in wave height occurred with the increase in latitude. Buoy data closer to the Caribbean study location showed significant wave heights of above 11 m which were attributable to TC Category 4 & 5 storms. The 5 m raster calculation was used to

represent lower hurricane strength category storms. The 10 m raster calculation was used to represent the more intense but less frequent hurricane strength storms.

- Raster inundation levels were calculated for the entire country. Storm surges are localized to the coastal regions. The potential for significant inland flooding may result from extreme precipitation and runoff as a result of TCs. These meteorological and hydrological/hydraulic processes are not modelled in this thesis.

Phase 3: Temporal analysis of hurricane track convergence patterns in the North Atlantic basin.

- GIS temporal analysis utilizing observed and derived historical hurricane tracks (1979 – 2011) impact paths over the NA basin.
- Divide the dataset into several temporal groupings
    - Split the data set in half (1979 – 1995 and 1996 – 2011) to examine changes in track convergence patterns over the two time fames
    - Spilt the three datasets (1979 – 2011, 1979 – 1995, and 1996 – 2011) into monthly groupings (June/July/August, September, October/November/December) to examine early and late season variations between the two time frames
- Utilize GIS overlay analysis of each temporal grouping to examine hurricane track convergence patterns over time and season.

2 Literature Review

This chapter contains a review of current research in the fields of tropical cyclones and rising ocean waters to gain a better understanding of how these systems can impact coastal populations. Significant damage to property as well as loss of human lives are possible from these powerful storms. Hurricane Sandy occurred in 2012 inflicting billions of dollars in damages and left many homeless. There was also loss of human life during and after this intense storm passed. Review of:

- Tropical cyclone structure, wind size, and storm surges produced by these winds was completed to appreciate contributing factors in resulting storm damage.
- Rising ocean levels influence storm surge heights.
- A discussion of climate science as well as factors contributing to global warming were investigated.

Vulnerability literature was reviewed to obtain an understanding of the social, economic, and recovery efforts required during and after disaster events for population and food production regions. Finally, scientific modelling as well as a discussion on the use of non-traditional scientific software was explored.

2.1 Tropical Cyclones and Hurricanes

2.1.1 Structure

Tropical Cyclones (TC), also referred to as hurricanes, are formed in warm ocean waters located in the tropics and rotate in a counter clockwise circular motion in the Northern Hemisphere (Colin J. McAdie, Landsea, Neumann, David, & Blake, 2009). An initial understanding of TCs structure was developed using meteorological data that included storm position, central pressure, temperature and a variety of wind speeds (George & Gray, 1976). George and Gray found typical TCs are asymmetrical with circular maximum wind speeds located in the right front quadrant to the direction travel. Figure 2.1.1 shows Hurricane Ike on September 7, 2008 one hour from the Cuban shore. The “trajectory” arrow shows the forward direction of travel.

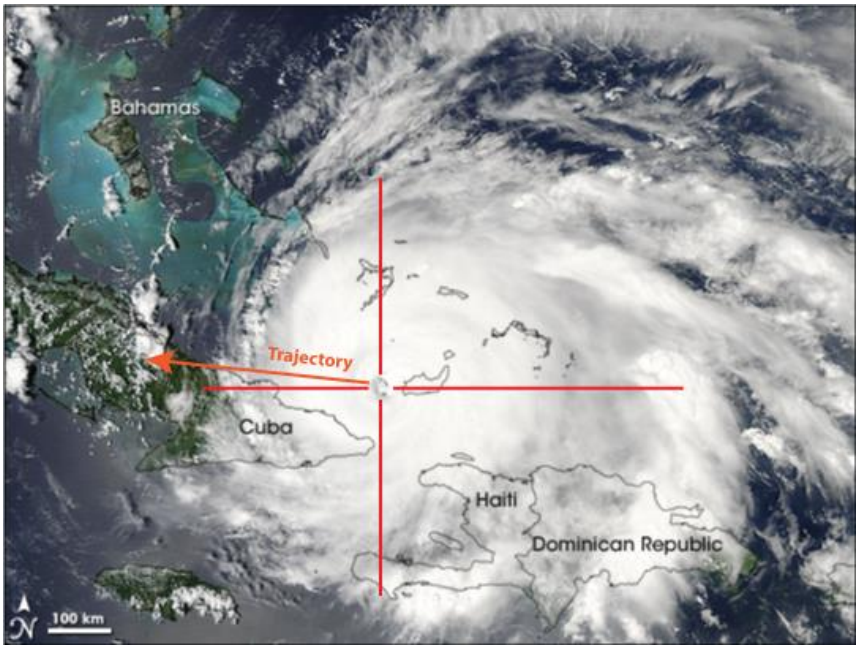

Figure 2.1.1: Hurricane Ike - September 7, 2008. This image shows Hurricane Ike one hour from Cuba. At this point, Ike was a Category 3 storm. The "Trajectory" arrow shows the direction of travel. The four quadrants are centered over the eye of the storm. (Schmaltz, 2010)

Spiral rain bands (Guinn & Schubert, 1993) form around the circular "eyewall" portion of the hurricane (Figure 2.1.2) which is located around a calm, rain free hurricane "eye" (Hence & Houze, 2011; Houze, Chen, Smull, Lee, & Bell, 2007). The eyewall contains intense winds and thunderstorms producing precipitation.

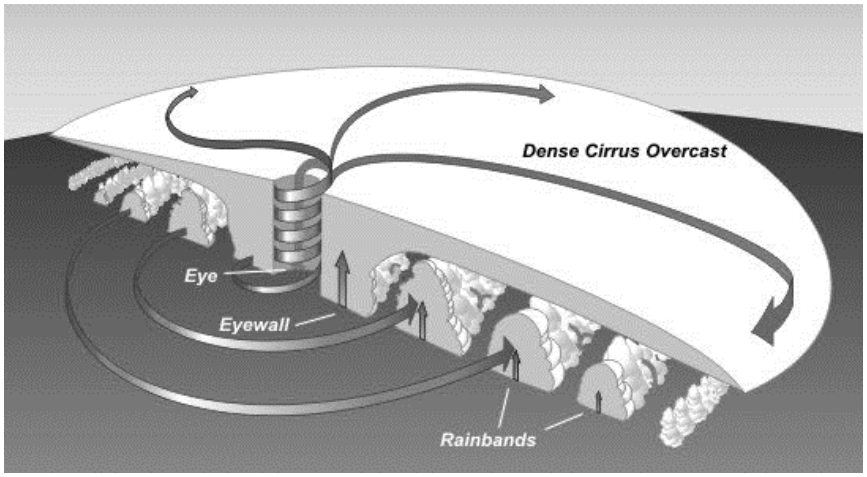

Figure 2.1.2: Typical Hurricane Structure. The Eye of the hurricane is a calm wind and rain free zone. Rain bands form in a circular fashion around the eyewall. (NWS, 2010)

Tropical cyclones have highly varied scale and storm intensity over the storm lifetime (Jury, Rios-Berrios, & García, 2012). Houze et al (2007) found clouds will merge outside the existing eyewall causing it to die out and be replaced a new emerging eyewall as seen in Figure 2.1.3. The TC becomes weaker during this process but re-intensifies as the new eyewall contracts and emerges.

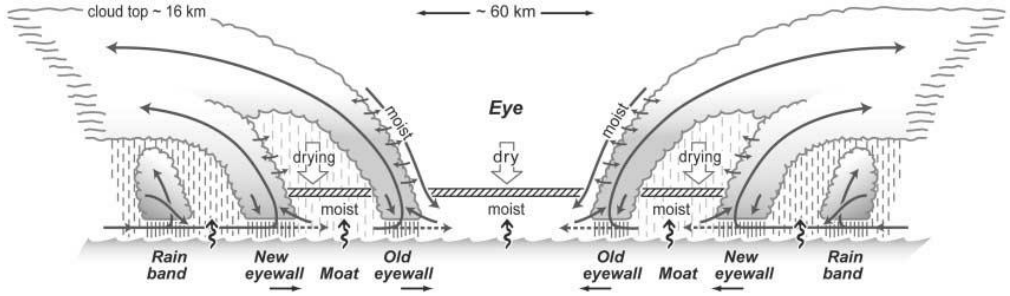

Figure 2.1.3: Hurricane Eyewall Replacement. Outside the existing eyewall, clouds begin to come together. The eyewall dies out causing the TC to become weaker. As the newly emerging eyewall forms, the TC re-intensifies. (Houze et al., 2007)

Storms will also decay (lose intensity) when coming in contact with land as energy required to sustain the TC is significantly reduced (Kaplan & DeMaria, 1995).

2.1.2 Wind radii

The circular motion of a TC must reach a minimum of 64 knots (kt) (119 km/hr or 74 mph) to be considered a hurricane category storm (Colin J. McAdie et al., 2009). The forward trajectory velocity of the TC is separated from the recorded circular wind speed. The most intense winds in the hurricane are located at the eyewall. The TC wind speed data is provided at three distance locations in the IBTrACS NA basin dataset for each storm quadrant; 64 kt, 50 kt, and 34 kt; measured from the center of the hurricane (Knapp et al., 2010; Colin J McAdie, 2004). The 64 kt wind radii is the distance from the TC center in nautical miles (nm) where minimum 64 kt hurricane category winds are observed. Statistical analysis of wind profiles show asymmetric patterns with the largest wind radii distances to the right of the hurricane trajectory (Bell & Ray, 2004) as well as estimating wind fields (James P. Kossin et al., 2007).

2.1.3 Storm Surge Inundation

The elevation of water higher than natural tide cycles is part of meteorological processes present in TCs. As TCs pass over landmasses, storm surge inundation occurs with maximums located to the right of the

hurricane eye (Hagen, Bacopoulos, Cox, & Cardone, 2012). High resolution bathymetric (oceanic water depths), topographic (land formation, features, and characteristics), wind (movement of air above the ground), and barometric pressure (the pressure caused by the weight of the atmosphere) data are required to determine normal tide levels in order to model wave dynamics of storm surge (Forbes, Luettich, Mattocks, & Westerink, 2010; Goring, Stephens, Bell, & Pearson, 2011; Westerink et al., 2008). Water depth modelling for deep water and near shore waves contribute to overall storm surge inundation (Bunya et al., 2010). Preliminary findings proposed by Hagen et al indicate surge heights will differ depending on hurricane trajectory and which side (left or right) the landmass is hit. Depending on location, storm surge heights off the US coast and in the Gulf of Mexico vary from 1 meter to almost 12 meters (Komar & Allan, 2008).

2.1.4 Hurricane Modelling and Forecasting

Hurricane models simulate storm size, intensity, and trajectory, and some models may be used to predict current and future TC activity. Some models utilise satellite and instrument observations (Amarin et al., 2012), statistical analysis techniques (DeMaria, 2009; DeMaria & Kaplan, 1999), and a combination of both statistical and observational readings. Several forecast models for present day hurricane activity attempt to predict rapid intensification (Kaplan, DeMaria, & Knaff, 2010), wind field size and trajectory paths (Cha & Wang, 2013; DeMaria et al., 2009) for a timeframe 72 hours ahead of the storm. Forecast models have improved in recent years but there is significant variation in predictions of storm track, intensity, and size between models. Hurricane Sandy struck the USA east coast in fall 2012, causing major damages to New York and New Jersey; and substantial life loss. Track and intensity predictions for Sandy were based on 12 models (Blake, Kimerlain, Berg, Cangialosi, & Beven, 2013). The European Center for Medium-range Weather Forecasts (ECWMF) model computed Sandy's track, including the unusual storm path diversion into the US eastern seaboard, 5 days before the storm hit the USA.

Predicting future hurricane activity for a range of climate scenarios is a challenge. Under global warming conditions, differing hurricane models provide conflicting projections of hurricane intensity, frequency, and duration (Knutson, Tuleya, et al., 2010; Kunkel et al., 2013). Historical hurricane data has not been consistently recorded (C. W. Landsea, Harper, Hoarau, & Knaff, 2006; C. W. Landsea, Vecchi, Bengtsson,

& Knutson, 2009) prior to the early 1990's although efforts are being made to re-evaluate past TCs and update datasets using standardized techniques. A substantial literature exists that argues hurricane intensity will increase in future, i.e. we can expect more of the powerful storms, but most analyses to date suggest no data supports an increase in the overall number of storms (James B. Elsner, Kossin, & Jagger, 2008; K. A. Emanuel, 2013; Malmstadt, Elsner, & Jagger, 2010). Debate still exists regarding hurricane frequency due in part to decadal climate patterns (James P Kossin, Camargo, & Sitkowski, 2010; Michael E Mann & Emanuel, 2006; Vimont & Kossin, 2007) that strongly impact in annual total storm occurrences. However, recent work from Emanuel shows hurricane frequency increasing may increase as well under some climate warming scenarios (K. A. Emanuel, 2013).

Statistical models attempt to create long term predictions based on numerous historical meteorological data inputs such as atmospheric wind profiles and temperature profiles (Jagger & Elsner, 2010) to detect trends. Factors such as hurricane genesis (Bender et al., 2010), forward storm velocity (Jury et al., 2012), atmospheric wind field profiles (Vickery, Masters, Powell, & Wadhera, 2009), and power dissipation (K. Emanuel, 2005) impact model outputs, and therefore aid in the understanding and accuracy of TC activity. Sea Surface Temperature (SST) (James B. Elsner et al., 2008; J. B. Elsner, Trepanier, Strazzo, & Jagger, 2012) is a key storm input and hence has been a key hurricane modelling input variable. Refinements to the model accuracy focuses on obtaining a better understanding of the hurricane structure components: circular velocity and vorticity (K. Emanuel & Jagger, 2010; Tang & Emanuel, 2012), eyewall structure (Hence & Houze, 2011), eyewall formation and banding (Vigh, Knaff, & Schubert, 2012), and near surface ocean temperatures (Lloyd & Vecchi, 2011). Recent work from Emanuel proposed removing SST as a determinant to TC genesis and intensity changes (K. Emanuel, Solomon, Folini, Davis, & Cagnazzo, 2013) as fluctuating ocean-atmospheric thermodynamic processes are more important and not actual SSTs. Emanuel et al (2013) propose total heat differences between ocean and the tropopause layer of the atmosphere should be used in prediction models instead of SST.

2.2 Sea Level Rise

Sea-level oscillates over time and is not uniform over the globe (Carbognin, Teatini, Tomasin, & Tosi, 2010). Over geologic time, global sea level has varied by hundreds of metres due to natural climate cycles.

But the expected increases in global sea level due to human induced climate warming will be much more rapid than events in the geologic record.

Sea-level rise (SLR) is measured over time with averaged monthly and annually tide gauge readings to establish rates of change. Short term data records of less than 35 years indicate a rising sea-level trend at Moturiki Island, Bay of Plenty, New Zealand of 1.5 mm per year (Goring et al., 2011). The north western coast of Germany in the German Bight area on the North Sea showed a slightly higher rate of 1.64 to 1.74 mm per year based on over 80 years of data (Albrecht, Wahl, Jensen, & Weisse, 2011); however when the time frame was shorted to under 40 years, an accelerated rate of 3.8 mm per year emerges. Using a combination of global altimeter and in situ data, Church and White (2011) established a trend for the 1993 – 2009 of 2.8 to 3.2 mm/year. In a review of SLR literature, the IPCC has determined "it is very likely SLR will continue with upward trends in the future" (IPCC, 2012).

The mechanisms that are causing the current sea level rise include increased oceanic heat content (Kevin E. Trenberth, 2010) resulting in thermal expansion of the water profile (Church et al., 2011). Glacier and ice sheet melt also contribute modestly to SLR (Alley, Clark, Huybrechts, & Joughin, 2005; IPCC, 2012) with Greenland producing the largest volume. Understanding and projecting future glacial and ice flows contributions to sea level are limited due to incomplete modelling of friction forces, bedrock influences, and thermal states (Alley & Joughin, 2012). A number of studies have predicted catastrophic sea level rise is possible due to failure of ice shelves in Greenland and/or Antarctica (refs). The likelihood of those failures is quite low but if one or more should occur, humanity would have to deal with sea level rise of on the order of metres in very short time frames (ref). However, even conservative estimates of sea level rise (IPCC 2014) will enhance coastal flooding in concert with TC storm surges.

Marine deposits in cave landforms located in Bermuda and the Bahamas indicate sea levels were more than 20 meters higher than today during the middle Pleistocene epoch (Hearty P. J., 1999). Using a combination of paleoclimate data, current sea-levels, atmospheric temperatures, and anthropogenic levels, projections are current sea level will continue to rise for the next 50-100 years. Reversal or slowing of SLR will

require anthropogenic carbon dioxide (CO_2) emission levels to be reduced to zero in order to reduce the current atmospheric temperature increases (Schaeffer, Hare, Rahmstorf, & Vermeer, 2012). Such progress on GHG emission sis highly unlikely; hence coastal population have to prepare for sea level rise. Tropical regions subject to TC will have to adapt for major coastal flooding events.

2.3 Climate Variability, and Global Warming

This section is included to examine factors that may contribute to changing climate over time and to obtain a better understanding of how these components may influence future climate. Global temperatures have been increasing in recent decades and are contributing to more extreme weather events on earth. Governments must now look at global warming issues and impacts on future policies. However, "global warming" and "climate change" deniers exist in many levels of government as well as the general public.

Over the course of earth's history, climate has varied greatly with extreme cooling and warming events. Climate refers to the long term trends and patterns of weather conditions including land and ocean temperature, wind, air pressure, and water content in the atmosphere (IPCC, A.P.M. Baede, E. Ahlonsou, Y. Ding, D. Schimel, 2001). Precipitation and weather elements are unique in any given location on earth and depend on many variables including incoming and outgoing solar electromagnetic radiation (EMR), and the variation in orientation and time period of earth's orbit. The study of paleoclimatology examines climate change over the course of earth's history. Proxy data such as analysis of ice cores, tree rings, sediment, corals, and other historical data are used to determine climate at given eras. These studies indicate the earth has cycled through glacial-interglacial periods; intervals of warm, ice-free periods as well as epochs during which the earth was in a cooled state with ice-sheets covering vast continental and ocean areas (Michael E. Mann, 2007). Reconstruction of surface temperatures from coral fossil and other proxy data indicates climate warming and cooling events varying regionally. In the 11^{th} century, Europe experienced a warming period while the western United States contended with a tendency for drought. During the 17^{th} century, a cooling period occurred in Europe and the western United States experienced wet conditions (Michael E. Mann, 2007).

The European Project for Ice Coring in Antarctica (EPICA) was established for the purposes of investigating past climate patterns by extracting and analysing ice cores in Antarctica. A 3,190 m ice core extracted by EPICA was analyzed using a laser sensor and high resolution counting instrument. EPICA indicates cold glacial periods correspond to increased dust fallout in the ice. A reduction in dust grain size also indicates a trend towards a glacial period (EPICA, 2004). Dust concentration measurements showed a high correlation between dust and temperature during the glacial periods that were absent during interglacial periods (Lambert et al., 2008). Results of the analysis showed the ice core contained eight glacial-interglacial climate change cycles going back to 800,000 years before present and observed climate was characterized by 100,000 year glacial-interglacial cycles.

CO_2 concentrations obtained by dry extraction techniques from the EPICA ice core were measured using a combination of laser absorption spectroscopy and gas chromatography at the University of Bern and the Environmental Laboratory of Geology and Geophysics in Grenoble. Findings showed CO_2 concentrations in the atmosphere are clearly linked to temperature. Ice core samples contained CO_2 concentrations averaging in the range of 180 to 300 parts per million by volume (p.p.m.v.) per cycle. Slight variations in CO_2 measurements of 172 to 300 p.p.m.v. occurred during the oldest two glacial-interglacial cycles. Analysis indicated these cycles were also influenced by increases and decreases in Methane (CH_4) concentrations in the atmosphere (Luthi et al., 2008). These increasing gases create a "greenhouse" effect causing the earth to warm. Long wave solar radiation becomes trapped in the atmosphere and is reflected back onto the surface of the earth resulting in rising global surface temperatures (Hansen & Sato, 2012; K. E. Trenberth & Fasullo, 2010).

2.4 Population, Industry, and Agriculture/Food Production Vulnerability

Levels of vulnerability to environmental disasters differ depending on economic status. Particular vulnerability is related to poverty, gender and age (especially children and the elderly), disability, and settlement patterns (Barros C.B. et al., 2012; Rygel et al., 2006; Senkbeil, Brommer, & Comstock, 2011). Social policies relating to the granting of access to emergency services, economic assistance, health care, and disaster support, assist with population coping and recovery abilities. Development of vulnerability

indicators takes into consideration ranking techniques as not all factors have equal levels of risk (Rygel et al., 2006). As well, levels of vulnerability can change over the course of the disaster and recovery process. For example, after a flood event, there is potential for the introduction of pathogens and bacterial contaminants in flood waters. These toxins remain in soils after water is removed from the site of the original disaster and must also be removed.

Examination of urban and rural infrastructure and services are also required to assess vulnerability. Transportation systems, utilities (electrical, water, sewer), critical and essential facilities (medical and public safety response capacity) require the capacity to meet demands during disasters. Governing functions, personal and public building infrastructures (Pita, Pinelli, Gurley, & Hamid, 2013) as well as access to basic living necessities such as food and provisions need to in sufficient quantities for survival during the recovery process (Frazier, Wood, Yarnal, & Bauer, 2010). Development of vulnerability and capacity assessment maps (Krishnamurthy, Fisher, & Johnson, 2011) assists in identifying possible impacts of disasters and extreme events. Short and long term economic wellbeing, physical infrastructure (housing, public systems, roads and safety shelters) and population risks should be determined for a given natural event. Information gathered from local communities is one source to help identify frequency and exposure to disasters. This local knowledge and input has the potential to assist governments in the development of structural and economic policies to aid in disaster management mitigation, emergency response, and recovery. Developing countries have little risk mitigation and adaptation capacity, and disaster management policies may require humanitarian relief to cope with and recover from extreme events (Barros C.B. et al., 2012).

Vulnerabilities are much greater in regions with populations in the poorer economic classes. These populations live in substandard housing more susceptible to extreme event damage (Krishnamurthy et al., 2011). The poor may not have the financial means to purchase adequate insurance policies - that compound disaster recovery efforts. In Jakarta, the urban poor settle in informal communities consisting mostly of undocumented or illegal residents. Often, they migrate in groups, generally to empty low lying areas, along the coast, riverbanks, and canals prone to flooding (Baker, 2011a). These residents settle on

private and government owned land. Scrap building materials found on construction sites, mostly concrete and brick, are used to construct temporary shelters that become permanent homes. Land use planning and policies are required to reduce impacts from SLR and/or TC related coastal inundation (Vafaee, Harati, & Sabbaghian, 2012).

2.4.1 Tropical Cyclone and Hurricane Risks

Mortality either directly or indirectly related to hurricanes is a major concern. Evacuation plans and emergency shelters have reduced death tolls over time (Blake, Landsea, & Gibney, 2011). Efforts are hampered when inadequate transportation infrastructures cannot effectively evacuate populations, or when people refuse to vacate the danger area (Krishnamurthy et al., 2011; Wolshon, 2006). Coastal population vulnerabilities continue to increase as more people migration to coastal cities (K. Emanuel, 2005; Frey et al., 2010).

As TC frequency and wind speeds increase, construction damage also increases (K. Emanuel, 2011). Insurance companies use engineering models of housing construction characteristics such as building material types, roof type, number of stories and the ability to withstand TC high wind speeds to establish insurance rate structures (Cole, Macpherson, & McCullough, 2010; Pinelli, Gurley, Subramanian, Hamid, & Pita, 2008). Improved building standards and materials in Florida post Hurricane Andrew in 1992 reduced the number of hurricane related insurance claims (Cole et al., 2010). Identifying and reinforcing building construction in hurricane prone locations (Bjarnadottir, Li, & Stewart, 2011) has the potential benefit of reducing disaster recovery costs (Greenblatt & Wills, 2011). Costly damage also occurs to public infrastructures such as electrical networks (Ball, 2006), roadways (Krishnamurthy et al., 2011), public buildings, and flood protection systems (Mlakar, 2006).

2.4.2 Sea Level Rise, Storm Surge, and Inundation

Public health risks exist from slow rising sea-levels, subsidence, and inundation in coastal areas. Changing disease and infection rates due to standing water and flooding increases the frequency of mosquito-borne diseases and dengue fever (Craig, 2010; S. D. Indonesia & Task-Force, 2011). In Jakarta, it is estimated for every 9.73 mm of increased monthly rainfall, an additional 67 cases of dengue occur (S. D. Indonesia &

Task-Force, 2011). Increased toxic algae blooms and agriculture nutrient runoffs are also problematic (Craig, 2010). Vulnerability modelling shows Jakarta and the Philippines are highly vulnerable to the effects of SLR (Yusuf & Francisco, 2009).

Salt water intrusion into aquifers reduces available potable water (ECLAC, 2010; Howard & Mullings, 1996). In Barbados, 98% of the rechargeable fresh water resources were being consumed. Desalinization plants have been constructed to remove salt from sea water and augment low water supplies (ECLAC, 2010). Bangladesh river systems are particularly prone to salt water intrusion in the dry summer months due to the flat terrain near the coast (Bhuiyan & Dutta, 2012).

During and after the Hurricane Katrina storm surge, locations of New Orleans near sea level, experienced toxins flowing into inundated waters from sewage treatment plants, oil and gas facilities, and chemical plants (Reible, Haas, Pardue, & Walsh, 2006) hampering rescue and cleanup efforts. Potable water was transported to the disaster site while toxic water was removed from the city. Modelled storm surge projected losses of infrastructure along the US Gulf of Mexico border are expected to increase as sea levels continue to rise (Hoffman et al., 2010).

2.4.3 Economic Vulnerability

SLR, tropical cyclone, and storm surge threats and damage have huge economic implications especially in tropical locations (Morenoa & Beckenb, 2009). In coastal regions, tourism is reduced with the occurrence of significant damage to coral reefs, mangroves, fishing, and coastal beaches (Forster, Schuhmann, Lake, Watkinson, & Gill, 2012; Gable, 1997). Threat of imminent extreme weather also deters tourists from selecting those destinations. Coastal beaches and wetlands provide a buffer zone from the effects of hurricanes and storm surge inundation. Damage and removal of wetlands due to SLR or other developments reduces the natural protection (Dean, 2006). Coastal beaches are dynamic landscapes vulnerable to SLR and storm surge related erosion. The ability for beaches to recover after extreme events depends on sediment transport and redistribution, and the health of vegetation and ecosystems on and near beaches. There is the potential for some types of beaches to disappear (Cambers, 2009) resulting in a reduction of coastal attractions. After a hurricane hits a region, it takes several years for the tourism

industry to recover (Hsiang, 2010). These losses may compound as SLR and storm dynamics might eliminate beaches in some regions.

Sediment redistribution and changes in river systems resulting from SLR have the potential to disrupt flows (Huang, Zong, & Zhang, 2004) and change channel characteristics (Dean, 2006). Ships travelling in the Hong Kong Pearl River Delta containing "Just in Time" inventories cannot reach manufacturing plants located along the river system causing delays and substantial economic loss (Tracy et al., 2007). Similarly, significant employment losses and devaluation of land values may occur in the Nile delta (El-Raey, 1997).

Agriculture practices in hurricane prone regions have changed in an attempt to reduce economic losses from the effects of wind and storm surge inundation. In Mexico, crops have changed to sugar cane production since it is more resilient to wind and flooding than other more profitable crops (Krishnamurthy et al., 2011). Agriculture recovery efforts from Hurricane Mitch in Nicaragua included the introduction of Agro ecology (Holt-Giménez, 2002). Introduction of techniques used to protect topsoil for crop production include construction of barriers and stubble being left on fields to allow root systems to hold the soil in place. These methods aid in the protection of soils and crops during extreme weather.

2.5 Modelling the Science

Three-dimensional (3D) models are created to visually "sense" a geographical space. Traditionally, scientific data is modelled using software such as Esri ArcGIS. The use of New Media software such as Autodesk 3D Studio Max or Epic Unreal Game Engine, allows for the addition of textures to be placed on surfaces giving the data a more realistic representation. 3D data visualization has the potential to disseminate scientific and mathematical data of a space to both experts and laypersons in an easily understandable manner.

The interactive ability of game engines enables end users to explore locations, objects, and features of the modelled space in "real time". Seamless game-play animation requires game engines to display detailed realistic terrain at 30 frames per second. Technological advances in the Central Processing Unit (CPU) and the Graphics Processing Unit (GPU) design now make this possible. Advances in game engine Artificial

Intelligence (AI) design allow realistic "serious games" to be created based on "real-life" data (Prakash et al., 2009). Adaptive games, based on studies in human behaviour, are being integrated into game AI systems. Adaptive games allow environmental data, parameters, and variables to change in "real-time" providing immediate feedback in the modelled geographical space. In the case of climate change, programming of variables such as sea-level, storm surge, inundation levels, atmospheric temperature, and ocean temperature can be modified "on the fly" in the virtual world allowing changing conditions to be examined.

Research presented in this thesis uses traditional scientific modelling software with some maps enhanced using Adobe Photoshop. 3D modelling and game engine software research were explored with limited success and therefore were not included in this body of work. Continued investigation of these technologies to disseminate this research to the general public will be considered at a future date.

2.5.1 Digital Earth

The advent of a global "Digital Earth" has made geographical spatial data and thematic mapping (Gibin, Singleton, Milton, Mateos, & Longley, 2008; Sandvik, 2008) available to the general public (Craglia et al., 2011). Web based applications such a Google Earth provide 2D and 3D views of the earth. However, data accuracy is insufficient for scientific geo-spatial analysis (Yu & Gong, 2011). Various techniques have been developed for object and feature extraction modelling from photographic imagery to be "draped" over the globe (Homainejad, 2012). An approach was developed using pattern recognition to create a point cloud, consisting of vector data to overlay a single image onto a 3D model such as a digital terrain model (DTM), digital surface model (DSM), or digital elevation model (DEM). Image distortion was removed as part of this approach however gaps in the image remain where correction is completed requiring additional images to fill these gaps. In the case of digital earth, this technique allows features to be extruded from an image and correctly placed on the surface of the globe (Homainejad, 2012).

2.5.2 3D Modelling

Geographical Information Systems (GIS) are able to create 3D mathematical models. A computer generated 3D model for a coal mine in the Shandong Province of China was created to examine land

subsidence (Djamaluddin, Mitani, & Ikemi, 2012). Geological 3D dynamic ground movement over time was incorporated into the model. The model was compared to observational field data measurements. Additional ground movement and soil and water characteristics were required to remove slight differences between the model and field observational data.

3D modelling of the Pompeii Archaeological area was completed using OpenSceneGraph, open source 3D visualization software (Apollonio, Gaiani, & Benedetti, 2012). A back end database was constructed using architectural naming conventions to organize and relate artifacts. A data management pipeline was developed for modelling, texturing, segmenting, and placement of objects. Geospatial information was obtained using photogrammetric, laser scanning, and surveying techniques. Data verification using triangulation laser scanning was used to place artifacts in the 3D model to within 0.1 mm of the "real world" placement.

In 2002, researchers at MIT used the Epic Unreal Engine 2 to create a "real-time" virtual ecosystem based on "real-world" data (Thrane, Ojika, & Berry, 2002). A complex system was setup and configured using DEM, satellite imagery, photographic data, a web-based controller, a sun controller, and weather feed from a "real-time" online service. The DEM required several conversions resulting in the data not accurately represented in the game engine. Photographs of the locale were used to create changing seasonal textures. Live data feeds were programmed to control the appearance of environmental conditions, changing light levels as well as changing seasonal ground conditions. It was not possible to orient the virtual world to the "real world" therefore sun angle could not be accurately projected for lighting based on the time of day data feed. The direction of real-world roads, parking lots, and sizes of features were not correctly represented in the virtual world. The research team experienced difficulties due to the immature nature of computer technology available at the time. As well, there were inconsistencies in geographical data, photography, and satellite imagery when it was imported into the game engine. Significant progress was made by the MIT research team to move the technology forward by implementing custom computer programming.

A simulated environment of the Amazon River and floodplain was developed using Crysis game engine software at the University of Bristol (Ash, Romanillos, & Trigg, 2009). The Crysis engine was used for its ability to import "real-world" scientific DEM elevation data for terrain creation. The goal was to use interactive 3D visualization of a mathematical flood model to disseminate and communicate a sense of geographical scale in a manner that could be understood by non-scientific clients especially when on-site field visits were not possible. A sense of the vastness of the Amazon River could be conveyed by the length of time it took to traverse the virtual world.

A three dimensional virtual construction of the archaeological site of Casal de Freiria located in the coastal area of Cascais, Portugal was modelled in Autodesk 3DS Max and ported into the Bethesda game engine (Rua & Alvito, 2011). The environment was modelled using varying scale data from topographical, archaeological, and photographic surveys. A Triangular Irregular Network (TIN) grid was created for the terrain. The stone foundation was the only physical data available for the site. Archaeologists were consulted to obtain a consensus for probable "time period" building materials, textures, and the overall structural footprint. Presenting the archaeological site in this manner was done to facilitate further research. Structural and building material scenarios could be easily modified as new excavation data or additional information about the site became available. An additional benefit of the virtual environment was public outreach regarding the historical site.

At the University of Rhode Island, the Unity 3D game engine was utilized to create a research and education environment for ocean floor exploration (Hervé et al., 2010). 3D models of the area were created using sonar, stereographic, video, and other sensor data. An avatar automatically follows a predefined path using a "first person" view but has an option to switch to manual control if desired. The simulation is recorded for post mission analysis.

3 Coastal Population Vulnerability to Sea Level Rise and Tropical Cyclone

3.1 Introduction

Global climate change will negatively affect coastal populations. Sea Level Rise (SLR) caused by melting glaciers and increased temperatures (Church & White, 2011; Vafaee et al., 2012) in coastal regions pose increasing public health risks. Standing water and land subsidence inundation in coastal areas change disease and infection rates such as increased frequency of mosquito-borne diseases such as malaria and dengue fever (Craig, 2010; S. D. Indonesia & Task-Force, 2011). Salt water intrusion into aquifers reduces available agricultural irrigation water supplies (Howard & Mullings, 1996) and potable water. Rising sea levels erode coastal beaches, impact habitats, wetlands (Vafaee et al., 2012), industry (Yin, Yin, Wang, & Xu, 2012), manufacturing processes (Tracy et al., 2007), and tourism (Gable, 1997). Urban and rural populations will be disrupted and displaced by rising sea levels (Baker, 2011b; Rowe, 2011).

Tropical cyclone (also referred to as hurricane) wind and storm surge damages to infrastructure and human health have been extensive. Property damages in the U.S. from 1900 to 2005 have occurred at an average rate of $10 billion per year based on estimated 2005 replacement values (Pielke et al., 2008). Damage in US coastal regions could increase as wealthy populations continue to migrate to hurricane prone coastal regions (Senkbeil et al., 2011). Risks of increased hurricane level storms has the potential to decrease travel to popular tourist destinations impacting local economies (Forster et al., 2012). Infrastructure in developing countries is especially prone to higher risks of damage from hurricanes, storm surges and inundation due to insufficient building construction policies and standards (Programme, 2011).

The objective of this research is to develop first order estimates of flooding potential for regions vulnerable to the combined impacts of global warming enhanced tropical cyclones, forecast SLR and storm surge inundation. Geographic Information System (GIS) analysis techniques use population data, hurricane tracks and Digital Elevation Model (DEM) datasets to identify a) densely populated coastal regions in the Caribbean and Asia; b) low lying coastal locations susceptible to SLR; and c) regions prone to tropical cyclone/hurricane activity. This research will produce maps of coastal populations under enhanced threats of coastal inundation in the Caribbean, Philippines, Bangladesh, Jakarta, parts of China, and the east coast

of India. Based on the results of this study, a regional study area will be selected for continued, in depth analysis.

3.2 Methods

The study area selected is located in the Northern Hemisphere where potential SLR and hurricane storms intersect with Asia (see Figure 3.2.1) and the Caribbean (see Figure 3.2.2) countries. Bangladesh has very low elevation throughout the country. The east coast of India has regions of low elevation. The North Indian hurricane basin affects both countries. China's coast is susceptible to rising ocean levels (Yin et al., 2012). The Shanghai region of China, Taiwan, and the Philippines are located in the Western Pacific hurricane basin. Jakarta frequently experiences inundation and land subsidence on a frequent basis. Rising sea levels compound flooding issues (Baker, 2011a; EASIS & Eng, 2008).

Figure 3.2.1: Asian Study Location. Includes Bangladesh, China (Shanghai and Taiwan), India (east coast), Jakarta, and the Philippines.

The Caribbean is located in the North Atlantic hurricane basin (Figure 3.2.2). Smaller island countries in the northern portion were grouped to improve the GIS processing time. The north island group contains Bermuda, Cayman Islands, and Turks & Caicos Islands. In a similar fashion, the island countries in the southern part of the Caribbean were grouped together consisting of Anguilla, Antigua & Barbuda, Aruba, Barbados, British Virgin Islands, Dominica, Grenada, Guadeloupe, Martinique, Montserrat, Netherlands Antilles, Saint Kitts and Nevis, Saint Lucia, Saint Vincent & the Grenadines, Trinidad & Tobago, and U.S. Virgin Islands. The balance of the island countries of the Bahamas, Cuba, Dominican Republic, Haiti, Jamaica, and Puerto Rico were kept separate for the analysis.

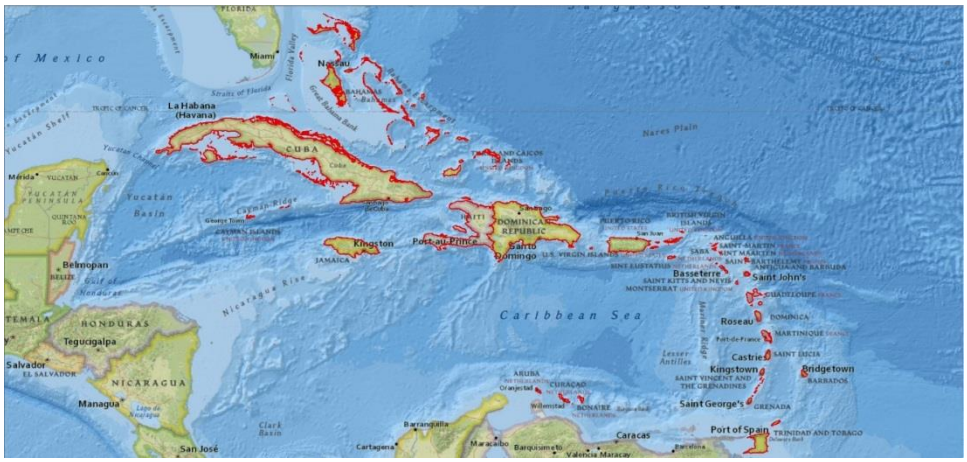

Figure 3.2.2: Caribbean Study Location. Includes the 26 island countries of the Anguilla, Antigua & Barbuda, Aruba, Bahamas, Barbados, Bermuda, British Virgin Islands, Cayman Islands, Cuba, Dominica, Dominican Republic, Grenada, Guadeloupe, Haiti, Jamaica, Martinique, Montserrat, Netherlands Antilles, Puerto Rico, Saint Kitts and Nevis, Saint Lucia, Saint Vincent & the Grenadines, Trinidad & Tobago, Turks & Caicos Islands, and U.S. Virgin Islands.

A GIS based inundation model was developed on Esri ArcGIS version 10.0 SP 5 with the "World Cylindrical Equal Area" map projection. The National Geographic world base map was used to visually identify countries in the study area (Geographic et al., 2011). Administrative and regional subdivision GIS shapefiles were obtained from Diva-GIS to limit analysis to each country and their internal territorial boundaries (Hijmans, 2009). Microsoft Excel 2010 was used for area and population density calculations as described later in this section.

Climate Change Ocean Inundation Level (CCOIL) was modelled using Aster GDEM Version 2 30 m raster data (Tachikawa et al., 2011a). Aster DEMs are available in tiles containing square grid cells 30 m long by 30 m wide with a vertical resolution of 1 m. Each grid cell contains a single elevation value representing the terrain height for that location (Tachikawa, Hato, Kaku, & Iwasaki, 2011b). Aster GDEM tiles were obtained for each country and region. Separate single mosaics were created using all tiles located within each country or region. This method was used to keep raster sizes as small as possible and decrease computational time required performing GIS analysis. To calculate inundation, Diva-GIS shapefile masks were used to limit CCOIL analysis to the country boundary. The inundation model used a "bathtub" model where water fills a grid cell if it is less than or equal to the CCOIL value being calculated. CCOIL was calculated for 0 m (sea level), 5 m, and 10 m. "Country" rasters were created capturing all grid cells within each country or region's boundary. Inundation area was calculated based on the number of grid cells

multiplied by the area of a square grid cell size of 900 m^2 and converted to area per square kilometer. The corresponding percentage was calculated using the number of grid cells divided by the total number of grid cells in the area "location/region" raster. Missing grid cell values were not factored into the calculations and no statistical Root Mean Square Error (RMSE) calculations were computed to compare the model results to any observed data.

Hurricane storm track analysis was completed using the IBTrACS (Knapp et al., 2010) database. Data is recorded in 6 hour increments along all identified storm tracks for all global hurricane basins. Each observation point contains statistics about the hurricane at the given time (C. Landsea, Franklin, & Beven, 2012). Hurricane maximum circular wind speed is recorded from satellite imagery, air reconnaissance, and/or other observational evidence to the nearest 5 kt; central pressure is recorded to the nearest millibar. IBTrACS data for the hurricane season, storm names, date, time, sustained wind speed (kt), and physical location (latitude/longitude) was obtained for the West Pacific Ocean (WP basin) from 1884 – 2011, North India Ocean (NI basin) from 1842 – 2011, and North Atlantic Ocean (NA basin) from 1851 – 2011. GIS overlays and tabulated results were created showing locations and counts of hurricane track segments intercepting each land location in the study area. Saffir-Simpson Hurricane Wind Scale (SSHWS) intensities (see Table 3.2.1) were calculated in ArcGIS using wind speed and subsequently classified into categories of less than 1 through to 5 for each track segment in all NI, WP, and NA basins. Missing wind speed data values must be factored into the analysis. Since each track segment is classified into levels of SSHWS categories, missing data counts for each location are required to determine the quality of the data and quantify regions more vulnerable to TCs. Wind speed data values of -999 indicate the segment contains "No Data" and are therefore considered missing data.

	Wind Speed Knots	**Wind Speed Metric**	**Wind Speed Imperial**
Category 1	64 – 82	119 – 153 km/h	74 – 95 mph
Category 2	83 – 95	154 – 177 km/h	96 – 110 mph
Category 3	96 – 112	178 – 208 km/h	111 – 129 mph
Category 4	113 – 136	209 – 251 km/h	130 – 156 mph
Category 5	137 or higher	252 km/h or higher	157 mph or higher

Table 3.2.1: Saffir-Simpson Hurricane Wind Scale. The scale used to categorize intense storms with circular wind speeds reaching a minimum of 64 knots.

Population densities were created using official census data obtained directly from each country's statistics department for the Bahamas (Mackey et al., 2012), Cuba (Informacion, 2002), Dominican Republic (Tactuk, Ureña, & Mejía, 2010), Haiti (Geohive, 2003), Jamaica (Geohive, 2001), Puerto Rico (Geohive, 2010), Trinidad & Tobago (Geohive, 2000), Bangladesh (B. B. o. Statistics, 2001), China (China, 2007), Taiwan (N. Statistics, 2012), India (Geohive, 2011), Jakarta (B. P. S.-S. Indonesia, 2010), and the Philippines (Board, 2007). Census data was assembled corresponding to administrative subdivisions for each country using the GIS polygon administrative boundary shapefile data obtained from Diva-GIS (Hijmans, 2009). Microsoft Excel was used to match population district data to the Diva-GIS administrative unit polygons within each reported country or region's shapefile. The ArcGIS built-in calculator was used to compute square kilometer (km^2) area of the Diva-GIS polygons in the study area to establish land area for each population district. Population density was categorized using Esri ArcGIS into standardized subdivisions for all reported locations and normalized based on the calculated area.

3.3 Results

Climate Change Ocean Inundation Level CCOIL) raster analysis was successfully calculated using 30 m Aster GDEM tiles for both the Asian and Caribbean study locations (see Table 3.3.1 and Table 3.3.2). The Shanghai region has the potential for 12,537 km^2 or 8% of physical area to be affected by a 5 m CCOIL. Flooding in Bangladesh is estimated to be 4% of its land mass (6,281km^2). Actual CCOIL inundation could be potentially higher than the reported values as several DEM tiles covering the northeast portion of Bangladesh contain significant numbers of missing data values and anomalies. At the 10 m CCOIL level, the same ranking exists for Asian study locations. In the Caribbean, Cuba has the largest area at 4,015 km^2 (3.5% of the country area) that could be affected by 5 m CCOIL and 15,921 km^2 (14%) at a 10 m CCOIL. The Bahamas will experience the second highest inundation levels for a 5 m CCOIL level 2,099 km^2 (15%) and 7,041 km^2 (51% of the country) at a 10 m CCOIL.

Location	Area (km^2)	Area (km^2) 5 m CCOIL		Area (km^2) 10 m CCOIL	
Bangladesh *	143,900	6,281	4 %	56,748	39.5 %
India	485,379	4,457	1 %	44,840	9 %
Philippines	286,434	3,311	1 %	15,764	5.5 %
Shanghai and region	160,446	12,537	8 %	71,778	45 %
Taiwan	37,258	192	0.5 %	1,334	3.5 %
Jakarta	631	17	3 %	156	25 %

* Anomalies and missing data exist in DEM tiles covering the northeastern region of Bangladesh. Reported CCOIL values can be higher than reported.

Table 3.3.1: Sea Level Rise in the Asian Study Area. Area calculations for the country size, 5m and 10m inundation are in km^2. Percentages are calculated based on how much of the country land area is inundated.

Location	Area (km^2)	Area (km^2) 5 m CCOIL		Area (km^2) 10 m CCOIL	
Bahamas	13,886	2,099	15 %	7,041	51 %
Cuba	112,682	4,015	3.5 %	15,921	14 %
Dominican Republic	48,115	380	1 %	1,513	3 %
Haiti	27,088	235	1 %	1,154	4 %
Jamaica	10,955	77	1 %	382	3.5 %
Puerto Rico	8,937	118	1 %	452	5 %
South Island Group	12,630	400	3 %	1,098	8.5 %
North Island Group	1,291	183	14%	522	40%

Table 3.3.2: Sea Level Rise in the Caribbean Study Area. Area calculations for the country size, 5m and 10m inundation are in km^2. The North Island Group contains Bermuda, Cayman Islands, and Turks & Caicos Islands. The South Island Group consists of Anguilla, Antigua & Barbuda, Aruba, Barbados, British Virgin Islands, Dominica, Grenada, Guadeloupe, Martinique, Montserrat, Netherlands Antilles, Saint Kitts and Nevis, Saint Lucia, Saint Vincent & the Grenadines, Trinidad & Tobago, and U.S. Virgin Islands.

GIS overlays of IBTrACS data were created identifying hurricane track line segments intersecting country shapefiles for both study area locations (see Table 3.3.3 and Table 3.3.4). The tables show storm segments broken down into SSHWS categories "< 1" through "5" which includes those not reaching hurricane intensity. "No data" values are also reported for each country and hurricane basin. The most severe SSHWS storms reaching category 5 in the NI and WP basins occurred in India. The Philippines experienced the greatest number of category 3 to 5 hurricanes with a quantity of 18 storm track recorded segments passing over the country. Jakarta experienced 0 hurricanes. A significant number of "no data" values exist in the NI and WP basins with 47,103 in the WP basin and 23,070 in the NI basin. SSHWS reported values could be much higher if "unknown" hurricane storm tracks intensity data were available for countries in the Asian study location. "No data" issues do not exist in the Caribbean study location as all intersecting track segments contain SSHWS intensities. The North Island Group experienced 76 storm

track segments in the most severe SSHWS categories 3 through 5 with Cuba containing 62. The largest quantity of SSHWS level hurricane segments was also in Cuba.

	< Cat 1	Cat 1	Cat 2	Cat 3	Cat 4	Cat 5	Sub Total	No Data	Total
Bangladesh	46	1	1	0	3	0	51	651	702
Philippines	1,333	123	57	16	2	0	1,531	1,859	3,390
India	521	8	4	2	1	2	538	9,328	9,866
China	2,618	85	2	1	0	0	2,706	2,123	4,829
Taiwan	193	49	11	5	0	0	258	295	553
Jakarta	0	0	0	0	0	0	0	0	0
WP basin	47,096	4,467	1,739	643	64	1	54,010	47,103	101,113
NI basin	1,847	104	37	25	20	3	2,036	23,070	25,106

Table 3.3.3: Hurricane Line Segment SSHWS Category Storm Counts in the Asian Study Location. Data is available in the NI basing from 1842–2011 and in the WP basin from 1884–2011. The Sub-Total column is the sum of all storms from "< Category 1" through to "Category 5".

	<Cat 1	Cat 1	Cat 2	Cat 3	Cat 4	Cat 5	SSHWS	No Data	Total
North Island Group	269	56	46	43	27	6	178	0	447
South Island Group	143	34	19	15	10	0	78	0	221
Cuba	301	107	44	42	18	2	213	0	514
Dominican Republic	96	26	8	4	3	1	42	0	138
Haiti	65	19	5	4	3	0	31	0	96
Jamaica	25	6	7	7	0	0	20	0	45
Puerto Rico	29	9	11	5	4	2	31	0	60
NA Basin	29,000	7,718	3,684	1,866	918	123	14309	10	43,319

Table 3.3.4: Hurricane Line Segment SSHWS Category Storm Counts in the Caribbean Study Location. Data is available in the NA basin from 1851 – 2011. In this analysis, the Bahamas is included in the North Island Group. The North Island Group contains the Bahamas, Bermuda, Cayman Islands, and Turks & Caicos Islands. The South Island Group consists of Anguilla, Antigua & Barbuda, Aruba, Barbados, British Virgin Islands, Dominica, Grenada, Guadeloupe, Martinique, Montserrat, Netherlands Antilles, Saint Kitts and Nevis, Saint Lucia, Saint Vincent & the Grenadines, Trinidad & Tobago, and U.S. Virgin Islands.

Population density for each country was successfully created from official census data and classified using standardized category subdivisions (see Table 3.3.5 and Table 3.3.6). The Asian study location has both the largest population and population density. Jakarta was ranked highest at 12,403 persons/km^2, followed by 3,346 persons/km^2 in Shanghai, and 1,029 persons/km^2 in the Philippines. In the Caribbean, population densities were calculated for island countries with the largest land area. Puerto Rico has the highest population density at 415 persons/km^2, followed by Haiti with 293 persons/km^2. Higher densities exist in the territorial regions. Ciudad de la Habana, Cuba has a population density of 2,689 persons/km^2 and New Providence, Bahamas has a population density of 1,070 persons/km^2.

Location	Census Year	Population	Area (km^2)	Population Density/km^2
Bangladesh	2011	124,355,263	139,647	890
China - Jiangsu	2006	78,690,000	101,699	774
China - Shanghai	2006	23,030,000	6,884	3,346
China - Zhejiang	2006	54,470,000	102,788	530
India – West Bengal	2011	94,777,446	295,857	320
Indonesia - Jakarta	2010	9,797,525	790	12,403
Philippines	2010	91,347,736	88,752	1,029
Taiwan	2006	23,282,670	36,224	643

Table 3.3.5: Population Density in the Asian study location. Calculations for the country area are in km^2; population densities are persons/km^2.

Location	Census Year	Population	Area (km^2)	Population Density/km^2
Bahamas	2011	351,461	13,388	26
- New Providence	2011	246,329	230	1,070
Cuba	2002	11,177,743	110,731	101
- Ciudad de la Habana	2002	2,201,610	819	2,689
Dominican Republic	2010	9,445,281	48,105	196
Haiti	2003	7,929,048	27,075	293
Jamaica	2001	2,607,631	11,000	237
Puerto Rico	2010	3,725,789	8,970	415
Trinidad & Tobago	2000	1,262,366	5,159	245

Table 3.3.6: Population Density of the Largest Island Countries in the Caribbean study location. Calculations for the country area are in km^2; population densities are persons/km^2. Population densities are also reported at the territorial level for the Bahamas and Cuba.

3.4 Discussion

The selection of coastal regions and island countries for the study area were specifically chosen to examine and identify impacts caused by inundation and intense hurricanes. Asia and the Caribbean are both situated in hurricane storm basins. With the use of a simple inundation "bathtub" model, it was possible to identify low-lying regions susceptible to CCOIL. Although current SLR estimates of 1 to 3 mm per year are well below the 5 and 10 m levels calculated in this study, other factors such as hurricane storm surge (Church & White, 2011; Komar & Allan, 2008), precipitation & runoff, and land subsidence (Baker, 2011a, 2011b) have the potential to cause much higher levels of inundation. To illustrate the physical size of flooding expanse, Jakarta was used to demonstrate the potential impact in a region. The calculated size of Jakarta's land area is 631 km^2. This equates roughly to a dimension of 25 km by 25 km. At the 10 m CCOIL level, 156 km^2 of Jakarta's land area could be inundated. This extent is approximately 12 km by 12 km and is calculated to be 25% of the total land area. In the Asian study location, both the Shanghai region with a flooding extent of 12,537 km^2 (8% of the region's land area approximately 112 X 112 km) and Bangladesh (Figure 3.4.1) with 6,281 km^2 (4%, extent of 79 X 79 km) are at risk of a 5m CCOIL inundation.

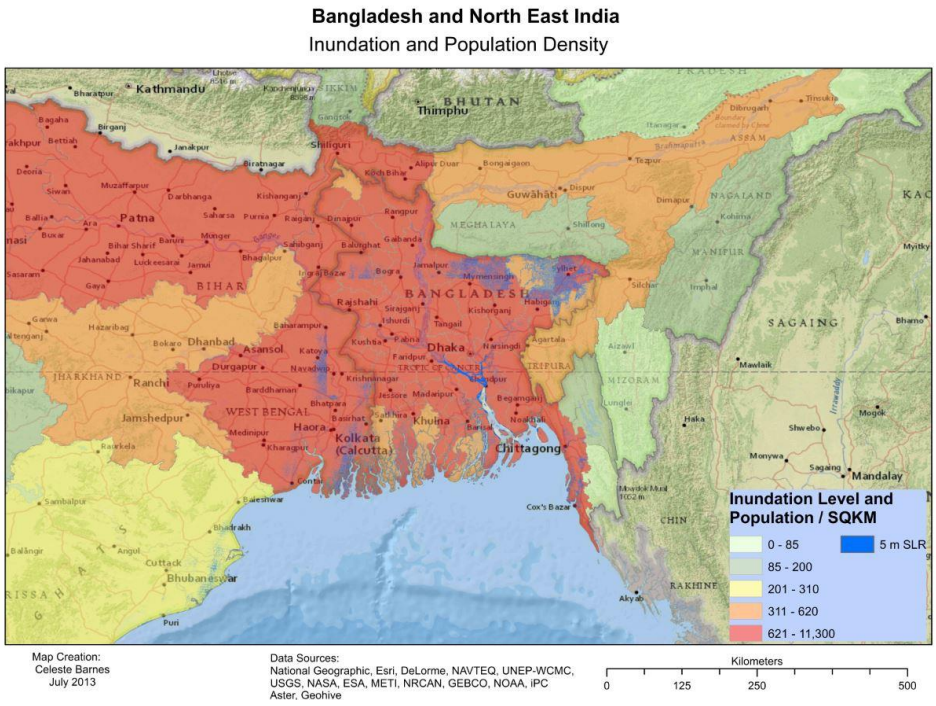

Figure 3.4.1: Bangladesh and North East India 5 m Inundation with Population density.

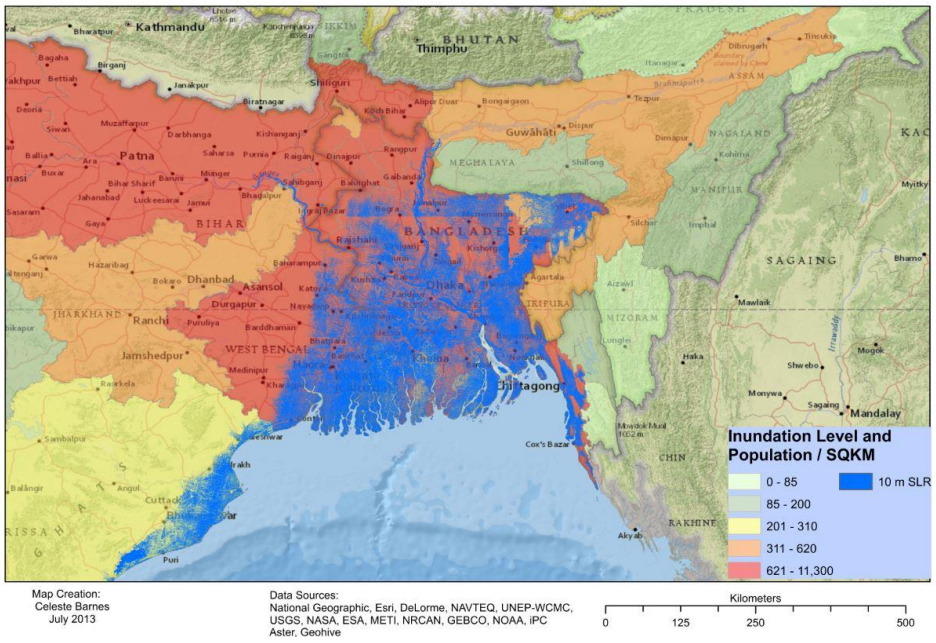

Figure 3.4.2: Bangladesh and North East India 10 m Inundation with Population density.

At a 10 m CCOIL level, the Shanghai region, Bangladesh (Figure 3.4.2), Jakarta, and the east coast of India are also prone to extensive inundation. The Philippines is the largest country in both the Asian and

Caribbean study locations. Although only 5.5% of the country would be inundated (15,764 km^2) at a 10 m CCOIL level, it is still roughly an area of 125 km by 125 km. In the Caribbean study location, Cuba has the potential to experience the largest inundation at 4,015 km^2 (3.5 % of its country area, extent of approximately 63 X 63 km) followed by the Bahamas with 2,099 km^2 (15 %, extent of 46 X 46 km). At the 10 m CCOIL level, Cuban inundation could be as high as 14% of its country size at 15,921 km^2. The Bahamas could experience a much greater impact with 51 % of its country being flooded at 7,041 km^2. Overall, the Asian study location will experience a larger area of inundation however; the Bahamas will experience a greater impact with 51% of its country susceptible to flooding.

GIS analysis of historical IBTrACS hurricane data indicate the Asian study location has been minimally impacted by intense SSHWS storms containing only 4 storm track segments at SSHWS category 5 and 84 segments at category 4. The NI and WP basins are located in the Asian study location and contain significant amounts of historical hurricane data that do not include wind speed and were therefore unclassified. In the WP basin, 47,103 out of 101,113 segments contain missing data and could not be categorized into SSHWS intensities. The issue is much greater in the NI basin where 23, 070 out of 25,106 segments contained missing wind speed data. As a result, a considerable number of unknown hurricane storm track intensities existed in the Asian study location making the identification of hurricane vulnerability in the NI and WP basins very difficult.

In the Caribbean study location, wind speed exists for all historical NA IBTrACS data with the exception of only 10 missing data segments out of 43,319. The NA basin contained 123 SSHWS category 5 and 918 category 4 storm tracks intersecting land in the Caribbean. Cuba ranked highest with 514 track segments of which 213 were SSHWS intensities. The North Island Group experienced 178 SSHWS track segments contacting land and it had the highest number of SSHWS category 2 through 5 storm track segments. Data for the NA basin contained 10 missing hurricane track segment wind speed values. With this more complete dataset, it was possible to calculate all SSHWS storm track intensities intersecting land located in the Caribbean.

Population density results show locations in Asia (Table 3.3.5) contain higher concentrations of people than in the Caribbean (Table 3.3.6). Jakarta ranked highest followed by Shanghai and the Philippines. In the Caribbean, Puerto Rico has highest density. The population density reported in the Caribbean countries is quite low when compared to Asia. However, the Caribbean does contain densely populated urban centers such as Ciudad de la Habana, Cuba and New Providence, Bahamas.

Population vulnerability to hurricane strength storms are difficult to identify in Asia due to the lack of a more complete IBTrACS dataset. In the Caribbean, these vulnerabilities can be more clearly identified using an overlay of population density, potential CCOIL, and Category 3, 4, and 5 hurricane storm tracks as shown in Figure 3.4.3. Island countries of the Bahamas, Cuba, Jamaica, Haiti, Dominican Republic, and Puerto Rico have experienced more intense hurricane strength storms. CCOIL is more pronounced in the Bahamas and Cuba (see Figure 3.4.4).

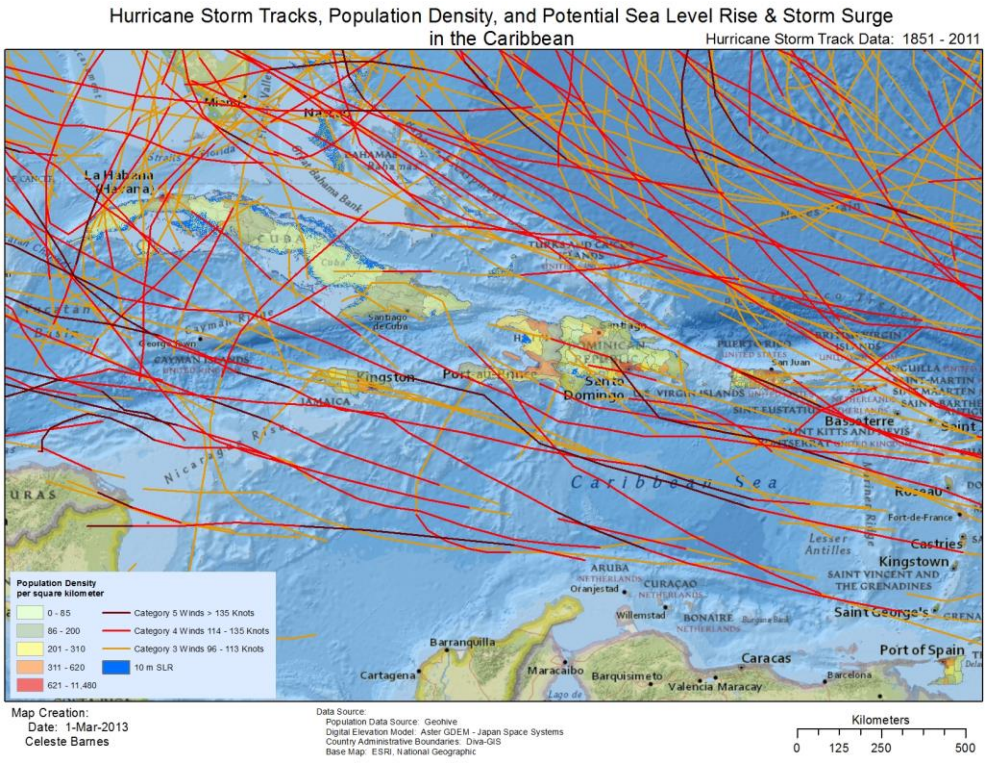

Figure 3.4.3: Caribbean Population Density, 10 m Inundation, and Category 3, 4, & 5 IBTrACS hurricane storm tracks.

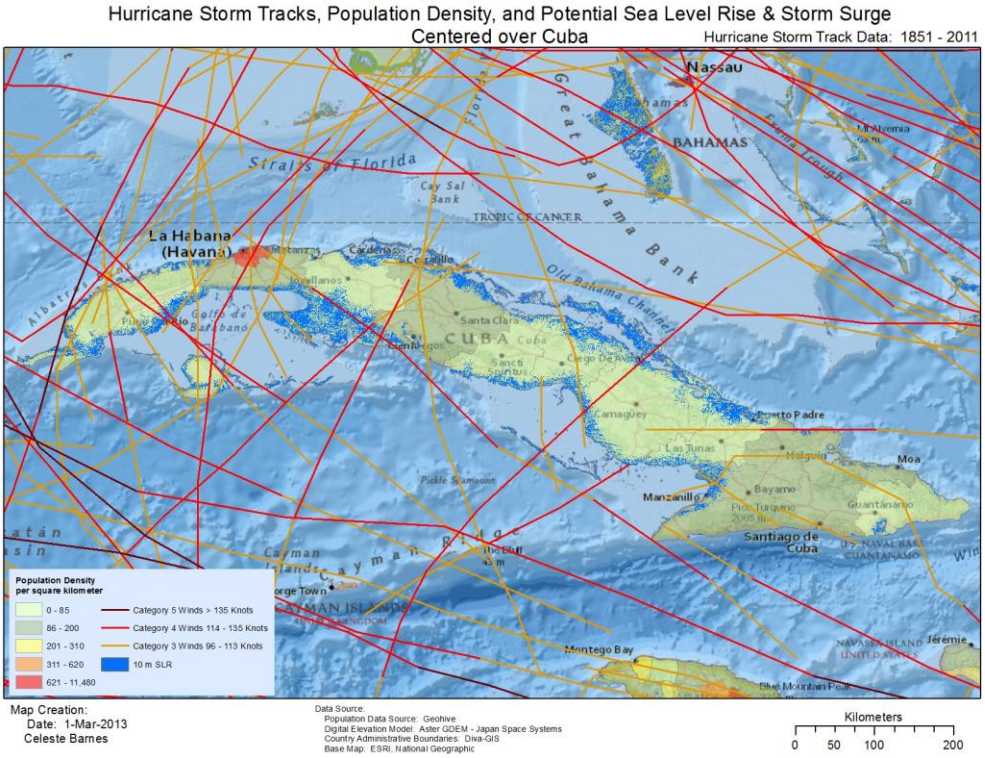

Figure 3.4.4: Centered over Cuba - Population Density, 10 m Inundation, and Category 3, 4, & 5 IBTrACS hurricane storm tracks.

3.5 Conclusion

GIS analysis in the Asian regions of Shanghai, Bangladesh, the east coast of India, Jakarta, the Philippines, and the Caribbean was used to study the effects of climate change ocean inundation level (CCOIL) combined with hurricane storm tracks on coastal populations. Aster GDEM 30 m grid cell DEM data showed all locations in both study locations were prone to coastal inundation. The Bahamas (51% of its country's land area), Shanghai (45%), Bangladesh (39.5%), Jakarta (25%), and Cuba (14%) were most susceptible to 10 m CCOIL flooding. North Indian (NI), Western Pacific (WP), and North Atlantic (NA) IBTrACS data was used to identify frequency and intensity of hurricane track segments for each site in the Asian and Caribbean study locations. The WP basin had no wind speed data for 47% of the segments while 92 % were missing wind speed data in the NI basin. Of the available data in the WP and NI basins, only a small percentage storm tracks that intersected land locations in Asia were classified as SSHWS intensity. The Philippines experienced the largest number of hurricanes while Jakarta did not experience any SSHWS storms. In the Caribbean, the NA basin had wind speed data values for all hurricane track segments intersecting land. Cuba experienced the highest number of SSHWS category storms with

Caribbean countries located in the northern region experiencing the next highest quantity. Official census data was obtained from each country's official statistics department in order to create population densities. Jakarta, Indonesia had the largest density with 12,403 persons/km^2. The Asian study location had higher density figures compared to all the Caribbean countries with the exception of Puerto Rico which had 415 persons/km^2. GIS overlays combined CCOIL, hurricane storm tracks, and population densities to identify locations most at risk.

3.6 Next Steps

Continued research of coastal population vulnerabilities to CCOIL and tropical cyclone intensification analysis requires a more localized study area. Selection criteria are based on results from this study to CCOIL, hurricane tracks, and population densities in coastal locations. A major factor required for future research is the frequency and intensity of tropical cyclones (hurricanes) within the proposed study area. SSHWS storm track analysis was very limited in the Asian study location due to a severe lack of available historical wind speed data in the NI and WP basins. The effects of tropical cyclones in these basins were difficult to fully examine. As a result, the Asian study location was removed from consideration leaving only the Caribbean study location.

A further refinement in the Caribbean study location was desired. Hurricane storm track analysis showed the largest concentration located in Cuba and the North Island Group followed by smaller concentrations in the South Island Group. The balance of the larger island countries of Dominican Republic, Haiti, Jamaica, and Puerto Rico were affected but to a lesser degree. CCOIL has the largest impact on land area in Cuba followed by the North Island Group then a lesser amount in the South Island Group. A further breakdown of the North Island Group shows the Bahamas to have the highest percentage of its country susceptible to inundation especially at the 10m CCOIL level. CCOIL in the South Island Group is most evident in Trinidad & Tobago. Population densities were computed for the largest of the island countries in the Caribbean. At the country level, Puerto Rico had the highest population density followed in order by Haiti, Trinidad & Tobago, Jamaica, Dominican Republic, Cuba, and the Bahamas. Trinidad & Tobago is too close to the equator to be impacted by hurricanes and was therefore removed from the study area selection. As Cuba and the Bahamas experienced the greatest impacts from both CCOIL and hurricane storm tracks,

further examination of intra-country population density was completed. Higher population density was found located in Ciudad de la Habana, Cuba and New Providence, Bahamas. The combination of CCOIL, hurricane storm track, and population density analysis indicated the larger island countries located in the north and central regions of the Caribbean could potentially be most at risk. Therefore the final country selection for continued research was The Bahamas, Cuba, Dominican Republic, Haiti, Jamaica, and Puerto Rico as shown in Figure 3.6.1.

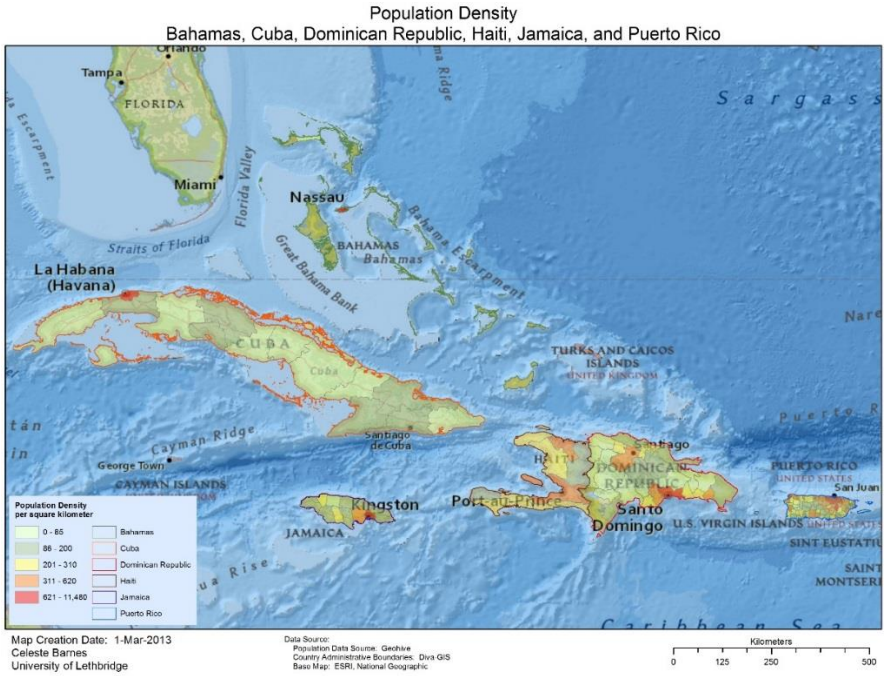

Figure 3.6.1: Caribbean Study Area for Continued Research. Caribbean countries included are the Bahamas, Cuba, Dominican Republic, Haiti, Jamaica, and Puerto Rico.

The objective the research will be to identify populations and food production areas that have been impacted by the effects of hurricanes on a frequent basis. A land cover/land use map of the study area will identify food production and urban locations. This study used GIS overlays of hurricane paths with no width dimension. The next study will put attempt to create a width buffer around each track and use it to examine the amount of land the hurricane path can impact in the study area. A hurricane must reach a minimum circular velocity of 64 kt in order to be classified as a SSHWS category storm. The 1851 – 2011 NA basin IBTrACS database contains 64 knot (kt) wind radii distances for each hurricane observation point in the four compass quadrants. The 64 kt wind radii data is the distance in nautical miles (nm) where 64 kt hurricane winds area observed. Unfortunately the 64 kt wind radii collection did not start until 2004.

Statistical linear regression analysis will used to extend the 2004 – 2011 64 kt radii data as far back as possible. GIS overlay analysis will create hurricane path impact zone maps using the 64 kt radii for the 2004 – 2011 time period as well as the extrapolated dataset.

4 Coastal Population Vulnerability to Sea Level Rise and Tropical Cyclone Intensification under Global Warming

Abstract
The potential for disruption to populations and food production areas due to global climate change is expected to be catastrophic in some regions. Among the most vulnerable regions are those impacted by the combined impacts of Sea Level Rise (SLR) and intensifying tropical cyclones (TC). The objective of this research is to identify coastal populations and food production vulnerabilities to multivariate driven inundation in the Caribbean. This work applies best estimates of climate change ocean inundation level (CCOIL) in concert with the International Best Track Archive for Climate Stewardship (IBTrACS) historical hurricane track database in a spatial and temporal analysis to evaluate inundation risk and impacts on a regional basis in the Caribbean. The inundation analysis is combined with coastal population and food production spatial data to define probable historic impacts. Further work will evaluate increasing vulnerabilities in the Caribbean under a range of climate change scenarios.

Country population statistics at a territorial administrative level are classified using a standardized category subdivision and normalized based on calculated square kilometer values within the study area. The 2008 Food and Agriculture Organization (FAO) of the United Nations 0.0833 decimal degree (~9 km) land cover data provides the basis for assessing possible impacts on food production areas. Raster analysis of 30 m Aster digital elevation models (DEM) is used to estimate potential CCOIL plus storm surge flooding. Spatial analysis of the IBTrACS Wind Radii hurricane data from 2004 to 2011 is used to identify varying levels of historical impact zones from tropical cyclones. Results of the study will provide digital data defining impact zones and levels of vulnerability for populations to both displacement and loss of food production.

4.1 Introduction

Tropical cyclone wind and accompanying storm surge in the North Atlantic hurricane basin has the capability to inflict significant damage (Blake et al., 2011) to populations and food production regions. Coupling tropical cyclone impacts with rising global sea level (Claudia et al., 2012) enhances coastal population risks. The objective(s) of this study is to identify vulnerabilities of populations and food production locations in the Caribbean islands of the Bahamas, Cuba, Dominican Republic, Haiti, Jamaica,

and Puerto Rico to coastal inundation due to the net impacts of CCOIL & storm surges due to enhanced tropical cyclones. Steps in the analysis will be:

1. Adding 2-Dimensional width buffers around all hurricane strength storm tracks from 2004 – 2011 to identify locations where one or more hurricane strength storms have made contact with land (impact zone areas) in the Caribbean study area.
2. Utilizing Multiple Linear Regression (MLR) to extend the IBTrACS dataset back to 1979 to analyze a longer time period of hurricanes making contact with land locations.
3. Utilizing Geographic Information System software to create inundation maps from Digital Elevation Models (DEM). Creating GIS population maps to identify more densely populated locations.
4. Creating GIS land cover/land use maps to identify urban and food production locations.
5. Creating overlays of hurricane strength storm impact zone area, CCOIL, population density, and land cover/land use to identify locations most vulnerable.

4.1.1 Background

The IBTrACS (Knapp et al., 2010) database contains hurricane observation point data for all global hurricane basins since 1842, recorded in 6 hour increments along the storm track. A data record for each observation point containing numerous hurricane features (C. Landsea et al., 2012; Colin J McAdie, 2004) such as hurricane season, name, date/time in Universal Time Coordinate (UTC), sustained wind speed, central pressure, physical location in latitude/longitude, and wind radii data. Hurricane wind speed is the maximum circular velocity of the hurricane observation recorded to the nearest 5 kt. Minimum central pressure of the hurricane observation is the recorded to the nearest 1 millibar (mb). Central pressure data values exist in the North Atlantic (NA) IBTrACS dataset consistently starting in the 1979 hurricane season. Wind radii data (see Figure 4.1.1) are distance values recorded to the nearest 5 International Nautical Miles (nm) where hurricane wind speeds categorized into 34, 50, and 64 kt (or greater) are observed from the center of a hurricane. Wind radii are recorded for each of the four quadrants based on compass direction where the 0, 360° location points north with Quadrant 1 being the North East (NE) quadrant. The data value in each radii quadrant is the maximum observed distance where wind speeds for each category are observed. A storm must reach a minimum wind speed of 64 kt in order to be classified in the lowest

hurricane category that being category 1. The 64 kt wind radii data collection is available in the North Atlantic (NA) Ocean basin IBTRACS database starting in the 2004 hurricane year.

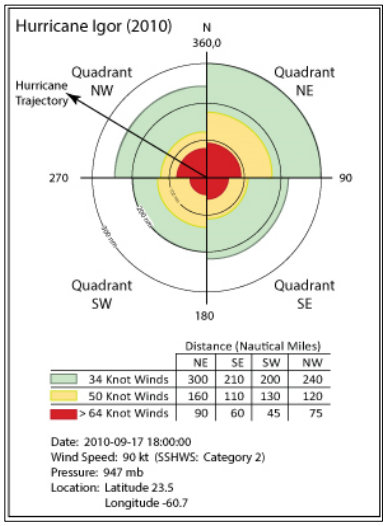

Figure 4.1.1: Hurricane Igor (2010). Hurricane Wind Speed, Pressure, and Wind Radii data for the 34 kt, 50 kt, and >64 kt distances from the center of the hurricane recorded for the 17-Sep-2010 at 6:00 p.m. UTC observation point. The Hurricane Trajectory is the forward direction of the storm.

SSHWS Strength	Wind Speed Knots	Wind Speed Metric & Imperial
Category 1	64 – 82	119 – 153 km/h 74 – 95 mph
Category 2	83 – 95	154 – 177 km/h 96 – 110 mph
Category 3	96 – 112	178 – 208 km/h 111 – 129 mph
Category 4	113 – 136	209 – 251 km/h 130 – 156 mph
Category 5	> 137	> 252 km/h > 157 mph

Table 4.1.1: Saffir-Simpson Hurricane Wind Scale. The scale used to categorize intense storms with circular wind speeds reaching a minimum of 64 knots.

GIS vector point and line shapefiles are available containing hurricane observation data from IBTrACS. Vector point shapefiles are specific physical locations where hurricane observation readings are recorded. Vector line segment data differs in that each hurricane observation reading has a physical start and end point and duration of 6 hours. The start point of each line segment record contains data for the current reading. The end point contains only the physical location of the observation point taken 6 hours later. Vector lines express the data in a continuous path for the life of the hurricane. Since a hurricane trajectory path varies greatly throughout its lifecycle, over time, it is possible for storm tracks to travel along similar paths causing locations to be hit by multiple hurricanes. A hurricane track impact path was created by adding a right and left width dimension to each hurricane line observation using 64 kt wind radii distance data. Geographic Information Systems (GIS) overlay analysis of storm track impact paths were used to create an impact zone overlay of the tracks for the study area identifying the frequency of hurricane "hit" counts as well as impacted size (km^2). Locations cannot be in more than one frequency hit count group. This means if a location was identified as being impacted by 2 hurricanes, it is only included in the "2"

frequency classification. The impact zone analysis allowed for the examination of locations where SSHWS (see Table 4.1.1) strength hurricanes were most frequent.

The 64 kt wind radii data exists in IBTrACS for 8 years of the analysis from 2004 - 2011. A method was required to extend the time period to investigate hurricane impact trends over a longer time frame. Statistical and modelling techniques used by hurricane prediction centers were examined to obtain an approach for estimating hurricane 64 kt wind radii size. Steed et al used a statistical approach with up to 28 independent variables to estimate wind radii (Steed, Swan, Jankun-Kelly, & Fitzpatrick, 2009). The "radii-CLIPER" model was developed to calculate hurricane path wind radii for 34, 50, and 64 kt wind radii using up to 60 predictors (Knaff et al., 2007). DeMaria compared the Statistical Hurricane Intensity Prediction Scheme (SHIPS) that uses a hurricane growth rate to the Logistic Growth Equation Model (LGEM) which uses a multiple linear regression model to estimate wind radii size (DeMaria, 2009). Holland et al estimated maximum wind radius using a mathematical vorticity model based on factors such as atmospheric density, hurricane wind speed, multiple atmospheric pressure values, physical location, and Sea Surface Temperature (SST) (Holland, Belanger, & Fritz, 2010). Another technique used to estimate hurricane wind radii data is from observational hurricane reconnaissance flight level data. Statistical regression and correlation methods are applied to collected hurricane wind speeds as well as to derive other influencing characteristics such as estimated central pressure, latitude, and SST. (Bell & Ray, 2004; Vickery & Wadhera, 2008). In this study, a statistical linear regression model based on $Y = b + \sum_{i=1}^{n} b_i x_i$ (where Y is the dependent variable, X_i is the i^{th} predictor variable, n is the total number of predictor variables, and b is a constant) was created using the 2004 – 2011 IBTrACS GIS vector line segment data (as described in Section 4.3.1). The statistical model was used to derive the 64 kt wind radii right and left width dimensions extending the time period for the 1979 – 2003 hurricane tracks.

DEM modelling was used to identify low areas susceptible to potential climate change ocean inundation level (CCOIL) and storm surge inundation. DEMs define terrain shape and therefore are dependent on the resolution (grid cell size) as well as elevation point increment values. Figure 4.1.2 shows a portion of a DEM raster located in the Bahamas with a resolution of 30 m X 30 m (900 m^2). It should be noted that

raster data can extend past a country boundary edge as it is not possible to use a partial raster grid cell. Elevation data values within each grid cell are calculated using the average or mean height value within the given cell. Flat terrain will have relatively the same elevation value throughout a grid cell whereas rugged terrain can have significantly different elevations. Since the elevation value used for any given grid cell is averaged throughout the cell, the larger the resolution, the less accurate the DEM will be. Raster grid cells covering a large ground area produce less accurate analysis and modelling (Kienzle, 2004; Poulter & Halpin, 2008) with respect to slope (steepness of terrain), aspect (direction the slope is facing), area (physical size), wetness (amount of water accumulation in the soil), and curvature of terrain. Depending on the type of terrain, using the smallest grid cell size possible will produce the most reliable results. The smallest available DEM resolution for this research study in Caribbean is 30 m.

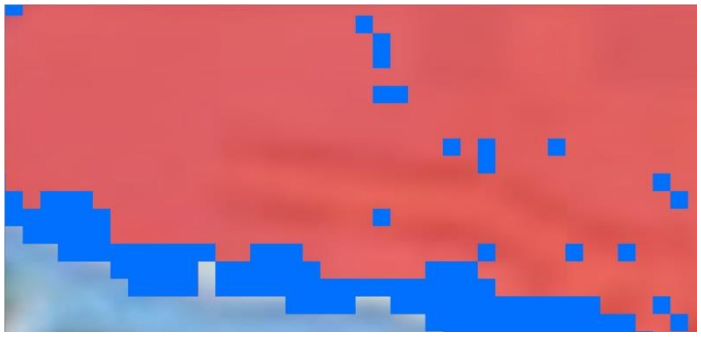

Figure 4.1.2: Raster 30m Grid Cell data. The image shows a small section of the Bahamas with potential CCOIL and storm surge inundation. Each square represents one 30 m X 30 m grid cell (900 m2).

The 2008 FAO (Nachtergaele, 2008) 5 arc minute or 0.0833 decimal degree grid cell size (~9 km) Land Cover/Land Use raster data was used to identify land designated for food production as well as populous locations in the study area. Although this resolution is quite coarse, generally large blocks of land are usually devoted to specific land use type areas such as urban or agricultural activities. As well, official population census data was categorized into standardized population densities for each country in the study area to locate population concentrations. GIS overlay analysis of urban and food production land, historical hurricane tracks, and potential CCOIL & storm surge inundation identified population and food production vulnerabilities in the Caribbean.

4.1.2 Study Area

This research study is located in the Caribbean, defined by the spatial extent of 17° N to 28° N latitude and -64° to -86° longitude, and includes the island countries of The Bahamas, Cuba, Dominican Republic, Haiti, Jamaica, and Puerto Rico (See Figure 4.1.3). Statistical information (see Table 4.1.2) is provided describing physical size of each country, physical size of each of 3 land types (see Figure 4.1.4), and population density. The land type classified as "Other" represents land designated to protected areas, forest, and wetlands. Population density is categorized using 5 standardized breakpoints for all countries.

Location	**Area (km^2) Total**	**Area (km^2) Urban**		**Area (km^2) Agriculture & Grazing**		**Area (km^2) Other**		**Census Population Density per km^2** Year	Population	Density
Bahamas	13,418	285	2%	2,511	19%	10,622	79%	2011	351,461	26
Cuba	111,025	9,654	9%	79,262	71%	22,109	20%	2002	11,177,743	101
Dom. Rep.	48,254	4,902	10%	34,141	71%	9,210	19%	2010	9,445,281	196
Haiti	27,158	538	2%	19,907	73%	6,713	25%	2003	7,929,048	292
Jamaica	11,035	2,521	23%	6,619	60%	1,895	17%	2001	2,607,631	236
Puerto Rico	8,999	6,040	67%	1,833	20%	1,125	13%	2010	3,725,789	414

Table 4.1.2: Study Area Statistics per Country. Total Area – the land size within the country. Land Cover/Land Use area broken into Urban, Agriculture & Grazing, and Other (remaining land use such as protected areas, forest, wetlands). Percentage values are calculated as land use area value / total country area. Population Density uses official Census data for the reported year.

The rationale for the selection of this study locale is:

- It is located in the Northern Hemisphere with hurricane tracks intersecting potential CCOIL & storm surge inundation
- Low coastal and inland elevations exist in most of the countries
- It is situated in the North Atlantic (NA) hurricane basin
- There are several densely populated centers
- Food production lands are diverse with large quantities devoted to agriculture and grazing activities
- Good quality data is availability for hurricane, digital elevation model (DEM), population, and land cover/land use analysis

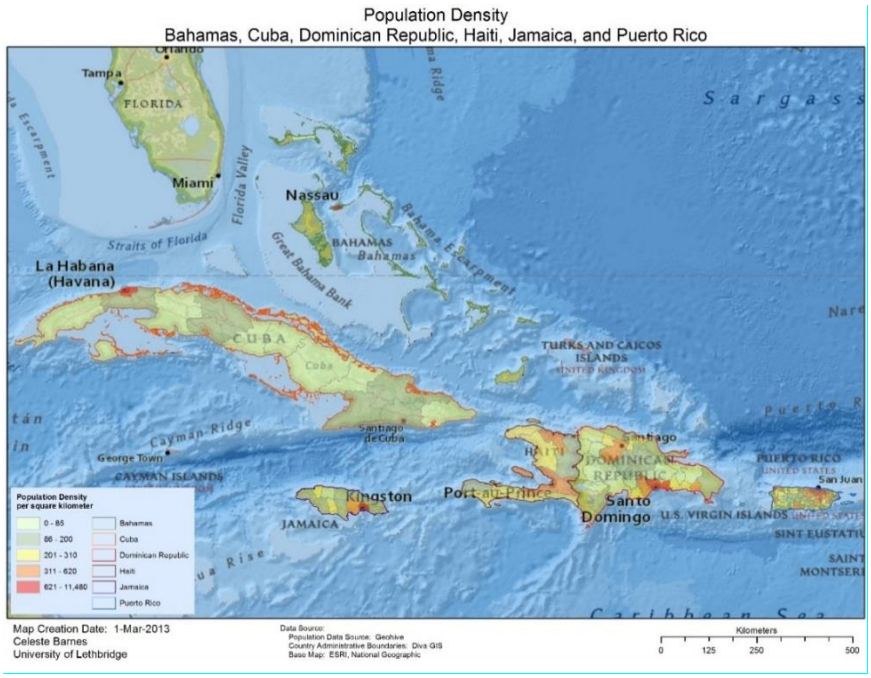

Figure 4.1.3: Population Density for The Bahamas, Cuba, Dominican Republic, Haiti, Jamaica, and Puerto Rico based on persons per square kilometer.

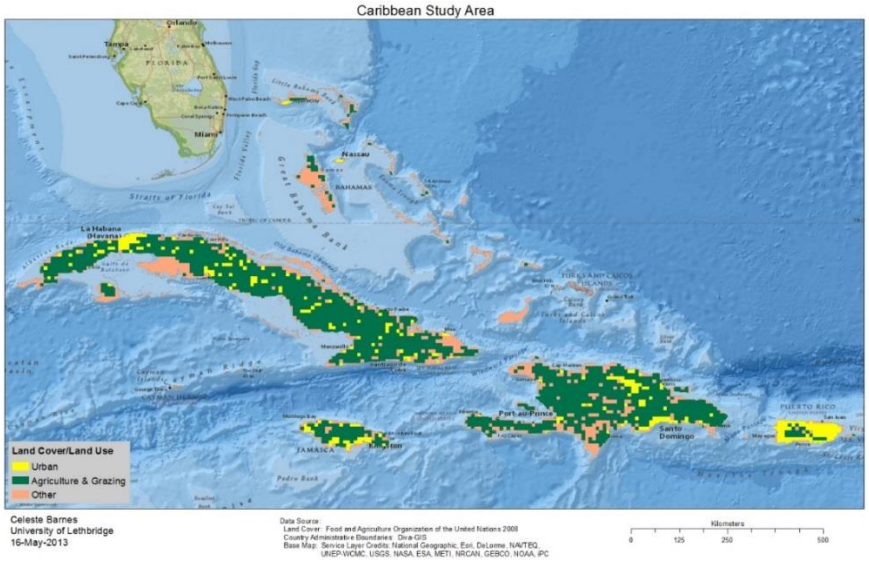

Figure 4.1.4: Land Cover/Land Use for the Bahamas, Cuba, Dominican Republic, Haiti, Jamaica, and Puerto Rico

4.2 Methods

Utilizing the 2004-2011 NA basin IBTrACS dataset, a 64 kt impact path was derived around each storm track using Geographic Information Systems (GIS) overlay analysis. Appendix B (IBTrACS data Multiple Linear Regression Analysis (MLR)) contains the methods and results to extend the 2004 – 2011 impact path data an additional 24 years. The resultant MLR dataset allowed for the creation of 64 kt impact paths

for all storms from 1979 – 2003; thus providing an expanded observed and derived time series from 1979-2011. Using a modified overlay analysis technique provided hurricane frequency hit count occurrences for 64 kt impact zones in all geographic regions. FAO Land cover/land use raster overlay analysis identified population centers and food production areas impacted by 64 kt storm paths including the corresponding frequency counts. DEM raster analysis of potential 5 and 10 m CCOIL & storm surge located inundation zones related to population densities.

4.2.1 Data

4.2.1.1 Geographical Information Systems (GIS) Base Data

ESRI ArcGIS version 10.0 SP 5 & 10.1 GIS software was used to complete this analysis. Microsoft Excel 2010 was used to calculate data variables as well as final results. The "Sphere Cylindrical Equal Area" map projection centered over the study area with the central meridian located at -74.83 and standard parallel at 22.5 was applied to the data. An equal area projection was used to minimize area calculation errors for population densities, land cover/land use, and hurricane impact zones. The linear unit was set to nautical mile since the IBTrACS database records hurricane observation readings in this unit of measure. The map extent covers a distance north to south of ~1,000 km and east to west of ~2,200 km. The "National Geographic World Map" base map provided a means to visually identify at a global level each country within the study area (Geographic et al., 2011). Diva-GIS administrative polygon shapefiles at both the country and regional levels were used to constrain analysis to each boundary (Hijmans, 2009).

4.2.1.2 Combined Sea Level Rise (CCOIL) and Storm Surge Inundation

Combined CCOIL and storm surge inundation was modelled using Aster GDEM 30 m grid cell size (900 m^2) DEM data (Tachikawa et al., 2011a). Raster tile files are 1 arc-degree by 1 arc-degree and contain 1 meter increment elevation values in each grid cell. An accompanying error matrix per cell per tile is available; however, no Root Mean Square Error (RMSE) calculations were computed.

4.2.1.3 Population Density

Official population census data were obtained directly from each country's department of statistics for the Bahamas, Cuba, Dominican Republic, Haiti, Jamaica, and Puerto Rico (Geohive, 2001, 2003, 2010;

Informacion, 2002; Mackey et al., 2012; Tactuk et al., 2010). Population statistics were assembled corresponding to administrative area subdivision boundaries for each country using Diva-GIS polygon data.

4.2.1.4 Land Cover/Land Use

The 2008 FAO land cover/ land use raster data was converted to vector format for easier data manipulation of the land classification data. The land cover/land use data contains 38 unique classification types. An additional data field was added to split the 38 land classes into three data types; Urban, Agriculture & Grazing, and Other. The "Agriculture & Grazing" type contains all land cover/land use locations either heavily or partially allocated to food production consisting of "Agriculture - large scale Irrigation" to "Sparsely vegetated areas - with low livestock density". The "Other" type contains land and water areas marked as protected or unmanaged as well as "No Data" available for the grid cell.

4.2.1.5 Hurricane Strength Track Impact Zones using 64 knot Wind Radii

The GIS vector line segment data from the IBTrACS NA basin subset was used for this analysis. The data fields utilized are Season (hurricane year), Name (hurricane name), ISO_time (date and hour in UTC format), WMO_WIND (10 minute sustained wind speed to nearest 5 kt), WMO_PRES (central pressure to nearest 1 mb), 64 kt wind radii to nearest 5 nm data variables ATC_w64_r1 (NE Quadrant 0 - 90° on a compass), ATC_w64_r2 (SE Quadrant 90 - 180°), ATC_w64_r3 (SW Quadrant 180 - 270°), and ATC_w64_r4 (NW Quadrant 270 - 360°).

4.2.1.6 Hurricane Strength Storm Impact Zone Analysis Computed Data Variables

SSHWS hurricane tracks were used in this analysis beginning with the 2004 season, to the end of 2011. IBTrACS contain data for the life cycle of a storm track, as well as including those not reaching SSHWS category 1 intensity. Storm tracks below category 1 were removed from the analysis, as those observations do not have 64 kt wind radii data. To reduce the dataset to a more manageable size, a new data file was created selecting only GIS vector line data from IBTrACS for the 2004 - 2011 time period where storms reached a minimum of category 1.

Hurricane trajectory was required to locate the right and left width dimensions for each observation. Using the 64 kt wind radii data, the right side width value was obtained from the 64 kt wind radii value one

quadrant to the right of the quadrant where the hurricane trajectory is located as shown in Figure 4.1.1. The left side value was taken one quadrant to the left of the trajectory. Data variables required to compute the trajectory, right, and left width dimensions were computed in both ArcGIS and Microsoft Excel. Each hurricane observation point was assigned an identification number to allow for data interchange between the software packages.

The first analysis requirement was to calculate the hurricane trajectory (NORTH_0_360) using the latitude and longitude coordinates for both the start and end position of the ArcGIS vector line. The latitude start coordinates (X_START, Y_START) as well as the end coordinates (X_END, Y_END) were calculated using built-in ArcGIS functions. All hurricane characteristics for a given vector line record are associated with the start latitude/longitude position. The end coordinates were only used to calculate the trajectory of the line segment. The ArcGIS data table was exported as a dbase (dbf) format for import into Microsoft excel in order to calculate the vector line segment trajectory, right and left width dimension data variables.

The forward hurricane trajectory path (NORTH_0_360 – see Appendix A: Program Block 1) is calculated based on the 360 degree angular direction of travel where the 0°, 360° mark points north on compass. The calculation is based on the line segment *x*,*y* start position being placed at the origin (0, 0) of a Cartesian plane. The difference is computed in both the latitude and longitude direction to obtain the quadrant of the end point. An intermediary angle is calculated for the line segment followed by the final trajectory.

The right width dimension (RIGHT_DIMENSION – see Appendix A: Program Block 2) is obtained from the 64 kt wind radii (ATC_w64_r?) distance variable located one quadrant to the right of the hurricane line segment trajectory. Using the "QUAD" variable (see Program Block 1) in the NORTH_0_360 trajectory computation, calculate the right quadrant located one to the right of the hurricane trajectory quadrant.

The left width dimension (LEFT_DIMENSION – see Appendix A: Program Block 3) is obtained from the 64 kt wind radii (ATC_w64_r?) distance variable located one quadrant to the left of the hurricane line

segment trajectory. Using the "QUAD" variable in the trajectory computation, calculate the left quadrant located one to the left of the hurricane trajectory quadrant.

The hurricane observation data containing the new variables for trajectory (NORTH_0_360), right dimension (RIGHT_DIMENSION), and left dimension (LEFT_DIMENSION) are imported back into ArcGIS using the hurricane observation number as the matching field.

The IBTrACS database contains storm records for both SSHWS and non-SSHWS category levels. SSHWS_MAX is used as a filter to separate and remove storms not reaching a minimum of Category 1 wind speeds. An excel pivot table was created listing each storm track with the corresponding highest SSHWS value reached during its lifecycle. Each hurricane observation in the dataset was assigned its corresponding SSHWS_MAX storm track value. All storms with a zero SSHWS_MAX value were removed from the analysis.

4.2.2 Analysis and Modelling Method

4.2.2.1 Impact Zone Analysis for NA IBTrACS data

The 6 hour GIS vector line data in IBTrACS contains observation readings that form a path of travel for all recorded storms. In the 2004 hurricane season, a width dimension in the form of 64 kt wind radii was added to the latitude/longitude position of each reading. Using the computed right (RIGHT_DIMENSION) and left (LEFT_DIMENSION) variables, it was possible to create a width dimension for each SSHWS strength observation. Over time, storms traveling over the same physical paths impact the same land and ocean locations (see Figure 4.2.1). Since storms change intensity during their life cycle, portions of the path may go below hurricane SSHWS category levels. Therefore, only those storm line segments reaching a minimum of Category 1 are included in the analysis. Impact zones with frequency counts are identified for every location being hit by one or more hurricane strength storms.

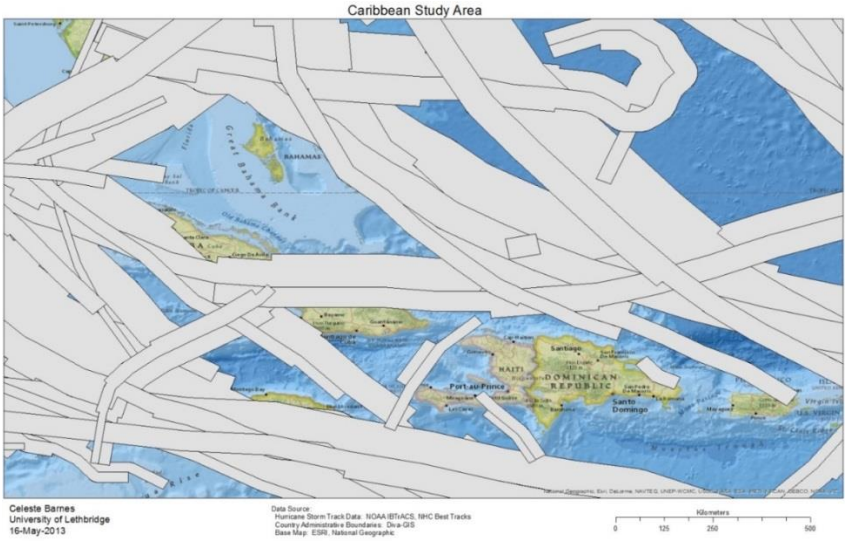

Figure 4.2.1: Hurricane Impact Zone Analysis. Hurricane storm tracks reaching a minimum of Category 1 status showing the right and left width dimension. Over time hurricane storm tracks overlap.

To identify locations impacted on a frequent basis by hurricane strength storms, the modified 2004-2011 IBTrACS NA dataset was utilized to derive 64 kt wind radii buffers around each storm track using a modified Esri ArcGIS "Spaghetti and Meatballs" GIS overlay technique (Honeycutt, 2012a, 2012b). A distance buffer was created for the right (RIGHT_DIMENSION) and left (LEFT_DIMENSION) with the "end point" set to "flat" and "dissolve fields" set to hurricane "season" and "name" to ensure a complete hurricane track path was created. Data observation 6 hours reading intervals caused an issue in the analysis. If the hurricane wind radii value changed to either a greater intensity or went below SSWHS category between successive intervals, the line buffer's path reflected an abrupt change in size instead of a gradual change. Since hurricane intensity for a given GIS vector line segment applies to the start point not the end point, using a flat end type for the buffer ensures the end distance buffer will not extend past the end of the line segment.

The final shapefile produced by the modified GIS technique contains polygons with a count of the number of hurricanes each physical location encountered. A unique identifier (FID_Overla) contains an identification number for each hurricane impact zone. GIS polygons with duplicate "FID_Overla" numbers indicate locations that were impacted by more than one hurricane strength storm. A second variable (Join_Count) contains the number of storms that impacted the same location (see Table 4.2.1). The

variable "IZONE_SQKM" (km^2) was added to the dataset. The ArcGIS built-in geometry calculator computed the hurricane impact area. Excel was used to ensure polygons with "Join_Count" values greater than 1 were only included once for the final area calculation per location.

Season	Name	FID_Overla	Join_Count	NAME_ENGLI	IZONE_SQKM
1992	ANDREW	9515	6	Bahamas	229.26
1995	ERIN	9515	6	Bahamas	229.26
1999	FLOYD	9515	6	Bahamas	229.26
2004	FRANCES	9515	6	Bahamas	229.26
2004	JEANNE	9515	6	Bahamas	229.26
2011	IRENE	9515	6	Bahamas	229.26

Table 4.2.1: Impact Zone Frequency Counts. The modified overlay analysis technique illustrates the same physical location impacted by 6 different hurricanes. Identical FID_Overla values indicate the physical land area was impacted by multiple hurricanes. The Join Count represents the number of hurricanes passing over the same location with IZONE_SQKM containing the physical area impacted in km^2.

The create right (RIGHT_DIMENSION) and left (LEFT_DIMENSION) variables to include the 1979 – 2003 time period, statistical linear regression analysis equations were used to extend the dataset. Using Honeycutt's modified "Spaghetti and Meatballs" overlay analysis technique developed for the 2004 – 2011 analysis two analyses were conducted on the 1979 – 2011 extended dataset. The first one created the "buffer dissolve fields" based on season and name. The second was SSHWS category strength, season, and name, which allowed for the identification of hurricane line segments to be broken into the 5 hurricane intensities.

4.2.2.2 2008 FAO Land Cover/Land Use Data

The 2008 FAO land cover/land use data exists in raster format with a spatial grid cell resolution of 5 arc minutes (~ 9 km). Since the area of each grid cell was quite large, the raster was converted into vector polygon format to aid in data manipulation. A land classification (LAND_CLASS) variable was added to the new shape file to simplify the number of land cover/land use types into three categories, those being "Agriculture & Grazing", "Urban", and "Other" (see Appendix D for data reclassification categories).

The "Impact Zone Frequency" shapefile had to be simplified before a GIS overlay could be completed with the land classification shapefile. A new "Simplified Impact Zone Frequency" shapefile was created by removing all duplicate polygons. The variable "FID_Overla" identified multiple hurricane frequency hit count polygons existing for each land location. The number of occurrences each location was impacted by

hurricanes is contained in the "Join_Count" variable. This method simplified the identification of land classes as well as impact zone area calculation as only one polygon existed for each physical location.

A GIS overlay of the simplified impact zone and land class shapefiles was then applied producing a new shapefile containing impact zone frequency per land class. A land class area (LUS_SQKM) variable was added to the shapefile and calculated using the ArcGIS built-in area calculator. The data was exported into Excel for final calculation of total impacted area per land class within each country in the study area.

4.2.2.3 Combined Sea Level Rise and Storm Surge Impacts on Population Density

Official population census data for the Bahamas, Cuba, Dominican Republic, Haiti, Jamaica, and Puerto Rico was used to calculated population density. The administrative region names in the census data did not consistently match the Diva-GIS shapefile polygon name data. Microsoft excel was used to match region names to enable population data (POP20XX – XX corresponding to census year) to be imported into ArcGIS. The variable SQKM (area in km^2) was added to the shapefile with the data value obtained from the ArcGIS built-in area calculator. Population densities for each country were classified using the same density subdivision values and normalized based on calculated square kilometer for the region.

Combined CCOIL & storm surge was modelled using 30 m grid cell size (900 m^2) Aster GDEM raster datasets. Tiles were obtained covering each country in the study area. Raster mosaics for each country were created and constrained to the country boundary using Diva-GIS country shapefiles (mask) to keep raster sizes as small as possible. This method decreased the computational time required to perform raster analysis in the study area. DEMs containing missing grid cell data values could not be factored into any of the area calculations.

The flooding methodology used in this study was based on a "bathtub" model where water "fills" an individual grid cell if it is less than or equal to the elevation value being calculated. "CCOIL value" rasters, 5 for each country in the study area, were created for each calculated inundation level starting at sea level (0 m) going up by increments of 5 m to a final level of 20 m. Combined CCOIL and storm surge inundation area was calculated for each country using CCOIL value rasters containing the total number of

inundated grid cells multiplied by 900 m^2 and converted to square kilometer. The percentage value was calculated from the total number of grid cells in the CCOIL value raster divided by the total number of grid cells in the country raster. CCOIL value raster files at different inundation levels were then displayed over population density to locate regions vulnerable to combined CCOIL and storm surge.

4.3 Results

The analysis of hurricane impact zones containing frequency hit counts, potential CCOIL & storm surge inundation of urban and agriculture & grazing land in the Caribbean study area was successfully completed. Results of this study increased the ability to identify population centers and food production regions more vulnerable to the effects of tropical cyclones and potential CCOIL & storm surge inundation. Appendix C (2004 – 2011 IBTrACS Data Analysis) contains results for the 2004 – 2011 time period.

4.3.1 Statistical Analysis Linear Regression Equations

This research utilizes the 64 kt wind radii data values from the IBTrACS NA basin. The 64 kt wind radii are distance values recorded in IBTrACS beginning in the 2004 hurricane season. The 64 kt wind radii is recorded for each of the 4 compass quadrants (0-90°, 91-180°, 181-270°, 271-360°); measured outward from the center of the hurricane eye extending to the point where wind speed intensity drops below SSHWS category 1. Statistical Multiple Linear Regression (MLR) was used to extend the 64 kt wind radii from 2004 back to 1979. Three MLR models were successfully run using the 2004 – 2011 IBTrACS NA 64 kt wind radii to acquire the right and left width dimensions for the hurricane strength storm track line segments. The first regression model was required to obtain the maximum 64 kt wind radii distance (Max_64) from the center point of each hurricane strength storm observation. This value was then used as an input to calculate the right and left width dimensions. The intermediary value, right, and left width dimensions were computed for each hurricane strength storm observation using the following set of equations: The linear regression output produced coefficients "B" for estimating 64 kt wind radii (see Appendix B: Table 9.3.2, Table 9.3.3, Table 9.3.4). The intermediary as well as final right and left width dimensions were computed for each hurricane observation using the following set of equations:

$$m = 788.124 + 0.824\gamma + 0.017\theta + 0.385v - 0.809p + 0.268s \quad (1)$$

$$RIGHT = 16.506 + -0.152\gamma + 0.004\theta + 0.024v - 0.016p + 0.052s + 0.978m \quad (2)$$

$$LEFT = 221.151 + 0.252\gamma - 0.009\theta - 0.370v - 0.223p + 0.092s + 0.372m \quad (3)$$

where:

m – maximum 64 kt distance of all four quadrants in the hurricane observation
γ – latitude of the hurricane observation point
θ – hurricane trajectory
v – hurricane forward velocity
p – central pressure
s – SSHWS observation time series number within the hurricane

(1) $R^2 = 0.714$, Standard Error = 14.2
(2) $R^2 = 0.984$, Standard Error = 3.4
(3) $R^2 = 0.773$, Standard Error = 8.2

To obtain more accurate historical wind radii distance values, it is desirable to use a well-developed hurricane statistical model in future analyses.

4.3.2 1979 – 2011 Hurricane Strength Storm Impact Zones

The relationships derived in section 4.3.1 are used to extend the analysis functionality of the 1979 – 2003 IBTrACS NA dataset. The older dataset was imported into excel to link to the 2004 – 2011 64 kt wind radii dataset. Equations 1, 2, and 3 derived from the statistical linear regression were used to calculate Max_64 (maximum 64 kt distance), RIGHT_DIMENSION, and LEFT_DIMENSION wind radii widths using hurricane observation computed data NORTH_0_360, HURR_FCAT_OBSER, wmo_pres, HR_VEL_KT_fine, Y_START_ROUND. The resulting 64 kt right and left widths were imported into ArcGIS. The modified GIS overlay analysis technique was run on the newly extended 1979 – 2011 64 kt wind radii dataset with the 2004 – 2011 data being unaltered. A right and left width buffer was created for each storm track containing SSHWS intensities (see Table 4.3.1 and Table 4.3.2). Although 33 hurricane tracks made landfall within the study area, Hurricanes Dennis, Rita, and Tomas did not contribute significantly to the impacted area. The 2008 hurricane season (see Table 4.3.2 and Figure 4.3.1) affected the largest area with 61,818 km^2 contacting land throughout the study area followed by 1998 with 61,052 km^2 then 1979 at 53,734 km^2. By splitting the 1979 – 2011 dataset into two time periods 1979 – 1995 and 1996 - 2011, storms that made landfall in the Caribbean study area experienced greater land impacts in the second time frame than the first.

1979 – 2011 Name	Season	Total Impact Area (km^2) *	Name	Season	Total Impact Area (km^2) *
ALLEN	1980	8,245	HUGO	1989	3,100
ANDREW	1992	3,426	IKE	2008	44,784
CHARLEY	2004	3,495	IRENE	2011	5,311
DAVID	1979	53,502	ISIDORE	2002	5,155
DEAN	2007	6,601	IVAN	2004	11,029
DENNIS	1999	25	JEANNE	2004	4,090
DENNIS	2005	32,331	KATE	1985	22,260
EMILY	1987	16,890	KATRINA	1981	394
ERIN	1995	2,482	LILI	1996	17,205
FLOYD	1999	2,823	LILI	2002	7,414
FRANCES	2004	4,714	MARILYN	1995	109
FREDERIC	1979	232	MICHELLE	2001	20,720
GEORGES	1998	61,052	PALOMA	2008	2,643
GILBERT	1988	11,000	RITA	2005	2
GUSTAV	2008	13,996	TOMAS	2010	1
HANNA	2008	429	WILMA	2005	1,937
HORTENSE	1996	1,304			

Table 4.3.1: 1979 – 2011 Hurricanes Intersecting the Study Area. Hurricanes impacting the Caribbean Study Area of The Bahamas, Cuba, Dominican Republic, Haiti, Jamaica, and Puerto Rico from 1979 – 2011. * Area calculation differences for the 2004 – 2011 time period are caused by rounding errors in ArcGIS field calculator (ESRI, 2010). 149 polygons exist in the 2004 – 2011 data set whereas there are 1,030 polygons in the 1979 – 2011 data set. The differences in area size between the 2 data sets are within 1%.

Hurricane Season	Total Impact Area (km^2)	Hurricane Season	Total Impact Area (km^2)
1979	53,734	1998	61,052
1980	8,245	1999	2,848
1981	394	2001	20,720
1985	22,260	2002	12,569
1987	16,890	2004	23,328
1988	11,000	2005	34,270
1989	3,100	2007	6,601
1992	3,426	2008	61,852
1995	2,591	2010	1
1996	18,509	2011	5,311
		Total	**368,701**

Table 4.3.2: Hurricane Impacts per Season over the Study Area. Differences in area calculations for 2004 - 2011 are caused by rounding errors in the ArcGIS field calculator.

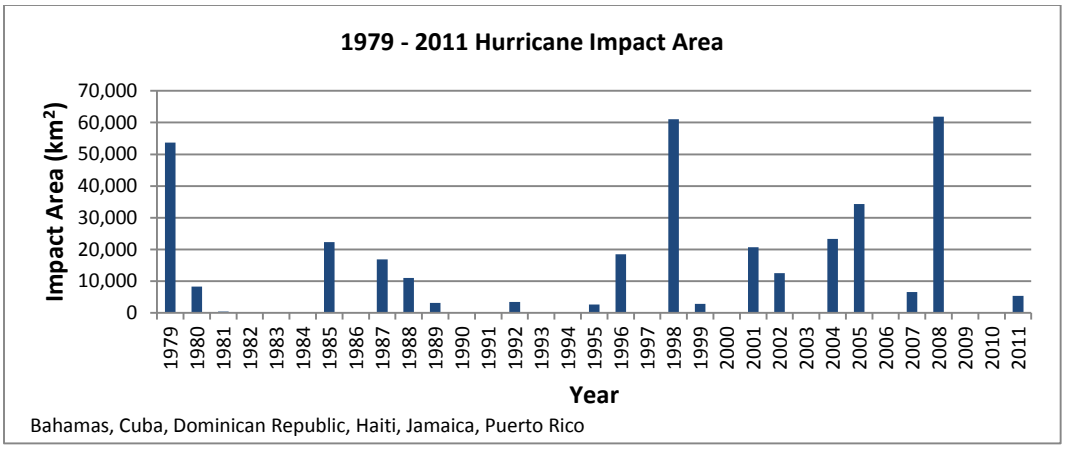

Figure 4.3.1: 1979 – 2011 Hurricane Land Area Impact per Season in the Study Area. The bar represents the total physical land area impacted by one or more hurricanes per season.

Examining both the NA basin and the Caribbean study area (see Figure 4.3.2), the total seasonal category level hurricane counts also shows a greater number of storms in the second time period than the first. This is partially due to the Atlantic Multi-decadal Oscillation (AMO) pattern in which small changes in sea surface temperature cycle over a 20 – 50 year time period. The AMO has the effect of changing hurricane storm intensity and duration (James P Kossin et al., 2010; Vimont & Kossin, 2007). This study did not examine the influence of AMO, only the physical land impacts.

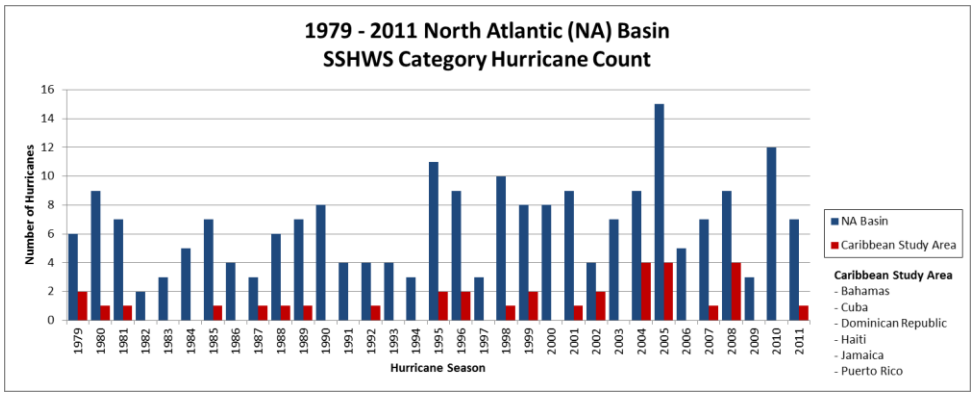

Figure 4.3.2 1979 – 2011 Hurricane Counts for the NA basin and Study Area. The left bar represents the total number of hurricanes per season in the NA basin. The right bar represents the total number of hurricanes intersecting with the Caribbean study area.

The modified GIS overlay analysis technique using the derived right and left 64 kt wind radii distances was run for the 1979 – 2011 hurricane dataset. Only two additional hurricane impact frequency counts appeared in the extended timeline although a significantly greater land area was hit. Figure 4.3.3 shows the study area with categorized impact frequency land locations. The only country in study area hit by 6

hurricanes was the Bahamas, which affected 13,260 km^2 (see Table 4.3.3). Cuba experienced a frequency of 5 storms impacting 180 km^2. Jamaica and Puerto Rico were also significantly impacted as 100 % of their total country land area was hit by hurricanes during the 1979 – 2011 time period.

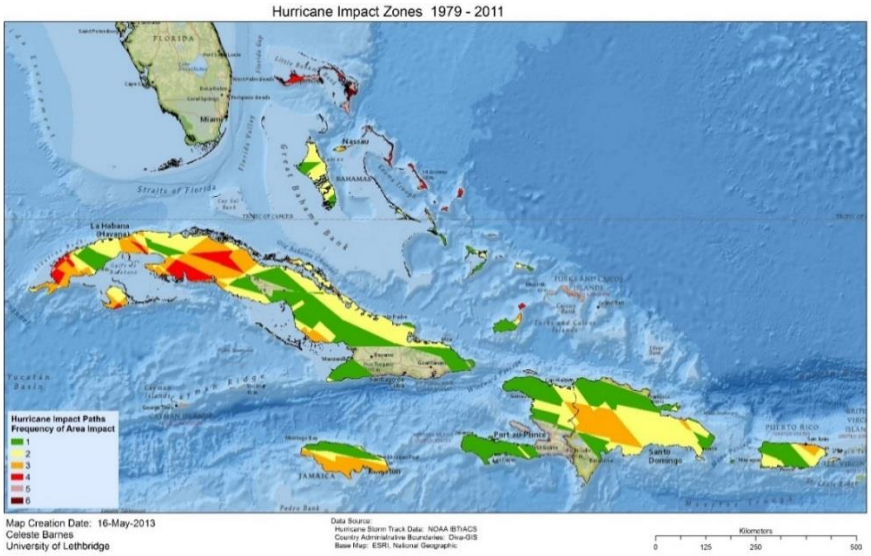

Figure 4.3.3: 1979 – 2011 Hurricane Impact Zones. Frequency of impact is a maximum of 6 occurrences in the same location.

Location 1979 – 2011	Country Area (km^2)	Area (km^2) 1	Area (km^2) 2	Area (km^2) 3	Area (km^2) 4	Area (km^2) 5	Area (km^2) 6	Area (km^2) Total	
Bahamas	13,418	3,753	5,242	536	1,822	1,351	558	13,260	99%
Cuba	111,025	31,684	34,339	19,773	7,750	180	0	93,721	84%
Dom. Rep.	48,254	13,286	18,491	9,710	0	0	0	41,484	86%
Haiti	27,158	14,693	5,021	541	0	0	0	20,253	75%
Jamaica	11,035	3,665	1,815	5,520	0	0	0	10,999	100%
Puerto Rico	8,999	4,567	3,462	940	1	0	0	8,968	100%

Table 4.3.3: 1979 – 2011 Total Impact Zone Area. The total area per country and per impact occurrence of hurricanes hitting the same location measured in square kilometers.

Over the course of a hurricane lifecycle, wind speeds change intensity (SSHWS_CATEGORY) fluctuating below category 1, to category 5. The size of the wind radii dimensions also expands and contracts. As well, hurricanes generally decay or decrease intensity over land (Kaplan & DeMaria, 1995). To examine hurricane intensities, a second impact zone overlay was completed based on hurricane category level. In this analysis right and left distance dimensions were created based on hurricane name, season, and SSHWS category. An interesting outcome from this GIS overlay was Jamaica only experienced category 3 and 4

storms (see Table 4.3.4) and Puerto Rico was only significantly impacted by category 1 to 3 hurricanes. The Dominican Republic experienced the greatest land area hit by category 5 storms.

Location 1979 - 2011	Country Area (km^2)	Area (km^2) Category 1	Area (km^2) Category 2	Area (km^2) Category 3	Area (km^2) Category 4	Area (km^2) Category 5
Bahamas	13,418	8,937	4,769	6,659	2,827	1,813
Cuba	111,025	44,841	49,038	35,350	45,184	5,030
Dom. Rep.	48,254	9,581	10,551	21,183	20,021	14,874
Haiti	27,158	8,652	0	8,176	2,883	6,047
Jamaica	11,035	0	0	11,000	7,335	0
Puerto Rico	8,999	2,136	8,970	2,931	170	0
Total Area	219,889	74,147	73,328	85,299	78,420	27,764

Table 4.3.4: 1979 - 2011 Total Impact Area by SSHWS Category. The total area per country based on the same SSHWS category level storm intensity hitting the same location.

4.3.3 Land Cover/Land Use Reclassification

The 2008 FAO land cover/land use data was reclassified into three new land classes those being urban, agriculture & grazing, and other land (see Appendix D: Table 11.1.1). Although the spatial resolution is quite course at ~ 9 km X 9 km, the data does provide land type information at a country level.

The physical land area for each of the three land classifications was calculated for each country (see Table 4.3.5). Cuba is the largest country in the study area at 111,025 km^2. It also has the largest land area in each of the three categories with urban at 9,654 km^2 (9% of its total country area), agriculture and grazing at 79,262 km^2 (71%), and other at 22,109 km^2 (20%). Puerto Rico has second highest urban land value of 6,040 km^2, covering 67% of the country. Haiti has 19,907 km^2 (73%) of its land area devoted to agriculture and grazing. The Bahamas and Haiti only have 2% of the land allocated to urban use.

Location	Area (km^2) Total	Area (km^2) Urban		Area (km^2) Agriculture & Grazing		Area (km^2) Other	
Bahamas	13,418	285	2%	2,511	19%	10,622	79%
Cuba	111,025	9,654	9%	79,262	71%	22,109	20%
Dom. Rep.	48,254	4,902	10%	34,141	71%	9,210	19%
Haiti	27,158	538	2%	19,907	73%	6,713	25%
Jamaica	11,035	2,521	23%	6,619	60%	1,895	17%
Puerto Rico	8,999	6,040	67%	1,833	20%	1,125	13%

Table 4.3.5: Land Classification Area per country. Country and classification area are calculated in km^2. The percentage values for each land classification type are based on the area in relation to the total country size.

4.3.4 1979 – 2011 Hurricane Strength Impact Zones on Land Cover/Land Use

An overlay of the 1979 – 2011 GIS hurricane impact zone shapefile was combined with the reclassified 2008 FAO land cover/land use data (see Figure 3.2.1). In the extended time period, the entire urban and agriculture & grazing land types located in the Bahamas, Jamaica, and Puerto Rico were completely impacted by one or more hurricanes (see Table 4.3.6). Urban land situated in Haiti was impacted least with only 266/538 km^2 (49%) affected by storms. Cuba and Dominican Republic are also significantly impacted by one or more hurricanes in their urban and agriculture & grazing areas.

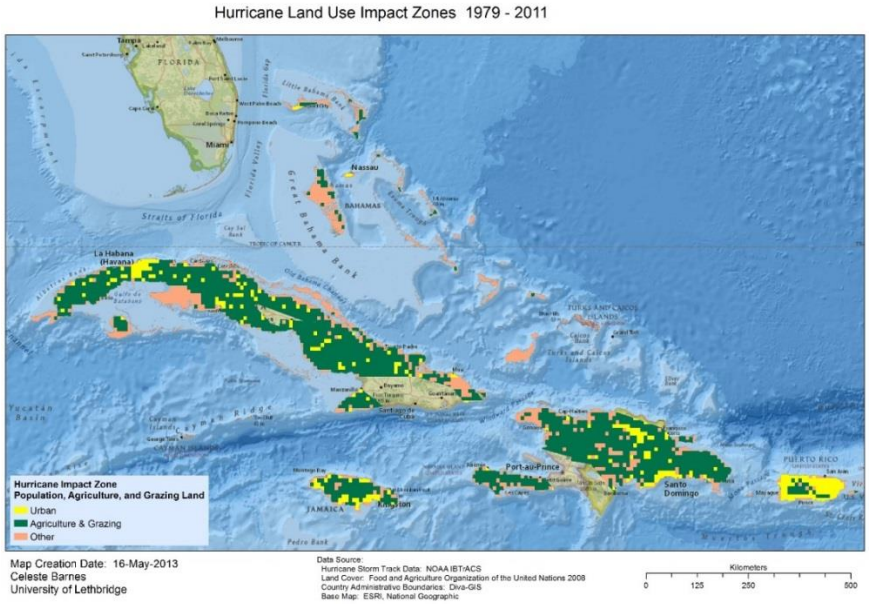

Figure 4.3.4 1979 - 2011 Land Classification Impact Zone - hurricane impact zones based on land cover/land use reclassification.

Location 1979 - 2011	Country Area (km^2)	Area (km^2) Urban		Area (km^2) Agriculture & Grazing		Area (km^2) Other		Area (km^2) Total Impact Zones	
Bahamas	13,418	285	100%	2,511	100%	10,496	99%	13,292	99%
Cuba	111,025	8,246	85%	65,908	83%	19,817	90%	93,971	85%
Dom. Rep.	48,254	4,749	97%	30,582	90%	6,282	68%	41,613	86%
Haiti	27,158	266	49%	15,233	77%	4,818	72%	20,316	75%
Jamaica	11,035	2,521	100%	6,619	100%	1,895	100%	11,035	100%
Puerto Rico	8,999	6,040	100%	1,833	100%	1,125	100%	8,999	100%

Table 4.3.6 1979 - 2011 Hurricane Impact Zones based on Land Classification. Country size and land reclassification are expressed in km^2. Percentage values of each land classification are based on land area for the class. Total impact zone percentage is based on country size.

The 1979 – 2011 hurricane frequency counts broken down by land type (see Table 4.3.7) shows the Bahamas was hit by 6 hurricanes impacting 210/2,511 km^2 (8%) of agriculture & grazing land. Cuba

experienced 5 hurricane impact zones however the amount of urban and agriculture & grazing land hit was minimal. Urban land in Jamaica (1,781/2,521 km^2 or 71%), Puerto Rico (663/6,040 km^2 or 11%), and Dominican Republic (430/4,902 km^2 or 9%) were hit by 3 hurricanes. Agriculture & grazing land in Jamaica (3,026/6,619 km^2 or 46%) and Dominican Republic (7,534/34,141 km^2 or 22%) were also hit by 3 hurricanes. Haiti was impacted the least with 2 hurricanes hitting the urban and agriculture & grazing land types.

1979 – 2011 Land Use	Area (km^2)	Area (km^2) 1		Area (km^2) 2		Area (km^2) 3		Area (km^2) 4		Area (km^2) 5		Area (km^2) 6	
Bahamas	13,418												
Urban	285	4	2%	45	16%	81	29%	77	27%	77	27%	0	0%
Ag & Grazing	2,511	187	7%	1,344	54%	32	1%	386	15%	352	14%	210	8%
Other	10,622	3,571	34%	3,865	36%	424	4%	1,362	13%	924	9%	350	3%
Cuba	111,025												
Urban	9,654	2,154	22%	3,131	32%	2,488	26%	465	5%	8	0%	0	0%
Ag & Grazing	79,262	26,288	33%	23,197	29%	12,114	15%	4,200	5%	110	0%	0	0%
Other	22,109	3,328	15%	8,101	37%	5,221	24%	3,105	14%	62	0%	0	0%
Dom. Rep.	48,254												
Urban	4,902	1,770	36%	2,550	52%	430	9%	0	0%	0	0%	0	0%
Ag & Grazing	34,141	9,229	27%	13,818	40%	7,534	22%	0	0%	0	0%	0	0%
Other	9,210	2,327	25%	2,180	24%	1,775	19%	0	0%	0	0%	0	0%
Haiti	27,158												
Urban	538	144	27%	122	23%	0	0%	0	0%	0	0%	0	0%
Ag & Grazing	19,907	10,479	53%	4,212	21%	542	3%	0	0%	0	0%	0	0%
Other	6,713	4,115	61%	702	10%	0	0%	0	0%	0	0%	0	0%
Jamaica	11,035												
Urban	2,521	586	23%	154	6%	1,781	71%	0	0%	0	0%	0	0%
Ag & Grazing	6,619	2,442	37%	1,151	17%	3,026	46%	0	0%	0	0%	0	0%
Other	1,895	649	34%	515	27%	731	39%	0	0%	0	0%	0	0%
Puerto Rico	8,999												
Urban	6,040	2,610	43%	2,766	46%	663	11%	1	0%	0	0%	0	0%
Ag & Grazing	1,833	1,479	81%	347	19%	7	0%	0	0%	0	0%	0	0%
Other	1,125	492	44%	360	32%	273	24%	0	0%	0	0%	0	0%

Table 4.3.7: 1979 - 2011 Hurricane Impact Zone Frequency and Land Classification Breakdown. Country size and land Classification totals are expressed in km^2. Percentage values of each land classification are based on land area for that class.

4.3.5 Population Density and Combined Sea Level Rise & Storm Surge

Census data at the territorial level for Bahamas, Cuba, Dominican Republic, Haiti, Jamaica, and Puerto Rico was used to calculate 5 standardized population density categories for the study area (see Figure 4.3.5). Combined CCOIL and storm surge was calculated using 30 m Aster DEM data with the 10 m level displayed overtop the ArcGIS population density shapefile.

Figure 4.3.5: Potential CCOIL & Storm Surge Impact on Population. Combined CCOIL and storm surge are displayed at 10 m. The standardized population densities for the Bahamas, Cuba, Dominican Republic, Haiti, Jamaica, and Puerto Rico are grouped into 5 categories for persons/km^2.

Results for each country of the 30 m Aster DEM raster mosaics were tabulated (see Table 4.3.8). The calculated country size (area in km^2) in the study area for the combined CCOIL and storm surge differs from the land classification areas due to differences between raster and vector data. Raster mosaics are square grids and can extend past the edge of the vector shapefile country boundaries. The area calculation for all countries in the study area differs by a maximum of 3%. Cuba has the largest land area affected by potential CCOIL and storm surge at both 5 m (4,015 km^2 or 3.5%) and 10 m (15,921 km^2 or 14%). The Bahamas experiences the highest percentage of inundation for the 5 m (2,099 km^2 or 15%) and 10 m (7,041 km^2 or 51%) levels. Dominican Republic, Haiti, Jamaica, and Puerto Rico have a relatively modest impact in both 5 and 10 m analyses.

Location	**Area (km^2)**	**Area (km^2) 5 m CCOIL**		**Area (km^2) 10 m CCOIL**	
Bahamas	13,886	2,099	15 %	7,041	51 %
Cuba	112,682	4,015	3.5 %	15,921	14 %
Dom. Rep.	48,115	380	1 %	1,513	3 %
Haiti	27,088	235	1 %	1,154	4 %
Jamaica	10,955	77	1 %	382	3.5 %
Puerto Rico	8,937	118	1 %	452	5 %

Table 4.3.8: Potential CCOIL & Storm Surge. Area calculations for this analysis are based on raster grid data. Reported total country area differs by a maximum of 3% from vector data.

The Caribbean study area contains land territories varying from "very sparse" to "densely populated". Table 4.3.9 shows population density statistics for the regions in the highest category of 621 - 11,480 persons/km^2. Population census collection dates vary between countries. The Jamaica census year is 2001, Cuba is 2002, and Haiti is 2003. The Bahamas, Dominican Republic, and Puerto Rico census year is 2010. Although there is a gap in census years, this is acceptable as density values for countries with earlier dates are well above the cut-off level for the highest population density category with the exception of Haiti. The largest population density in Haiti is in the region of Ouest, which covers over 5,000 km^2. A population increase of over 35,000 people would be required to move this region into the highest population density category. The Distrito Nacional region of the Dominican Republic has the largest population density in the study area. Puerto Rico has a significant number of highly populated regions.

Country	**Region**	**Population Density Persons /km^2**	**Census Year**	**Potential 10 m CCOIL and Storm Surge Impacts**
Dominican Republic	Distrito Nacional	11,466	2010	Some coastal flooding
Jamaica	Kingston	7,468	2001	Coastal flooding
Puerto Rico	San Juan	3,075	2010	Some inland flooding
Cuba	Ciudad de la Habana	2,689	2002	Coastal flooding and some inland flooding in the northeastern half
Puerto Rico	Cataño	2,161	2010	Some inland flooding
Dominican Republic	Santo Domingo	1,863	2010	Some coastal flooding and flooding along the central region
Puerto Rico	Bayamón	1,794	2010	
Puerto Rico	Toa Baja	1,452	2010	
Puerto Rico	Carolina	1,429	2010	Some inland flooding
Puerto Rico	Guaynabo	1,406	2010	Some inland flooding in the north
Puerto Rico	Trujillo Alto	1,335	2010	
Jamaica	Saint Andrew	1,270	2001	
Bahamas	New Providence	1,070	2010	Significant coastal and inland flooding
Puerto Rico	Toa Alta	1,041	2010	
Puerto Rico	Caguas	937	2010	
Puerto Rico	Aguadilla	641	2010	
Puerto Rico	Dorado	633	2010	
Haiti	Ouest	614	2003	Coastal flooding

Table 4.3.9: Population Density Statistics. Population density statistics based on the most densely populated regions in the Bahamas, Cuba, Dominican Republic, Haiti, Jamaica, and Puerto Rico as defined by the ArcGIS map grouping for 621 – 11,480 persons/km^2.

In the locations where highest population densities exist as identified in Table 4.3.9, New Providence, Bahamas is significantly impacted at the 10 m CCOIL and storm surge inundation level. Regions of Carolina, Cataño, Guaynao, and San Juan located in Puerto Rico will have some coastal and inland flooding. Locations that may be significantly inundated in Cuba are for the most part located in sparely populated areas although Ciudad de la Habana is susceptible to coastal and inland flooding.

4.3.6 Vulnerabilities to Tropical Cyclone and Sea Level Rise & Storm Surge

The GIS analysis results for the hurricane strength storm track impact paths with hit count frequencies and the CCOIL & storm surge inundation were overlaid on the population density and land type to identify vulnerabilities to population and food production for each country in the study area (see Table 4.3.10). Locations identified in the table are where hurricane hit counts are greatest within each country. The corresponding 5 m combined CCOIL & storm surge were reported using general categories for those sites. Utilizing land type classification for "Urban" and "Agriculture & Grazing" along with the population density for the corresponding areas allows for identification of vulnerabilities. The Bahamas and Cuba had the highest hurricane hit counts as well as potential inundation.

Country Region	Urban Population	Agriculture and Grazing	Hurricane Hit Counts	5 m CCOIL & Storm Surge Impacts
The Bahamas				
• North Eleuthera	Sparse	Minor Amount	6	Significant flooding
• Central Abaco	None	Minor Amount	6	Significant flooding
• North Abaco	Sparse	Minor Amount	6	Significant flooding
• East Grand Bahama	Sparse	Half the Region	5	Significant flooding
• West Grand Bahama	Medium urban center	Minor Amount	5	Significant flooding
Cuba				
• Pinar del Río	Small urban centers	Most of the Region	5, 4	Coastal & inland flooding
• Cienfuegos	Sparse	Minor Amount	4	Some coastal flooding
• Isla de la Juventud	Sparse	Half the Region	4	Inland flooding
• La Habana	Small urban centers	Most of the Region	4	Some coastal flooding
• Matanzas	Sparse	Half the Region	4	Significant flooding
• Villa Clara	Sparse	Most of the Region	4	Some coastal flooding
Dominican Republic				
• San Cristóbal	Large urban center	Half the Region	3	Minor coastal flooding
• Santiago	Medium urban center	Most of the Region	3	No flooding
Haiti				
• Centre	Sparse	Most of the Region	3	No flooding
Jamaica				
• Clarendon	Medium urban center	Part of the Region	3	Coastal & inland flooding
• Kingston	Large urban center	Negligible Amount	3	Coastal & inland flooding
• Manchester	Medium urban center	Half the Region	3	Minor coastal flooding
• St. Andrew	Medium urban center	Part of the Region	3	Coastal & inland flooding
• St. Catherine	Medium urban center	Half the Region	3	Coastal & inland flooding
• St. Elizabeth	Sparse	Most of the Region	3	Minor coastal flooding
• St. Thomas	Sparse	Most of the Region	3	Minor coastal flooding
• Westmoreland	Medium urban center	Part of the Region	3	Minor coastal flooding
Puerto Rico				
• Carolina	Large urban center	Negligible Amount	3	Minor inland flooding
• Cataño	Large urban center	Negligible Amount	3	Minor inland flooding
• Culebra	Sparse	Negligible Amount	3	Minor coastal flooding
• Fajardo	Medium urban center	Negligible Amount	3	Minor coastal flooding
• Guaynabo	Large urban center	Negligible Amount	3	Minor inland flooding
• Loíza	Medium urban center	Negligible Amount	3	Minor inland flooding
• Luquillo	Medium urban center	Negligible Amount	3	Minor coastal flooding
• Río Grande	Medium urban center	Negligible Amount	3	Minor inland flooding
• San Juan	Large urban center	Negligible Amount	3	Minor inland flooding
• Toa Baja	Large urban center	Negligible Amount	3	Minor inland flooding
• Vieques	Sparse	Part of the Region	3	Minor coastal flooding

Table 4.3.10 Population and Food Production Vulnerabilities to Tropical Cyclone and Potential Combined CCOIL & Storm Surge

4.4 Discussion

Population and food production vulnerabilities in the Bahamas, Cuba, Dominican Republic, Haiti, Jamaica, and Puerto Rico to both tropical cyclone and potential CCOIL & storm surge were investigated in this study. IBTrACS GIS vector line segment data including 64 kt wind radii distances allowed for hurricane track right and left width dimensions to be computed. A deficiency exists in the data with regards to the 6-

hour time interval between hurricane observation readings. The GIS overlay analysis technique used in this study created a width around each hurricane track based on the data values applying to the start point of the vector line segment. Hurricanes travelling large distances and changing both intensity and size over a 6 hour period produced the effect of abrupt changes in both the hurricane track's direction and width. An improvement for future GIS modelling and research is to extrapolate the 6 hour data to a finer resolution. This will generate smoother hurricane storm paths as well as reduce large changes in wind radii dimension. Since this analysis is at the country level, the 6-hour data does provide information of where vulnerable locations exist.

The GIS frequency count impact zone overlay technique was successfully run for two time periods namely, 2004 – 2011 and 1979 - 2011. The output showed locations where hurricane impact path frequency hit counts are greatest in the study area. During the 8 hurricane seasons covering the time period of 2004 – 2011 (see Appendix C, Figure 10.2.1 and Table 10.1.2), the Bahamas and Cuba had the maximum impact in the study area at a frequency of 4 occurrences. When lengthening the period to 32 years covering seasons from 1979 – 2011 (see Figure 4.3.3 and Table 4.3.3), the frequency hit counts increased only by 2 for the Bahamas and one for Cuba. The Dominican Republic, Haiti, and Puerto Rico each experienced a relatively small area hit by hurricanes from 2004 – 2011 compared to a significant portion of each country being affected in the extended 1979 – 2011 time period. Jamaica experienced a significant amount of land area impacted by hurricanes during the time period of 2004-2011 with only one additional hit count in the 32 year time period.

In the extended 1979 – 2011 analysis time period, the regions of North Eleuthera, Central Abaco, and North Abaco situated in the northern region of the Bahamas were affected by 6 hurricane frequency hit counts. However, these locations are very sparsely populated with land type partially devoted to agriculture & grazing and the rest to other uses. The frequency count of 5 in the Bahamas covers the regions of East Grand Bahama of which approximately half is devoted to agriculture & grazing land and West Grand Bahama containing Freeport City. The 5 occurrences affecting Cuba are located in the western region of Pinar del Río region, which has mostly agriculture & grazing with some land devoted to smaller

urban centers and other land uses. The balance of the western portion of Cuba with regions Isla de la Juventud, La Habana, Matanzas, Cienfuegos, and Villa Clara were also hit by up to 4 hurricanes. For the most part, the land type is similar to that of the Pinar del Río region. Ciudad de la Habana which has a very dense population of 2,689 persons/km^2 is also located in this portion of the country although did not experience this hurricane frequency hit count.

Dominican Republic, Haiti, Jamaica, and Puerto Rico each experienced 3 hit counts. Land in the west central region of the Dominican Republic was affected by 3 hits comprising 7,534 km^2 of agriculture & grazing land and 430 km^2 of urban land. This location borders on the region of Centre, Haiti where the continuation of the affected area encompassed an additional 542 km^2 of agriculture & grazing land. In Puerto Rico 3 hurricane hits occurred in the northeastern tip of the country; a densely populated region containing the city of San Juan. In Jamaica, the southern half of the country consisting of mostly agriculture & grazing and urban land are impacted. The city of Kingston with a population density of 7, 468 persons/km^2 is in this zone.

A second GIS analysis was successfully run based on 1979 – 2011 SSHWS category data. The Bahamas, Cuba, and Dominican Republic experienced storms in all 5 hurricane category levels (see Table 4.3.4) with Haiti being hit with all intensities except for category 2. In Jamaica, only SSHWS category 3 and 4 hurricanes occurred. Puerto Rico was struck by category 1 through 3 as well as a very small land area off the eastern coast by category 4. The highly populated urban centers of New Providence located in the Bahamas, and Distrito Nacional & Santo Domingo, Dominican Republic were impacted by category 5 storms.

GIS raster analysis of potential inundation due to combined CCOIL & storm surge at a 10 m level has the potential to disturb the Bahamas with the highest percentage of inundation at 51% and Cuba at 14% of their respective country land areas. At the 5 m level, the Bahamas and Cuba are the only countries within the study area likely to be disturbed. At 5 m, the Bahamas is still affected by 15% inundation with a significant amount located in North Eleuthera, Central Abaco, North Abaco, East Grand Bahama, and West Grand

Bahama. The region of New Providence, which is the most densely populated centre (1,070 persons/km^2) in the Bahamas, contains portions of land both in the interior and along the coast where there is the potential for inundation to occur. In Cuba the location where a 5 m combined CCOIL & storm surge has the potential for largest inundation is Matanzas. The land type in this region is dedicated to roughly half for agriculture & grazing. Pinar del Río and Isla de la Juventud could also experience moderate inland inundation partially affecting agriculture & grazing land. There is also the possibility of considerable coastal inundation for the balance of Cuba.

The final step of combining the hurricane track impact path frequency counts with CCOIL & storm surge allows for identification of vulnerabilities to population and food production within the study area. Table 4.3.10 lists regions ordered by hurricane frequency count with corresponding level of inundation for each country. Sites in both the Bahamas and Cuba are at highest risk in the study area. In the Bahamas, a quantity of 6 hurricane hit counts affected North Eleuthera and North Abaco, which are also at risk to significant inundation. These two regions are both sparely populated and have limited agriculture & grazing. Populations and food production areas in East Grand Bahama and West Grand Bahama were hit by 5 hurricanes. These regions also have the potential for extensive flooding. In Cuba, the region of Pinar del Río has the potential for moderate inland flooding and was disturbed by 5 hurricanes. The countries of Dominican Republic, Haiti, Jamaica, and Puerto Rico were hit by 3 hurricanes and have minor amounts of coastal and inland flooding in these locations, making them the least vulnerable to the effects of tropical cyclones and CCOIL & storm surge inundation in the study area.

Global Warming Impact

Since 1972, hurricane data was collected and interpreted using a "Dvorak" technique to estimate intensity based on satellite imagery (C. W. Landsea et al., 2006). Meteorologists did not use standardized methods to read imagery and assign wind intensity values along the path of a hurricane, which resulted in inconsistencies in the recording process. A reanalysis of the 1978 – 1990 data estimated an additional 70 category 4 & 5 storms should have been recorded. Based on this historical data, statistical analysis may not accurately forecast future trends. Vimont and Kossin's study propose the AMO is influenced by climatic variability in NA basin and is strongly tied to Sea Surface Temperature (SST) (Vimont & Kossin, 2007).

With an increase in SST, it is possible for there to be an increase in AMO, which in turn will affect hurricane intensity and duration. Another method used to identify future hurricane trends is hurricane models. However, results differ depending on the model and setup, thus making it difficult to determine future trends (Knutson, McBride, et al., 2010). One study suggests hurricane frequency should be reduced while intensity should increase (K. Emanuel, 2011). Later work suggests both frequency and intensity will increase in the NA basin (K. A. Emanuel, 2013). Since there is still debate in regards to future hurricane trends, the IPCC's 2012 special report on "Managing the Risks of Extreme Events and Disasters to Advance Climate Change Adaptation" (Managing Risks) has a "low confidence" rating stating storm frequency will reduce and intensity will increase in some of the global hurricane basins (IPCC, 2012). GIS overlay techniques used in this study are dependent on the hurricane path trajectory. Under global warming conditions, the most vulnerable population and food production locations would still be at risk and will likely be dealing with greater intensity storms. Storm frequency changes in a warming climate are not well understood.

In the 2012 special report on Managing Risks, the IPCC indicates mean global sea level will continue to rise in the future. Since SLR varies from region to region throughout the globe, Church and White's study found the 1900 – 2009 rate of SLR was 1.7 – 3.2 mm per year (Church & White, 2011). Current storm surge wave heights also vary depending on location, tides, and sea floor topology (bathymetry). A study examining wave heights over a 30 year period using NOAA buoys (Komar & Allan, 2008) found hurricane category storms passing near the buoys generated waves above 3 m in height. Three buoys are located on the eastern US coast and 1 in the Gulf of Mexico. The most extreme waves observed from the Gulf of Mexico buoy during 1975 – 1990 were 8 m. From 1996 – 2005, the wave heights in the Gulf of Mexico increased to 11.6 m. The influence of global warming on combined CCOIL & storm surge would likely increase wave heights into the future. This study has identified locations within the study area susceptible to both a 5 and 10 m combined CCOIL & storm surge height. Under global warming, it is possible for this level of inundation to increase. GIS raster calculation at the 15 m elevation will identify a potentially larger area at risk to CCOIL and storm surge inundation.

4.5 Conclusion

This research study focused on identifying populations and food production regions susceptible to the effects of hurricanes including storm surge inundation and climate induced global sea level rise in the Caribbean. The countries of the Bahamas, Cuba, Dominican Republic, Haiti, Jamaica, and Puerto Rico were selected as preliminary results indicated this region located in the NA basin are potentially at risk. Tropical cyclone threat identification was developed with the use of the IBTrACS 64 kt wind radii dataset by defining a right and left distance buffer around each SSHWS hurricane storm track to identify impact zone frequency counts. Temporal analysis of two seasonal time periods, the first time period being 2004 – 2011 and the second 1979 – 2011, were completed. Since the 64 kt wind radii data is not tracked in IBTrACTS until 2004, multiple linear regressions were used to expand the dataset from 8 to 32 years. During the time period from 2004 – 2011, both the Bahamas and Cuba received the highest count of 4 hurricane impact hits in the study area. The affected land area in Cuba is however, significantly larger than that of the Bahamas. In the 1979 – 2011 extended data analysis, the Bahamas experienced the highest frequency of 6 hurricane impacts, while Cuba was struck by 5 occurrences. The Dominican Republic however, had the largest land area hit by Category 5 storms.

Aster GDEM raster data analysis of potential combined CCOIL and storm surge show the Bahamas and Cuba are most prone to 5 and 10 m coastal and inland inundation. Standardized population densities derived from official population census data as well as United Nations Food and Agriculture Organization land cover/ land use raster data were used to locate urban and food production areas. GIS overlay analysis identified potential coastal and inland flooding in the most populous locations in the study area. Although inundation is one factor used to identify regions at risk, further examination of these sites shows vulnerability to both tropical cyclones and potential CCOIL & storm surge is not as great in these locations. Sites dedicated to partial urban and agriculture & grazing lands in the Bahamas and Cuba are most vulnerable to tropical cyclones and combined CCOIL & storm surge particularly in East Grand Bahama, West Grand Bahama, and Pinar del Río, Cuba.

4.6 Future Research

The flooding method used in this study was a “Bathtub method” meaning each grid cell is set to the inundation value if it is at or below the calculated level. The effects of precipitation including land surface runoff and wave activity are not factored into any of the inundation calculations. Further examination of hydrological systems related to CCOIL & storm surge inundation and the effects on coastal regions is required.

5 North Atlantic Hurricane Basin Tropical Cyclone Track Convergence Patterns

Abstract

Disruption to populations and food production due to global climate change will be catastrophic in some regions. Among the most vulnerable regions are those impacted by tropical cyclones (TC). The objective of this research is to identify historical trends in TC tracks and regional circulation patterns that may indicate increasing risks due to TC intensification and/or frequency changes under global climate warming for the entire North Atlantic Hurricane basin. Spatial and temporal analysis is completed using the 1979 – 2011 International Best Track Archive for Climate Stewardship (IBTrACS) historical hurricane database. The data were divided into several subsets to allow analysis of trend in: (i) early (June/July/August/September - JJAS) and late (October/November/December - OND) seasonal trends; and (ii) multi-year intervals (1979-2011, 1979-1995, and 1996-2011 to differentiate possible long term trends. Geographical Information Systems (GIS) overlay analysis of the IBTrACS 64 knot hurricane wind radii data identified historical tropical cyclone track convergence in the North Atlantic (NA) basin. Results of the track convergence analysis provide a first order analysis for future research to identify potential population vulnerabilities due to changing seasonal or long-term tropical cyclone activity.

5.1 Introduction

This research is an extension of the storm track analysis methods developed in Barnes et al which included identifying coastal populations and food production vulnerabilities in the Caribbean at a potential increased risk from intensifying tropical cyclones (Barnes, Byrne, McDaniel, & Graham, 2013). The work used the IBTrACS historical hurricane database in a spatial and temporal analysis to evaluate risk and intensity changes on a regional basis in the Caribbean. Geographical Information Systems (GIS) spatial analysis of Saffir-Simpson Hurricane Wind Scale (SSHWS, see Table 5.1.1) category level storms obtained from IBTrACS utilized the 64 knot (kt) wind radii hurricane data from 2004 to 2011. Multiple linear regression analysis was used to extend the data to the time period of 1979 – 2011. The longer time series was used to identify varying levels of historical tropical cyclone SSHWS category level track location convergences. Results of the Barnes et al (2013) study provided hurricane strength storm impact zone frequency counts and levels of vulnerability for population displacement and loss of food production locations in the

Caribbean. Storm track analysis suggests that over time, hurricane track paths intersect one another and converge over the some locations in the Caribbean basin. Extending the analysis to the entire NA basin supports that contention.

This study applies spatial and temporal analysis to the 1979 – 2011 dataset for the entire North Atlantic (NA) hurricane basin. Results of GIS overlay analysis will be used in future work to identify tropical cyclone vulnerabilities in the NA basin where hurricane strength storm track convergence patterns have formed (see Figure 5.1.1). The greatest storm track frequency for the entire NA basin shows strong hurricane track convergence off the New England and Canadian Maritime coast. Historic tracking typically trends northeast across the Mid-Atlantic well offshore of the North American east coast. Hurricane Sandy was following this northeast path but was turned inland due to a high pressure-blocking ridge over Newfoundland and Greenland (see Figure 5.1.1). This ridge is suggested to be due in part to enhanced arctic ice melt during the summer of 2012 (Greene, Francis, & Monger, 2013). Greene et al suggest blocking patterns may increase in frequency in the fall due in part to global warming driven Arctic and Greenland ice melt. This poses a worrisome hypothesis. Will changing circulation patterns suggested by Greene et al force more of the storms that historically trended northeast offshore, to follow a path similar to Superstorm Sandy?

SSHWS Category	Intensity (knots)	Metric (km/h)	Imperial (mph)
1	64 – 82	119 – 153	74 – 95
2	83 – 95	154 – 177	96 – 110
3	96 – 112	178 – 208	111 – 129
4	113 – 136	209 – 251	130 – 156
5	>= 137	>= 252	>= 157

Table 5.1.1: Saffir-Simpson Hurricane Wind Scale.

Figure 5.1.1: 1979 – 2011 Hurricane Track Convergence Patterns with Hurricane Sandy's storm track. The Impact Frequency categorization shows the number of occurrences any given location was hit by hurricane strength storms during the June to December hurricane season.

5.2 Methods

This research utilizes the 64 kt wind radii data values from the International Best Track Archive for Climate Stewardship (IBTrACS) North Atlantic (NA) basin dataset (Knapp et al., 2010). The 64 kt wind radii are distance values recorded in IBTrACS beginning in the 2004 hurricane season. The 64 kt wind radii is recorded for each of the 4 compass quadrants (0-90°, 91-180°, 181-270°, 271-360°); measured outward from the center of the hurricane eye extending to the point where wind speed intensity drops below SSHWS category 1. Statistical Multiple Linear Regression (MLR) was used to extend the 64 kt wind radii from 2004 back to 1979. Three MLR models were successfully run using the 2004 – 2011 IBTrACS NA 64 kt wind radii to acquire the right and left width dimensions for the hurricane strength storm track line segments. The first regression model was required to obtain the maximum 64 kt wind radii distance

(Max_64) from the center point of each hurricane strength storm observation. This value was then used as an input to calculate the right and left width dimensions. The intermediary value, right, and left width dimensions were computed for each hurricane strength storm observation using the following set of equations:

$$m = 788.124 + 0.824\Upsilon + 0.017\theta + 0.385\nu - 0.809p + 0.268s \quad (1)$$

$$RIGHT = 16.506 + -0.152\Upsilon + 0.004\theta + 0.024\nu - 0.016p + 0.052s + 0.978m \quad (2)$$

$$LEFT = 221.151 + 0.252\Upsilon - 0.009\theta - 0.370\nu - 0.223p + 0.092s + 0.372m \quad (3)$$

where:

m – maximum 64 kt distance of all four quadrants in the hurricane observation

Υ – latitude of the hurricane observation point

θ – hurricane trajectory

ν – hurricane forward velocity

p – central pressure

s – SSHWS observation time series number within the hurricane

(1) $R2 = 0.714$, Standard Error = 14.2

(2) $R2 = 0.984$, Standard Error = 3.4

(3) $R2 = 0.773$, Standard Error = 8.2

Right and left distance buffers were added to each SSHWS category storm path. A modified Geographical Information Systems (GIS) overlay technique (Honeycutt, 2012a, 2012b) allowed for the creation of impact zone maps with frequency hit counts showing hurricane convergence patterns.

The modified IBTrACS NA dataset was analyzed in three time periods (analysis 1: 1979 – 2011; analysis 2: 1979 – 1995; and analysis 3: 1996 – 2011). The first analysis dataset 1979 – 2011 was split into four subsets to examine seasonal variability within the hurricane year (a) the entire hurricane season; (b) months of June, July, and August (JJA); (c) month of September; and (d) months of October, November, and December (OND). The second and third analysis datasets 1979 – 1995 and 1996 – 2011 focused on late

season activity when blocking highs in the North Atlantic potentially influence tropical cyclone trajectory, as was the case of Hurricane Sandy. The subsets were (e) 1979 – 1995 entire hurricane season, (f) 1996 - 2011 entire hurricane season, (g) 1979 – 1995 months of October, November, and December (OND), and (h) 1996 – 2011 months of OND. The modified GIS overlay technique was applied to each of the datasets to identify the location of hurricane track convergence patterns and potential population vulnerabilities to hurricane activity. Two standardized classification schemes were used to show hurricane strength storm impact concentration zones. The first classification was for dataset analysis of the entire season, JJA, and September. The classification for this set identified locations hit by hurricane strength storms using five separate categories with each of the group containing increments of three hit counts. To distinguish the change in concentration for the OND overlays, a second classification scheme was created that shows individual hurricane strength concentration hit count values. The colour scheme was also changed to distinguish this one from the first classification system.

5.3 Results and Discussion

Seasonal and annual trends of tropical cyclones were investigated using the modified dataset of Barnes et al (2013). Seasonal variability trends (for analysis 1) were examined by creating four GIS overlays from the 1979-2011 dataset; those being (a) the complete season shown in Figure 5.3.2-a; (b) June, July, and August (JJA) representing the early hurricane season shown in Figure 5.3.2-b; (c) the month of September shown in Figure 5.3.2-c; and (d) October, November, and December (OND) representing late season activity as shown in Figure 5.3.2-d.

The results of the overlay analysis of the NA basin for 1979 – 2011 full season presented in Figure 5.3.1-a suggests track impact frequencies are highly varied over the NA basin, but there are significant zones of concentration of storm tracks. The greatest concentration of storm tracks over the 33-year period formed on a line trending parallel to the east coast from New Jersey to Nova Scotia, approximately 400 to 600 km offshore. A substantial concentration extension of this track is notable all along the USA eastern seaboard. Another clearly discernable concentration track formed in the Mid-Atlantic roughly parallel to the North American coast approximately 1,200 to 1,300 km off shore. A smaller concentration was also present in the Gulf of Mexico roughly 350 km west of Florida and 400 km north of Cuba.

The GIS overlay for the early part of the season JJA in Figure 5.3.1-b shows smaller convergence zones with up to 5 track hit counts. In the Gulf of Mexico concentrations are 1) on the Louisiana coast near New Orleans, 2) just off the coast of the US/Mexico border as well as 3) approximately 350 km from the Florida coast. Another convergence zone exists approximately 100 km from the Bahamas. The last convergence zone near to land is present just off North Carolina coast. Smaller convergence zones also exist in the Mid-Atlantic.

A separate overlay (see Figure 5.3.2-c) for the month of September confirmed the volume of hurricane strength storm activity within this month was the most active within the season. The analysis shows up to 10 hurricane strength track convergence zones positioned from New Jersey to Nova Scotia with the largest concentration approximately 475 km off the Nova Scotia coast.

The last overlay in this series is for the months of OND as seen in Figure 5.3.2-d contains a much smaller set of convergence zone patterns with up to 5 hurricane track hit counts. Along the eastern seaboard, a larger concentration exists approximately 350 km off the coast of Nova Scotia with a smaller concentration approximately 350 km from the Carolinas to New Jersey. The highest number of hurricane track convergence frequency hit counts was located approximately 200 km southeast of the Yucatan Peninsula and 70 km north of Honduras. The highest frequency also is present in the Mid-Atlantic.

(a)

(b)

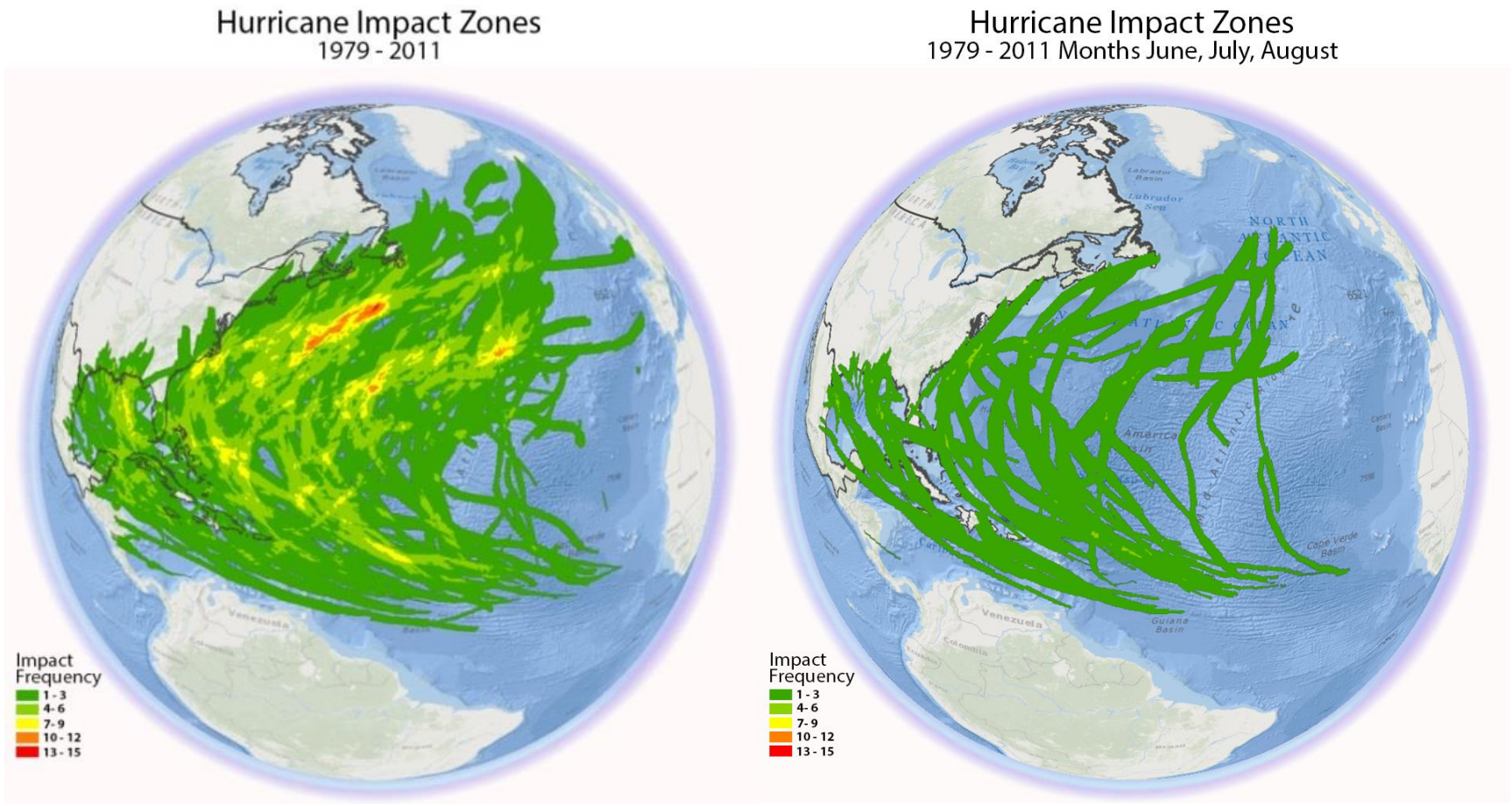

Figure 5.3.1: 1979 - 2011 Hurricane Convergence Zones. GIS overlay analysis convergences for (a) entire season, (b) JJA categorized in 5 groups of 3 hurricane strength storm impact frequency hit counts.

(c)

(d)

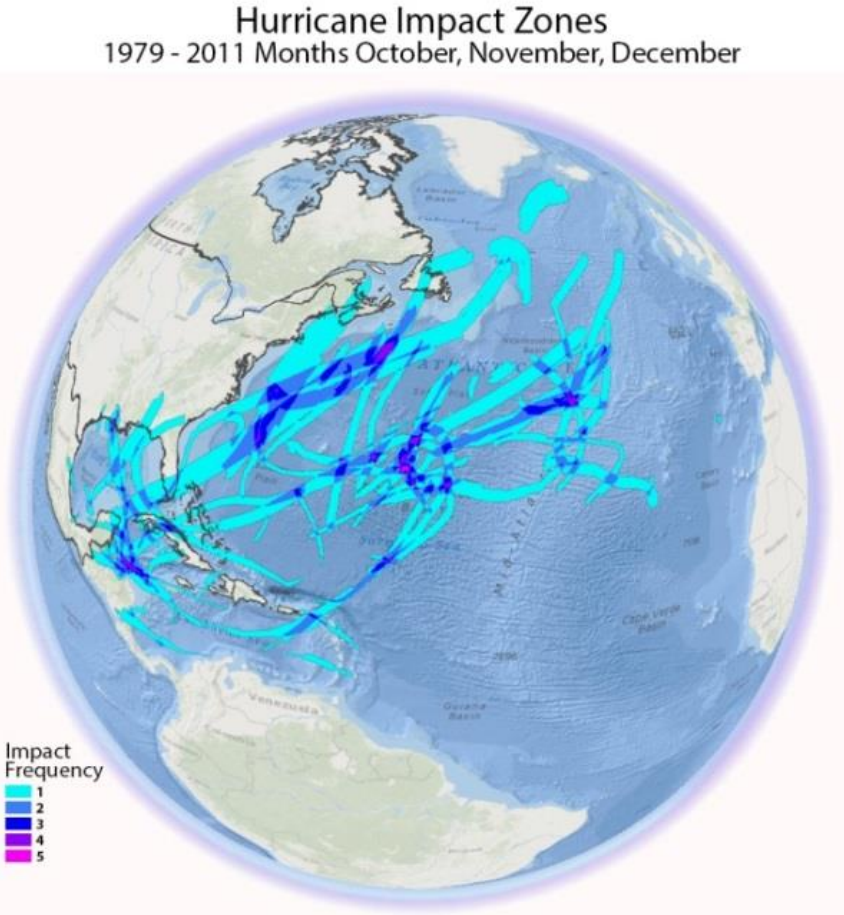

Figure 5.3.2: 1979 - 2011 Hurricane Convergence Zones. GIS overlay analysis displaying locations of hurricane strength storm track convergences for (c) September, and (d) OND. (c) is categorized in 5 groups of 3 hurricane strength storm impact frequency hit counts. The OND dataset (d) contains fewer hurricanes in the late season therefore the categorization is individual hit counts and a change in colour scheme in order to distinguish storm concentrations.

The second analysis was conducted to identify possible changes from the early to late parts of the hurricane season. The data set was divided into a 17-year early and 16-year later time span. Figure 5.3.3 shows yearly counts of total season (blue bars) and late season OND (October/November/ December red bars) hurricane strength storms for the NA basin. During 1979 – 1995, 93 SSHWS category level hurricanes occurred of which 24 were OND storms. From 1996 – 2011 the NA basin experienced a total of 125 storms where 29 were late season OND storms. This larger quantity of NA basin hurricane strength storms is due in part to the effect of the Atlantic Multi-decadal Oscillation (AMO) that influences increased and decreased hurricane activity cycles over a period of 20 to 50 years (James P Kossin et al., 2010; Vimont & Kossin, 2007). A linear trend line with its associated 95% confidence interval was computed for yearly storm count totals over time (see Equation 4). The chart shows an increasing trend in the number of SSHWS storms. However, the computed r^2 value of 0.13 is quite small therefore the trend of increasing hurricane strength storms over time is not conclusive.

$$y = 0.1126\,x - 218.1 \qquad (4)$$

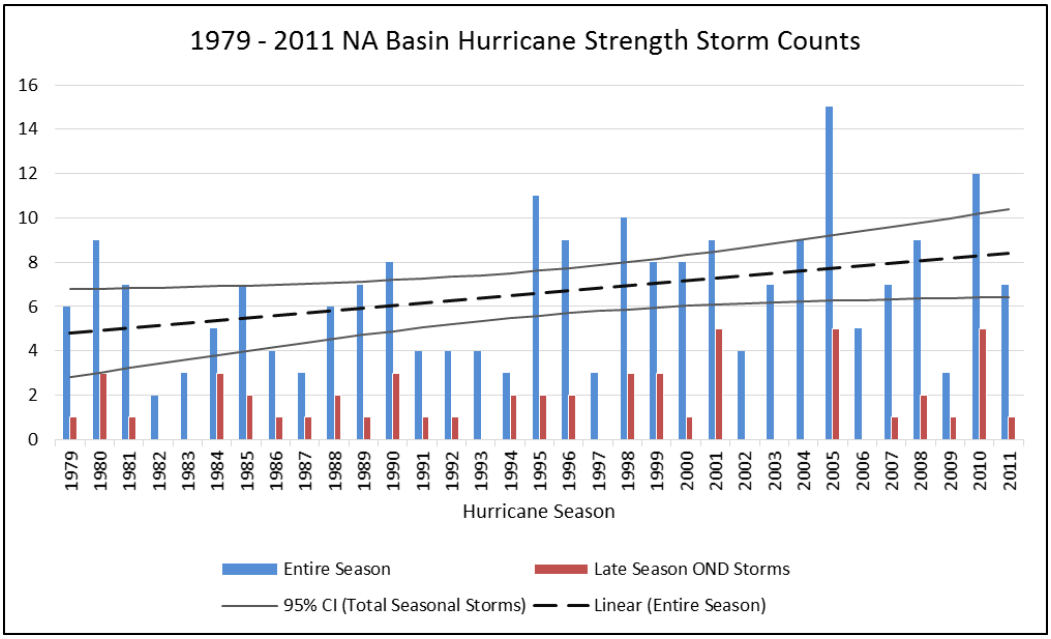

Figure 5.3.3: IBTrACS Hurricane Strength Storm Counts in the NA Basin from 1979 – 2011.

The GIS overlay technique was performed to create hurricane track impact zones for these two time periods as shown in Figure 5.3.4-e and f. During the 1979–1995 time period (Figure 5.3.4-e), a small convergence

zone positioned along the eastern seaboard located well off the New England coast intensified in the second time interval (Figure 5.3.4-f) and shifted northeast to settle off the coast of Nova Scotia. As well, two additional convergence zones emerged; one off the Carolinas coast and the other in the Caribbean Sea southeast of the Yucatan Peninsula.

(e)

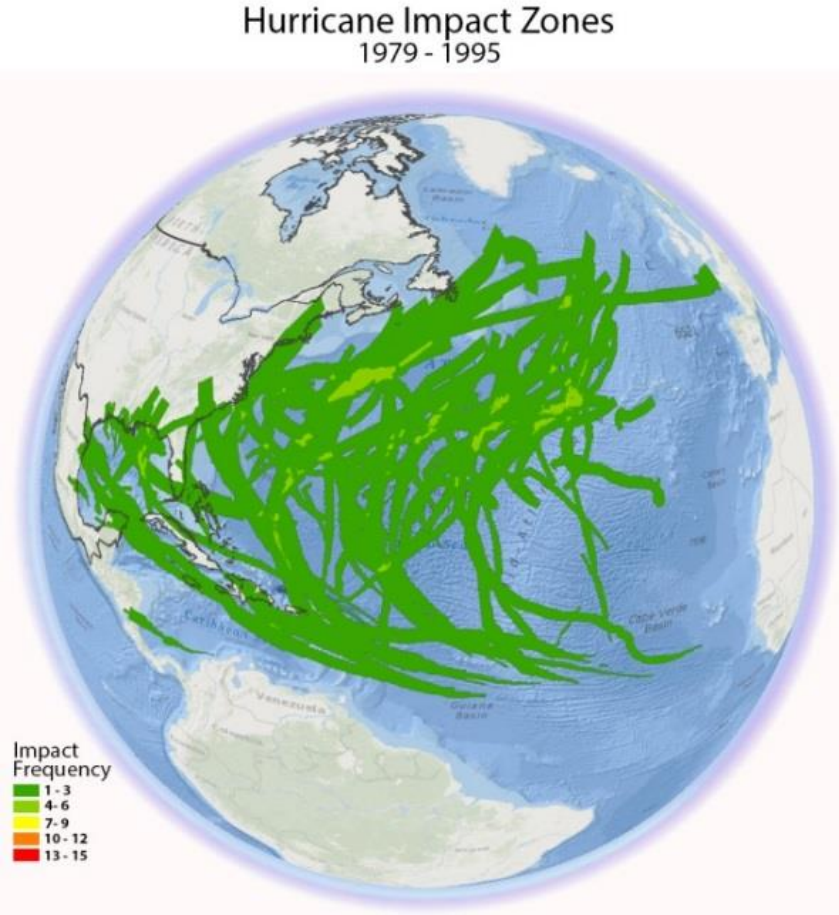

(f)

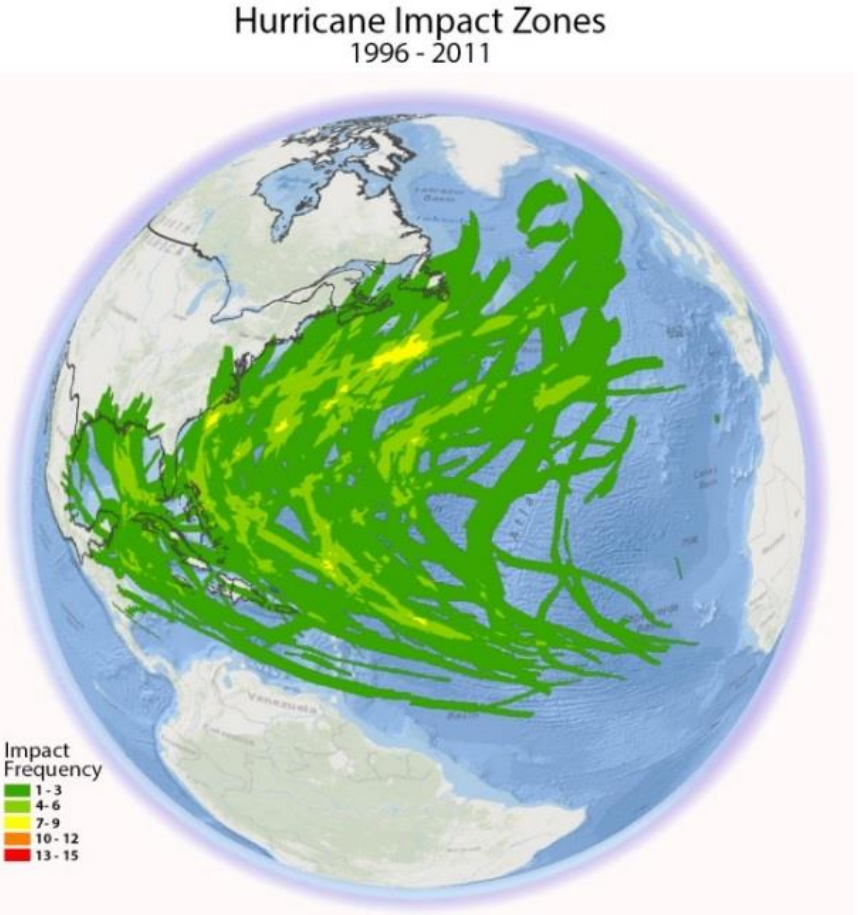

Figure 5.3.4: 1979 - 1995, 1996 - 2011 Hurricane Convergence Zones. GIS overlay analysis show concentrations of hurricane strength storm convergences for the entire. The dataset is split in two time periods. (e) the entire hurricane season for 1979 – 1995 and (f) the entire hurricane season for 1996 – 2011.

To investigate differences between the early and late seasons, the third GIS temporal analysis focused on OND data extracted for 1979 – 1995 and 1996 – 2011 as shown in Figure 5.3.5. The largest pattern of convergence for 1979 – 1995 was located in the Mid-Atlantic as seen in Figure 5.3.5-g. During the time period 1996 – 2011 time period (Figure 5.3.5-h), this concentration shifted westward toward the coast of Nova Scotia. Another convergence zone pattern emerged southeast of the Yucatan Peninsula.

Land locations impacted by hurricane strength storms in the 1979 – 1995 period (Figure 5.3.5-g) were situated in the southern portion of the NA basin in the Bahamas, Cuba, Nicaragua, the Yucatan Peninsula, and south-eastern US states situated off the Gulf of Mexico. In the later 1996 – 2011 time period (Figure 5.3.5-h) the formation of a hurricane track convergence pattern located southeast of the Yucatan Peninsula results in expanded land area being affected by SSHWS level storms. Belize, Guatemala, and Honduras were hit in Central America. Increased activity in the Caribbean affected the Bahamas, Cuba, and Haiti. Central Mexico, Louisiana, and Florida also experienced hurricane strength storm impacts. The convergence zone located off the coast of Nova Scotia contained hurricane tracks covering parts of the northern states of Maine and Rhode Island as well as the Canadian provinces of New Brunswick, Nova Scotia, and Newfoundland.

(g)

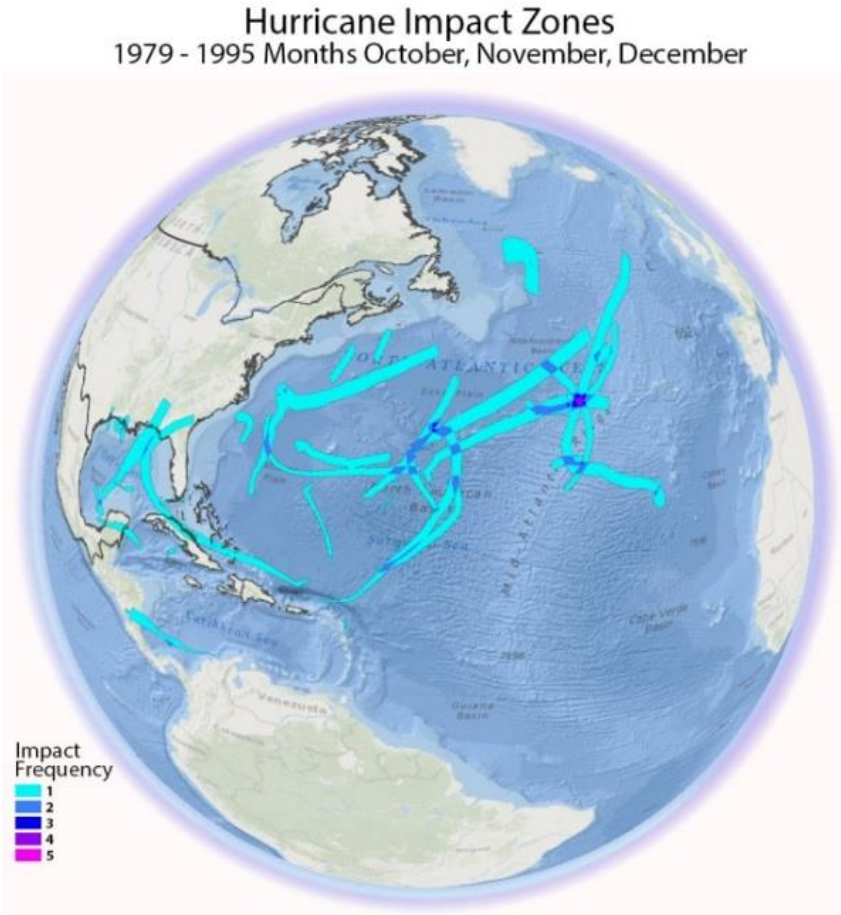

(h)

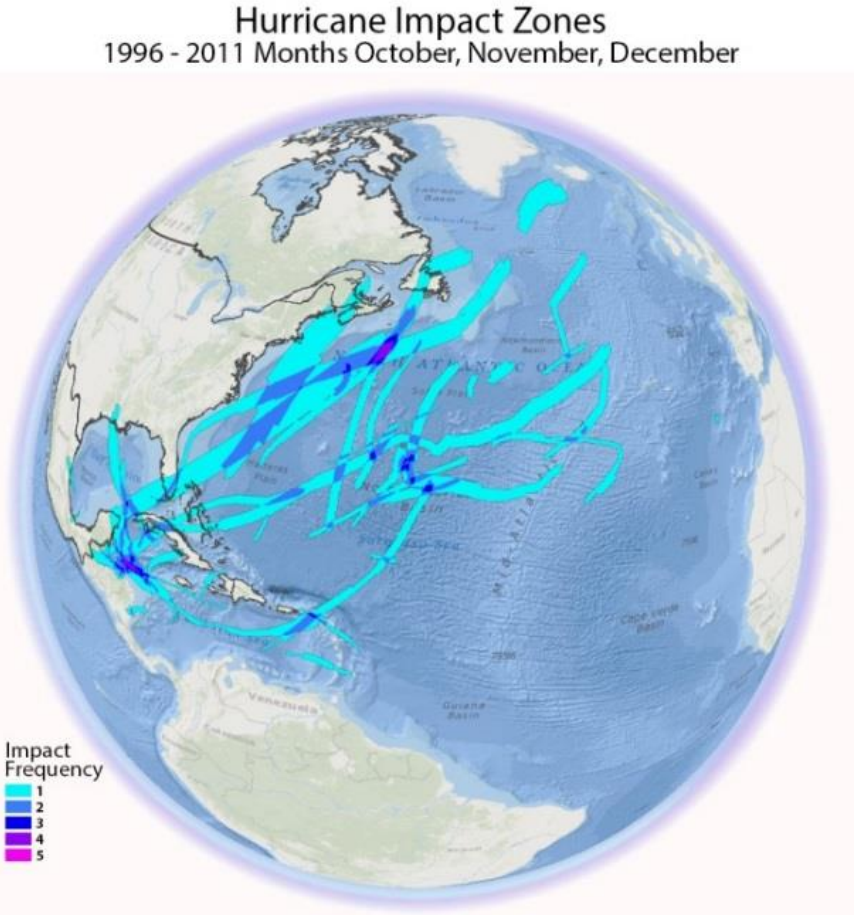

Figure 5.3.5: 1979 - 1995, 1996 - 2011 Hurricane Convergence Zones. GIS overlay analysis show convergences for the OND late hurricane season. The dataset is split in two time periods. (g) 1979 – 1995 and (h) 1996 – 2011.

The OND hurricane convergence overlays show storm tracks have moved westward and increased coverage from the Mid-Atlantic Ocean toward the Mid-Atlantic coast. Hurricane Sandy was a late season storm that diverted westward into the coast of New Jersey and New York (Blake et al., 2013) resulting in loss of life and significant infrastructure and property damage. Greene et al state this redirection was due to a blocking high over Greenland and Newfoundland that may have been related to the increased summer Arctic ice melt. Future blocking high formations similar to that of Sandy coupled with late season tropical cyclone activity have the potential to endanger the North American eastern seaboard. As well, there may be increasing vulnerability to late season OND tropical cyclones in the lower latitude regions of Central America, the Caribbean, and land locations off the Gulf of Mexico.

5.4 Conclusion

This research utilized the extended dataset from the Barnes (2013) study "Coastal Population Vulnerability to Sea Level Rise and Tropical Cyclone Intensification Under Global Warming" and expanded the study area to the entire North Atlantic hurricane basin. A temporal examination was conducted on all SSHWS category level storm paths to identify locations of converging hurricane strength storm track concentration patterns. Monthly inter-seasonal variability as well as annual trends were investigated by dividing the dataset into intervals from 1979-1995 and 1996-2011. Seasonal variability was examined by further sub-setting the data into the months of June/July/August (JJA), September, and October/November/December (OND). Convergence of hurricane track impact zones occurred in the Mid-Atlantic in all data subsets. During 1996 – 2011, two intensification patterns of hurricane strength storm concentrations along the eastern seaboard emerged with one off Nova Scotia and the other off the Carolinas coast. This pattern was also present when the 1996 – 2011 dataset was broken into seasonal JJAS and OND time intervals with the largest convergence occurring off the coast of Nova Scotia. In the 1996 – 2011 OND GIS overlay, a new convergence emerged southeast of the Yucatan Peninsula in the Caribbean Sea.

6 Summary and Recommendations

6.1 Summary

This research uses extensive GIS analysis to create a framework using limited course resolution datasets from the FAO, METI, and NOAA to provide a first order estimation to the impacts of tropical cyclone, and combined climate change ocean inundation level (CCOIL) & storm surge inundation in coastal locations. The first set of research focused on the countries of Bangladesh, the east coast of India, Jakarta, the Philippines, the east central coast of China, and the 26 Caribbean island countries. Tropical cyclone induced storm surge impacts coastal locations. Heavy precipitation and runoff is also typical in these intense storm events. However, meteorological, hydrological/hydraulic modelling was not completed in this thesis. A simple inundation model was used to identify low coastal and inland elevations of 5 m and 10 m above sea level for each country. Standardized population densities were calculated for each country to identify concentrations of people. These density maps were combined with the inundation maps to identify where more densely populated regions may be subjected to potential flooding. NOAA's IBTrACS hurricane storm track data for the North Atlantic, North Indian, and Western Pacific basins were categorized based on the Saffir-Simpson Hurricane Wind Speed scale to identify varying levels of storm tracks. Due to the excess quantity of missing data in the IBTrACS North Indian, and Western Pacific hurricane basin datasets, it was difficult to identify regions hit by intense storm events. IBTrACS for the North Atlantic hurricane basin contained the required data to identify countries located in the Caribbean that were hit on a frequent basis by hurricane strength storms. This allowed for the selection of a regional study to investigate tropical cyclone activity in the Caribbean.

The regional study was completed to investigate land locations in the Bahamas, Cuba, Dominican Republic, Haiti, Jamaica, and Puerto Rico hit by multiple hurricane strength storms. A minimum circular wind speed of 64 kt is required to classify a storm as hurricane strength. A 64 kt wind radii variable is available and obtained from the IBTrACS database. It was used to define hurricane strength storm impact zone frequency counts in the Caribbean and the extended NA basin. The 64 kt wind radii data collection began in 2004. Multiple linear regressions extended the time period from 2004 to back to 1979. This extended the dataset from 8 years of data to 33 years. Results from the Caribbean study showed the Bahamas and Cuba experience the highest frequency of hurricane impacts, however the Dominican

Republic had the largest land area hit by Category 5 storms. An overlay of the raster analysis of potential 5 and 10 m combined CCOIL and storm surge show the Bahamas and Cuba are most affected. Standardized population densities as well as land cover/land use were used to locate urban and food production areas. The results of this first order analysis also showed the Bahamas and Cuba have the potential to experience population vulnerabilities to tropical cyclones and combined CCOIL and storm surge. Global warming induced tropical cyclone storm surge is expected to increase inundation levels. As well, increased tropical cyclone intensity and frequency due to global warming will also continue to put coastal populations at risk impacts.

The temporal analysis of hurricane tracks showed convergence patterns emerged off the North American eastern seaboard in all three (1979 – 2011, 1979 – 1995, and 1979 – 2011) yearly datasets. Late season tropical cyclones have the potential to be especially dangerous as reduced Arctic sea ice causes changes in atmospheric blocking patterns in the north. During the months of October/November/December (OND), these blocking patterns can emerge off the Greenland and Nova Scotia coasts. Hurricanes that typically trend well offshore of the eastern seaboard have the potential to divert either over land was the case of Hurricane Sandy or out to sea. In the latter 1996 – 2011 OND time frame, convergence patterns shifted and were identified the coast of Nova Scotia and the Carolinas. The emergence of another convergence zone also appeared southeast of the Yucatan Peninsula in the Caribbean Sea. In the future, meteorological patterns similar to those present during hurricane Sandy coupled with late season tropical cyclone activity have the potential to endanger the North American eastern seaboard.

6.2 Recommendations for Future Research

This research developed a framework to obtain a first order estimation of locations susceptible to the effects of tropical cyclones. Results show increasing vulnerabilities in the North Atlantic hurricane basin.

The inundation modelling in this thesis did not consider any meteorological, hydrological, or hydraulic processes. Continued research in the Caribbean needs to take these processes into consideration. Investigation of the hydrological and hydraulic impacts of tropical cyclone storm surge, precipitation, and

runoff should continue for a limited coastal region. Several well developed flood mapping models exist. The Sea, Lake, and Overland Surge from Hurricanes (SLOSH) model was developed by the US National Weather Service and specifically used in the US to identify regions impacted by tropical cyclones. SLOSH does not factor precipitation or runoff into the inundation modelling. The GENESYS model developed at the University of Lethbridge is a physically based daily hydro meteorological model. Improved coastal and inland inundation modelling in the Caribbean can be completed with the use of the SLOSH and GENESYS models.

An improvement to the population and food production vulnerabilities in the Caribbean can be completed. Population vulnerability assessments to increasing risks of tropical cyclone and storm surge should focus on creating vulnerability and adaptive capacity indicators. Groups such as economic status, poverty, age, disability, and gender contain persons more at risk than others. Impoverished less developed countries are at higher risk and have fewer resources to recover from an extreme weather event. Building construction is usually substandard and can be completely destroyed during a tropical cyclone. An in-depth examination of evacuation and disaster recovery plans should be conducted to assess the ability of infrastructure to support transport and relocations during these events. Strong governmental infrastructure and social policies such as those in Cuba may be required to aid in the ability to cope with extreme events. Key performance indicators for factors such as disaster event mortality, infrastructure, and basic service survivability should be developed in order measure improvements in vulnerability and adaptive capacity to the effects of tropical cyclones.

Communication, outreach, and visualization of scientific data has the potential of being improved by using New Media software modelling methods. Recent improvements in computer graphic card (GPU) and video game engine technologies make possible real-time physics, volumes and fluids simulations. This shows considerable potential for simulating real-time simulations of tropical cyclone life cycles from development to dissipation and subsequent inundations. While these technologies still continue to be primarily associated with entertainment production, the adoption of modified gaming/graphics technologies, such as the NVIDIA Fermi by the Science community suggests that the potential for applying these high

performance computing technologies for non-entertainment data visualization purposes has considerable potential for real-time, interactive and visually-engaging scientific visualisation. (http://www.nvidia.ca/content/PDF/fermi_white_papers/NVIDIA_Fermi_Compute_Architecture_Whitepaper.pdf)

Communication and visual 3D modelling methods can be developed to disseminate population risks and vulnerabilities to the general public. A preliminary investigation using non-traditional 3D modelling and computer game engine software technologies was completed in 2011. The intent of the research was to reproduce portions of the Thrane, Ojika, and Berry (2002) MIT "Enhanced Environments: Large-Scale, Real-Time Ecosystems" study as described in section "2.5.2 3D Modelling". The investigation was to import high resolution terrain data into the Epic Unreal 3 (UE3) game engine to simulate the "real-world". High resolution 1 m City of Lethbridge GIS data (GIS, 2010) and 30 m Geobase (ASRD, 2008) Digital Elevation Model (DEM) topographic data were obtained for this study. To import the elevation data into UE3, data conversions were required. Data conversion software to import the 1 m City of Lethbridge data into the game engine was unavailable at the time of the study. The lower resolution 30 m Geobase dataset was imported in to UE3 with limited success. Two significant issues developed related to the representation of the terrain:

- Loss of elevation/height information for accurate scaling of the terrain in the "Z" direction.
- Loss of geographical map projection and orientation for accurate positioning of the terrain.

Research for methods to bring "real-world" topographic data into a game engine was unsuccessful and could only represent an approximation of the terrain. As a result, the continued investigation into the use of the Epic Unreal 3 game engine was discontinued due to the immaturity of the technology at the time. Another investigation of New Media visualization technology was conducted to model and simulate a tropical cyclone using the particle generator feature of Autodesk 3DS Max software. This technology showed promising results and could be pursued further.

With recent improvements in computer visualization hardware such as Fermi and computer gaming technologies, there now is potential to explore the use of New Media techniques for scientific visualization. Future research could be to use the Epic Unreal 4 game engine to create a "real-world" virtual environment

for individuals to role-play various socioeconomic individuals from an underprivileged third world country during a simulated sea-level rise and inundation event due to climate change. Policy structures and procedures would be incorporated into the simulated computer engine game environment with the intent for individuals to navigate through both the physical environment as well as policy and aid structures from the aftermath of a storm surge caused by a tropical cyclone. The simulation will also contain options to allow for (or not) settlement of environmental refugees to North America based on policy structure. Spatial extents in the game engine software are limited to a physical size of approximately 10 km by 10 km. The goal would be to deliver a realistic computer simulated environment based on real-world locational and environmental data to users with various levels of scientific understanding in an intuitive manner.

7 References

Albrecht, F., Wahl, T., Jensen, J., & Weisse, R. (2011). Determining sea level change in the German Bight. *Ocean Dynamics, 61*(12), 2037-2050. doi: 10.1007/s10236-011-0462-z

Alley, R. B., Clark, P. U., Huybrechts, P., & Joughin, I. (2005). Ice-sheet and sea-level changes. *Science, 310*(5747), 456-460.

Alley, R. B., & Joughin, I. (2012). Modeling ice-sheet flow. *Science, 336*(6081), 551-552.

Amarin, R. A., Jones, W. L., El-Nimri, S. F., Johnson, J. W., Ruf, C. S., Miller, T. L., & Uhlhorn, E. (2012). Hurricane Wind Speed Measurements in Rainy Conditions Using the Airborne Hurricane Imaging Radiometer (HIRAD). *Geoscience and Remote Sensing, IEEE Transactions on, 50*(1), 180-192. doi: 10.1109/tgrs.2011.2161637

Apollonio, F. I., Gaiani, M., & Benedetti, B. (2012). 3D reality-based artefact models for the management of archaeological sites using 3D Gis: a framework starting from the case study of the Pompeii Archaeological area. *Journal of Archaeological Science, 39*(5), 1271-1287. doi: 10.1016/j.jas.2011.12.034

Ash, J. N., Romanillos, J. L., & Trigg, M. (2009). Videogames, visuality and screens: reconstructing the Amazon in physical geographical knowledge. *Area, 41*(4), 464-474. doi: 10.1111/j.1475-4762.2009.00889.x

ASRD. (2008). *082H10, LETHBRIDGE*. Retrieved from: http://www.geobase.ca

Baker, J. L. (2011a). Jakarta Case Study Overview (I. B. f. R. and & D. T. W. Bank, Trans.) *Climate Change, Disaster Risk, and the Urban Poor - Cities Building Resilience for a Changing World* (pp. 16). Washington, DC: The World Bank.

Baker, J. L. (2011b). Summary - Climate Change, Disaster Risk, and the Urban Poor (I. B. f. R. and & D. T. W. Bank, Trans.) *Climate Change, Disaster Risk, and the Urban Poor - Cities Building Resilience for a Changing World* (pp. 33). Washington, DC: The World Bank.

Ball, B. (2006). Rebuilding Electrical infrastructure along the Gulf Coast: A Case Study. *The Bridge, 36*(Spring 2006), 6.

Barnes, C. C., Byrne, J. M., McDaniel, S. A., & Graham, J. R. C. (2013). *Coastal Population Vulnerability to Sea Level Rise and Tropical Cyclone Intensification Under Global Warming*. Paper presented at the 4th International Summit on Hurricanes and Climate Change, Kos, Greece. Poster retrieved from University of Lethbridge

Barros C.B., V., T.F. Stocker, D. Qin, D.J. Dokken, K.L. Ebi, M.D. Mastrandrea, . . . (eds.), P. M. M. (2012). Summary for Policymakers. In: Managing the Risks of Extreme Events and Disasters to Advance Climate Change Adaptation *A Special Report of Working Groups I and II of the Intergovernmental Panel on Climate Change* (pp. pp. 1-19). Cambridge, UK, and New York, NY, USA: IPCC.

Bell, K., & Ray, P. S. (2004). North Atlantic Hurricanes 1977–99: Surface Hurricane-Force Wind Radii. *Monthly Weather Review, 132*(5), 1167-1189. doi: 10.1175/1520-0493(2004)132<1167:nahshw>2.0.co;2

Bender, M. A., Knutson, T. R., Tuleya, R. E., Sirutis, J. J., Vecchi, G. A., Garner, S. T., & Held, I. M. (2010). Modeled Impact of Anthropogenic Warming on the Frequency of Intense Atlantic Hurricanes. *Science, 327*(5964), 454-458. doi: 10.1126/science.1180568

Bhuiyan, M. J. A. N., & Dutta, D. (2012). Assessing impacts of sea level rise on river salinity in the Gorai river network, Bangladesh. *Estuarine Coastal & Shelf Science, 96*, 219-227. doi: 10.1016/j.ecss.2011.11.005

Bjarnadottir, S., Li, Y., & Stewart, M. G. (2011). A probabilistic-based framework for impact and adaptation assessment of climate change on hurricane damage risks and costs. *Structural Safety, 33*(3), 173-185. doi: http://dx.doi.org/10.1016/j.strusafe.2011.02.003

Blake, E. S., Kimerlain, T. B., Berg, R. J., Cangialosi, J. P., & Beven, J. L. (2013). Tropical Cyclone Report Hurricane Sandy (pp. 157): National Hurricane Center.

Blake, E. S., Landsea, C. W., & Gibney, E. J. (2011). The Deadliest, Costliest, and Most Intense United States Tropical Cyclones From 1851 to 2010 (and other frequently requested hurricane facts) (N. W. Service, Trans.) (pp. 49). Miami, Florida: National Hurricane Center.

Board, R. o. t. P. N. S. C. (2007). *Philippines Population as of Aug 1, 2007* [Statistics]. Spreadsheet. Retrieved from: http://www.nscb.gov.ph/activestats/psgc/listprov.asp

Bunya, S., Dietrich, J. C., Westerink, J. J., Ebersole, B. A., Smith, J. M., Atkinson, J. H., . . . Roberts, H. J. (2010). A High-Resolution Coupled Riverine Flow, Tide, Wind, Wind Wave, and Storm Surge Model for Southern Louisiana and Mississippi. Part I: Model Development and Validation. *Monthly Weather Review, 138*(2), 345-377. doi: 10.1175/2009mwr2906.1

Cambers, G. (2009). Caribbean beach changes and climate change adaptation. *Aquatic Ecosystem Health & Management, 12*(2), 168-176. doi: 10.1080/14634980902907987

Carbognin, L., Teatini, P., Tomasin, A., & Tosi, L. (2010). Global change and relative sea level rise at Venice: what impact in term of flooding. *Climate Dynamics, 35*(6), 1055-1063. doi: 10.1007/s00382-009-0617-5

Cha, D.-H., & Wang, Y. (2013). A Dynamical Initialization Scheme for Real-Time Forecasts of Tropical Cyclones Using the WRF Model*. *Monthly Weather Review, 141*(3), 964-986. doi: 10.1175/mwr-d-12-00077.1

China, N. B. o. S. o. (2007). *China Population, Birth Rate, Death Rate and Natural Growth Rate by Region (1978-2006)* [Statistics]. Spreadsheet. Retrieved from: http://www.stats.gov.cn/english/

Church, J. A., & White, N. J. (2011). Sea-Level Rise from the Late 19th to the Early 21st Century. *Surveys in Geophysics, 32*(4-5), 585-602. doi: 10.1007/s10712-011-9119-1

Church, J. A., White, N. J., Konikow, L. F., Domingues, C. M., Cogley, J. G., Rignot, E., . . . Velicogna, I. (2011). Revisiting the Earth's sea-level and energy budgets from 1961 to 2008. *Geophys. Res. Lett., 38*(18), L18601. doi: 10.1029/2011gl048794

Claudia, T., Benjamin, H. S., & Chris, E. Z. (2012). Modelling sea level rise impacts on storm surges along US coasts. *Environmental Research Letters, 7*(1), 014032.

Cole, C. R., Macpherson, D. A., & McCullough, K. A. (2010). A Comparison of Hurricane Loss Models. *Journal of Insurance Issues, 33*(1), 31-53.

Craglia, M., de Bie, K., Jackson, D., Pesaresi, M., Remetey-Fülöpp, G., Wang, C., . . . Woodgate, P. (2011). Digital Earth 2020: towards the vision for the next decade. *International Journal of Digital Earth, 5*(1), 4-21. doi: 10.1080/17538947.2011.638500

Craig, R. K. (2010). A PUBLIC HEALTH PERSPECTIVE ON SEA-LEVEL RISE: STARTING POINTS FOR CLIMATE CHANGE ADAPTATION. *Widener Law Review, 15*(2), 521-540.

Dean, R. G. (2006). New Orleans and the Wetlands of Southern Louisiana. *The Bridge, 36*(Spring 2006), 8.

DeMaria, M. (2009). A Simplified Dynamical System for Tropical Cyclone Intensity Prediction. *Monthly Weather Review, 137*(1), 68-82. doi: 10.1175/2008mwr2513.1

DeMaria, M., & Kaplan, J. (1999). An Updated Statistical Hurricane Intensity Prediction Scheme (SHIPS) for the Atlantic and Eastern North Pacific Basins. *Weather and Forecasting, 14*(3), 326-337. doi: 10.1175/1520-0434(1999)014<0326:auship>2.0.co;2

DeMaria, M., Knaff, J. A., Knabb, R., Lauer, C., Sampson, C. R., & DeMaria, R. T. (2009). A New Method for Estimating Tropical Cyclone Wind Speed Probabilities. *Weather and Forecasting, 24*(6), 1573-1591. doi: 10.1175/2009waf2222286.1

Djamaluddin, I., Mitani, Y., & Ikemi, H. (2012). GIS-Based Computational Method for Simulating the Components of 3D Dynamic Ground Subsidence during the Process of Undermining. *International Journal of Geomechanics, 12*(1), 43-53. doi: 10.1061/(asce)gm.1943-5622.0000105

EASIS, I. S. D., & Eng, F. C. (2008). Indonesia - Jakarta Urgent Flood Mitigation Project - PROJECT INFORMATION DOCUMENT (PID) CONCEPT STAGE (Vol. 1 of 1): The World Bank Group.

ECLAC. (2010). CLIMATE CHANGE PROFILES IN SELECT CARIBBEAN COUNTRIES - REVIEW OF THE ECONOMICS OF CLIMATE CHANGE (RECC) IN THE CARIBBEAN PROJECT: Phase I: Economic Commission for Latin America and the Caribbean Subregional Headquarters for the Caribbean.

El-Raey, M. (1997). Vulnerability assessment of the coastal zone of the Nile delta of Egypt, to the impacts of sea level rise. *Ocean & Coastal Management, 37*(1), 29-40. doi: 10.1016/s0964-5691(97)00056-2

Elsner, J. B., Kossin, J. P., & Jagger, T. H. (2008). The increasing intensity of the strongest tropical cyclones. *Nature, 455*(7209), 92-95. doi: http://www.nature.com/nature/journal/v455/n7209/suppinfo/nature07234_S1.html

Elsner, J. B., Trepanier, J. C., Strazzo, S. E., & Jagger, T. H. (2012). Sensitivity of limiting hurricane intensity to ocean warmth. *Geophys. Res. Lett., 39*(17), L17702. doi: 10.1029/2012gl053002

Emanuel, K. (2005). Increasing destructiveness of tropical cyclones over the past 30 years. *Nature, 436*(7051), 3p.

Emanuel, K. (2011). Global Warming Effects on U.S. Hurricane Damage. *Weather, Climate, and Society, 3*(4), 261-268. doi: 10.1175/wcas-d-11-00007.1

Emanuel, K., & Jagger, T. (2010). On Estimating Hurricane Return Periods. *Journal of Applied Meteorology & Climatology, 49*(5), 8p.

Emanuel, K., Solomon, S., Folini, D., Davis, S., & Cagnazzo, C. (2013). Influence of Tropical Tropopause Layer Cooling on Atlantic Hurricane Activity. *Journal of Climate, 26*(7), 14p.

Emanuel, K. A. (2013). Downscaling CMIP5 climate models shows increased tropical cyclone activity over the 21st century. *Proceedings of the National Academy of Sciences*. doi: 10.1073/pnas.1301293110

EPICA, E. P. f. I. C. i. A. (2004). Eight glacial cycles from an Antarctic ice core. *Nature, 429*(6992), 623-628. doi: http://www.nature.com/nature/journal/v429/n6992/suppinfo/nature02599_S1.html

Fattah, M. A. (2010). Multicollinearity. Retrieved 21-Apr-2013, from http://www.chsbs.cmich.edu/fattah/courses/empirical/multicollinearity.html

Forbes, C., Luettich, R. A., Mattocks, C. A., & Westerink, J. J. (2010). A Retrospective Evaluation of the Storm Surge Produced by Hurricane Gustav (2008): Forecast and Hindcast Results. *Weather & Forecasting, 25*(6), 1577-1602. doi: 10.1175/2010waf2222416.1

Forster, J., Schuhmann, P. W., Lake, I. R., Watkinson, A. R., & Gill, J. A. (2012). The influence of hurricane risk on tourist destination choice in the Caribbean. *Climatic Change, 114*(3-4), 745-768.

Frazier, T. G., Wood, N., Yarnal, B., & Bauer, D. H. (2010). Influence of potential sea level rise on societal vulnerability to hurricane storm-surge hazards, Sarasota County, Florida. *Applied Geography, 30*(4), 490-505. doi: http://dx.doi.org/10.1016/j.apgeog.2010.05.005

Frey, A. E., Olivera, F., Irish, J. L., Dunkin, L. M., Kaihatu, J. M., Ferreira, C. M., & Edge, B. L. (2010). Potential Impact of Climate Change on Hurricane Flooding Inundation, Population Affected and Property Damages in Corpus Christi. *Journal of the American Water Resources Association, 46*(5), 1049-1059. doi: 10.1111/j.1752-1688.2010.00475.x

Gable, F. J. (1997). CLIMATE CHANGE IMPACTS ON CARIBBEAN COASTAL AREAS AND TOURISM. *Journal of Coastal Research*(ArticleType: research-article / Issue Title: SPECIAL ISSUE NO. 24. ISLAND STATES AT RISK: GLOBAL CLIMATE CHANGE, DEVELOPMENT AND POPULATION / Full publication date: Fall 1997 / Copyright © 1997 Coastal Education & Research Foundation, Inc.), 49-69. doi: 10.2307/25736087

Geographic, N., Esri, DeLorme, NAVTEQ, UNEP-WCMC, USGS, . . . iPC. (2011). *National Geographic World Map 16-Dec-2011* [Map]. Retrieved from: http://goto.arcgisonline.com/maps/NatGeo_World_Map

Geohive. (2000). *Trinidad & Tobago Population Census 2000*. Retrieved from: http://www.geohive.com/cntry/trinidad.aspx

Geohive. (2001). *Jamaica Population Census 2001*. Retrieved from: http://www.geohive.com/cntry/jamaica.aspx

Geohive. (2003). *Recensement Général de la population et de l'Habitat 2003* [Statistics]. Retrieved from: http://www.geohive.com/cntry/haiti.aspx

Geohive. (2010). *Population 2010-04-01 Census* [Statistics]. Spreadsheet. Retrieved from: http://www.geohive.com/cntry/us-pr.aspx

Geohive. (2011). *The Office of Registrar General & Census Commissioner of India Population Census 2011*. Retrieved from: http://www.geohive.com/cntry/india.aspx

George, J. E., & Gray, W. M. (1976). Tropical Cyclone Motion and Surrounding Parameter Relationships. *Journal of Applied Meteorology, 15*(12), 1252-1264. doi: 10.1175/1520-0450(1976)015<1252:TCMASP>2.0.CO;2

Gibin, M., Singleton, A., Milton, R., Mateos, P., & Longley, P. (2008). An Exploratory Cartographic Visualisation of London through the Google Maps API. *Applied Spatial Analysis and Policy, 1*(2), 85-97. doi: 10.1007/s12061-008-9005-5

GIS, D. o. (2010). *City of Lethbridge DEM Points and Breaklines*. Retrieved from: http://digitallibrary.uleth.ca/cdm/landingpage/collection/geo

Goring, D. G., Stephens, S. A., Bell, R. G., & Pearson, C. P. (2011). Estimation of Extreme Sea Levels in a Tide-Dominated Environment Using Short Data Records. *Journal of Waterway, Port, Coastal & Ocean Engineering, 137*(3), 150-159. doi: 10.1061/(asce)ww.1943-5460.0000071

Greenblatt, A., & Wills, E. (2011). SITES AT RISK. (Cover story). *Architect, 100*(9), 164-169.

Greene, C. H., Francis, J. A., & Monger, B. C. (2013). Superstorm Sandy: A series of unfortunate events? *Oceanography, 26*(1), 8-9.

Guinn, T. A., & Schubert, W. H. (1993). Hurricane Spiral Bands. *Journal of the Atmospheric Sciences, 50*(20), 3380-3403. doi: 10.1175/1520-0469(1993)050<3380:hsb>2.0.co;2

Hagen, S. C., Bacopoulos, P., Cox, A. T., & Cardone, V. J. (2012). Hydrodynamics of the 2004 Florida Hurricanes. *Journal of Coastal Research, 28*(5), 1121-1129. doi: 10.2112/jcoastres-d-10-00170.1

Hansen, J. E., & Sato, M. (2012). Paleoclimate Implications for Human-Made Climate Change. In A. Berger, F. Mesinger & D. Sijacki (Eds.), (pp. 21-47): Springer Vienna.

Hearty P. J., K. P., Cheng H., Edwards R. L. (1999). A +20 m middle Pleistocene sea-level highstand (Bermuda and the Bahamas) due to partial collapse of Antarctic ice. *Geology, 27*, 375 - 378. doi: 10.1130/0091-7613(1999)027<0375:AMMPSL>2.3.CO;2

Hence, D. A., & Houze, R. A. (2011). Vertical Structure of Hurricane Eyewalls as Seen by the TRMM Precipitation Radar. *Journal of the Atmospheric Sciences, 68*(8), 1637-1652. doi: 10.1175/2011jas3578.1

Hervé, J.-Y., Mullen, B., Yago Vicente, T. F., Allen, C. T. S., Morace, C., & Otterness, I. (2010). Using a Game Engine to Integrate Experimental, Field, and Simulation Data for Science Education: You Are the Scientist! *International Journal on Computing, 1*(1), 66-72. doi: 10.5176_2010-2283_1.1.11

Hijmans, R. (2009). *Global Administrative Areas, Country Level Data*. Retrieved from: http://www.gadm.org/country, http://www.diva-gis.org/gdata

Hoffman, R. N., Dailey, P., Hopsch, S., Ponte, R. M., Quinn, K., Hill, E. M., & Zachry, B. (2010). An Estimate of Increases in Storm Surge Risk to Property from Sea Level Rise in the First Half of the Twenty-First Century. *Weather, Climate, and Society, 2*(4), 271-293. doi: 10.1175/2010wcas1050.1

Holland, G. J., Belanger, J. I., & Fritz, A. (2010). A Revised Model for Radial Profiles of Hurricane Winds. *Monthly Weather Review, 138*(12), 4393-4401. doi: 10.1175/2010mwr3317.1

Holt-Giménez, E. (2002). Measuring farmers' agroecological resistance after Hurricane Mitch in Nicaragua: a case study in participatory, sustainable land management impact monitoring. *Agriculture, Ecosystems & Environment, 93*(1–3), 87-105. doi: http://dx.doi.org/10.1016/S0167-8809(02)00006-3

Homainejad, A. S. (2012). A novel approach for constructing a 3D model based on registering a mono image on a 3D model, applicable in Digital Earth. *International Journal of Digital Earth, 5*(2), 91-105. doi: 10.1080/17538947.2011.579396

Honeycutt, D. (2012a, 13-Nov-2012). More adventures in overlay: counting overlapping polygons with spaghetti and meatballs. Retrieved 14-Mar-2013, from http://blogs.esri.com/esri/arcgis/2012/11/13/spaghetti_and_meatballs/

Honeycutt, D. (2012b, 9-Nov-2012). More adventures in overlay: splitting polygons with cartographic spaghetti. Retrieved 14-Mar-2013, from http://blogs.esri.com/esri/arcgis/2012/11/09/splitting_polygons/

Houze, R. A., Chen, S. S., Smull, B. F., Lee, W.-C., & Bell, M. M. (2007). Hurricane intensity and eyewall replacement. *Science, 315*(5816), 1235-1239.

Howard, K. W. F., & Mullings, E. (1996). Hydrochemical Analysis of Ground-Water Flow and Saline Incursion in the Clarendon Basin, Jamaica. *Ground Water, 34*(5), 801-810. doi: 10.1111/j.1745-6584.1996.tb02074.x

Hsiang, S. M. (2010). Temperatures and cyclones strongly associated with economic production in the Caribbean and Central America. *Proceedings of the National Academy of Sciences of the United States of America, 107*(35), 15367-15372. doi: 10.1073/pnas.1009510107

Huang, Z., Zong, Y., & Zhang, W. (2004). Coastal inundation due to sea level rise in the Pearl River Delta, China. *Natural hazards, 33*(2), 247-264.

Indonesia, B. P. S.-S. (2010). *Population of Indonesia by Village Result of 2010 Population Census*. Retrieved from: http://bps.go.id/eng/download_file/Population_of_Indonesia_by_Village_2010.pdf

Indonesia, S. D., & Task-Force, E. (2011). Jakarta - Urban challenges in a changing climate *Mayors' Task Force On Climate Change, Disaster Risk & The Urban Poor* (Vol. 1 of 1, pp. 48). Jakarta: The World Bank and Indonesia Sustainable Devlpmnt (EASIS).

Informacion, O. N. D. E. E. (2002). *3.26- Población residente en ciudades, según sexo e Índice de masculinidad. Censo 2002* [Statistics]. Spreadsheet. Retrieved from: http://www.cubagob.cu/otras_info/censo/tablas_html/ii_4.htm

IPCC. (2012). Managing the Risks of Extreme Events and Disasters to Advance Climate Change Adaptation. A Special Report of Working Groups I and II of the Intergovernmental Panel on Climate Change. In C. B. Field, V. Barros, T.F. Stocker, D. Qin, D.J. Dokken, K.L. Ebi, M.D. Mastrandrea, K.J. Mach, G.-K. Plattner, S.K. Allen, M. Tignor, and P.M. Midgley (eds.) (Ed.), (pp. 582). Cambridge, UK, and New York, NY, USA.

IPCC, A.P.M. Baede, E. Ahlonsou, Y. Ding, D. Schimel. (2001). IPCC Third Assessment Report - Climate Change 2001: The Scientific Basis - The Climate System: an Overview. In IPCC (Ed.), *IPCC Third Assessment Report - Climate Change 2001* (pp. 87 - 98). Cambridge University Press IPCC.

Jagger, T. H., & Elsner, J. B. (2010). A Consensus Model for Seasonal Hurricane Prediction. *Journal of Climate, 23*(22), 6090-6099. doi: 10.1175/2010jcli3686.1

Jarvinen, B. R., Neuman, C., & Davis, M. (1988). A tropical cyclone data tape for the North Atlantic basin. *NOAA Tech. Memo. NWS NHC-22*.

Jury, M., Rios-Berrios, R., & García, E. (2012). Caribbean hurricanes: changes of intensity and track prediction. *Theoretical & Applied Climatology, 107*(1/2), 297-311. doi: 10.1007/s00704-011-0461-5

Kaplan, J., & DeMaria, M. (1995). A simple empirical model for predicting the decay of tropical cyclone winds after landfall. *Journal of Applied Meteorology, 34*(11), 2499-2512.

Kaplan, J., DeMaria, M., & Knaff, J. A. (2010). A Revised Tropical Cyclone Rapid Intensification Index for the Atlantic and Eastern North Pacific Basins. *Weather and Forecasting, 25*(1), 220-241. doi: 10.1175/2009waf2222280.1

Kienzle, S. (2004). The Effect of DEM Raster Resolution on First Order, Second Order and Compound Terrain Derivatives. *Transactions in GIS, 8*(1), 83-111. doi: 10.1111/j.1467-9671.2004.00169.x

Knaff, J. A., Sampson, C. R., DeMaria, M., Marchok, T. P., Gross, J. M., & McAdie, C. J. (2007). Statistical Tropical Cyclone Wind Radii Prediction Using Climatology and Persistence. *Weather and Forecasting, 22*(4), 781-791. doi: 10.1175/waf1026.1

Knapp, K. R., Kruk, M. C., Levinson, D. H., Diamond, H. J., & Neumann, C. J. (2010). The International Best Track Archive for Climate Stewardship (IBTrACS). *Bulletin of the American Meteorological Society, 91*(3), 363-376. doi: 10.1175/2009bams2755.1

Knutson, T. R., McBride, J. L., Chan, J., Emanuel, K., Holland, G., Landsea, C., . . . Sugi, M. (2010). Tropical cyclones and climate change. *Nature Geosci, 3*(3), 157-163. doi: http://www.nature.com/ngeo/journal/v3/n3/suppinfo/ngeo779_S1.html

Knutson, T. R., Tuleya, R. E., Sirutis, J. J., Vecchi, G. A., Garner, S. T., & Held, I. M. (2010). Modeled Impact of Anthropogenic Warming on the Frequency of Intense Atlantic Hurricanes. *Science, 327*(5964), 5p.

Komar, P. D., & Allan, J. C. (2008). Increasing Hurricane-Generated Wave Heights along the U.S. East Coast and Their Climate Controls. *Journal of Coastal Research, 24*(2), 479-488. doi: 10.2307/30137851

Kossin, J. P., Camargo, S. J., & Sitkowski, M. (2010). Climate modulation of North Atlantic hurricane tracks. *Journal of Climate, 23*(11), 3057-3076.

Kossin, J. P., Knaff, J. A., Berger, H. I., Herndon, D. C., Cram, T. A., Velden, C. S., . . . Hawkins, J. D. (2007). Estimating Hurricane Wind Structure in the Absence of Aircraft Reconnaissance. *Weather and Forecasting, 22*(1), 89-101. doi: 10.1175/waf985.1

Krishnamurthy, P. K., Fisher, J. B., & Johnson, C. (2011). Mainstreaming local perceptions of hurricane risk into policymaking: A case study of community GIS in Mexico. *Global Environmental Change, 21*(1), 143-153. doi: http://dx.doi.org/10.1016/j.gloenvcha.2010.09.007

Kunkel, K. E., Karl, T. R., Brooks, H., Kossin, J., Lawrimore, J. H., Arndt, D., . . . Wuebbles, D. (2013). MONITORING AND UNDERSTANDING TRENDS IN EXTREME STORMS: State of Knowledge. *Bulletin of the American Meteorological Society, 94*(4), 499-514. doi: 10.1029/2005jd006290.

Lambert, F., Delmonte, B., Petit, J. R., Bigler, M., Kaufmann, P. R., Hutterli, M. A., . . . Maggi, V. (2008). Dust-climate couplings over the past 800,000 years from the EPICA Dome C ice core. *Nature, 452*(7187), 616-619. doi: http://www.nature.com/nature/journal/v452/n7187/suppinfo/nature06763_S1.html

Landsea, C., Franklin, J., & Beven, J. (2012). The revised Atlantic hurricane database (HURDAT2) (pp. 6): National Hurricane Center.

Landsea, C. W., Harper, B. A., Hoarau, K., & Knaff, J. A. (2006). Can We Detect Trends in Extreme Tropical Cyclones? *Science, 313*(5786), 452-454. doi: 10.2307/3846789

Landsea, C. W., Vecchi, G. A., Bengtsson, L., & Knutson, T. R. (2009). Impact of Duration Thresholds on Atlantic Tropical Cyclone Counts*. *Journal of Climate, 23*(10), 2508-2519. doi: 10.1175/2009jcli3034.1

Lloyd, I. D., & Vecchi, G. A. (2011). Observational Evidence for Oceanic Controls on Hurricane Intensity. *Journal of Climate, 24*(4), 1138-1153. doi: 10.1175/2010jcli3763.1

Luthi, D., Le Floch, M., Bereiter, B., Blunier, T., Barnola, J.-M., Siegenthaler, U., . . . Stocker, T. F. (2008). High-resolution carbon dioxide concentration record 650,000-800,000[thinsp]years before present. *Nature, 453*(7193), 379-382. doi: http://www.nature.com/nature/journal/v453/n7193/suppinfo/nature06949_S1.html

Mackey, C., Dorsett, K., Lowe, C., Saunders, K., Frith, I., Williams, L., & Newbold, L. (2012). *2010 Census of Populatoin and Housing* [Statistics]. PDF. Retrieved from: http://statistics.bahamas.gov.bs/download/056411800.pdf

Malmstadt, J. C., Elsner, J. B., & Jagger, T. H. (2010). Risk of Strong Hurricane Winds to Florida Cities. *Journal of Applied Meteorology and Climatology, 49*(10), 2121-2132. doi: 10.1175/2010jamc2420.1

Mann, M. E. (2007). Climate Over the Past Two Millennia. *Annual Review of Earth and Planetary Sciences, 35*(1), 111-136. doi: 10.1146/annurev.earth.35.031306.140042

Mann, M. E., & Emanuel, K. A. (2006). Atlantic hurricane trends linked to climate change. *EOS, Transactions American Geophysical Union, 87*(24), 233.

McAdie, C. J. (2004). Development of a wind-radii CLIPER model. *DEVELOPMENT, 5*, 7.

McAdie, C. J., Landsea, C. W., Neumann, C. J., David, J. E., & Blake, E. S. (2009). *Tropical cyclones of the North Atlantic Ocean, 1851-2006* (6th rev., July 2009 ed.). Asheville, N.C.: U.S. Dept. of Commerce, National Oceanic and Atmospheric Administration, National Weather Service, National Environmental Satellite, Data, and Information Service,.

Mlakar, P. F. (2006). The Behavior of Hurricane-Protection Infrastructure in New Orleans. *The Bridge, 36*(Spring 2006), 7.

Morenoa, A., & Beckenb, S. (2009). A climate change vulnerability assessment methodology for coastal tourism. *Journal of Sustainable Tourism, 17*(4), 473-488. doi: 10.1080/09669580802651681

Nachtergaele, F. (2008). *Land Use Systems of the World* [Raster Digital Map]. TIFF. Retrieved from: http://www.fao.org/geonetwork/srv/en/resources.get?id=37139&fname=lust.zip&access=private

NWS (Producer). (2010, 7-Mar-2014). Tropical Cyclone Structure. Retrieved from http://www.srh.noaa.gov/jetstream/tropics/tc_structure.htm

Pielke, R., Gratz, J., Landsea, C., Collins, D., Saunders, M., & Musulin, R. (2008). Normalized Hurricane Damage in the United States: 1900–2005. *Natural Hazards Review, 9*(1), 29-42. doi: doi:10.1061/(ASCE)1527-6988(2008)9:1(29)

Pinelli, J. P., Gurley, K. R., Subramanian, C. S., Hamid, S. S., & Pita, G. L. (2008). Validation of a probabilistic model for hurricane insurance loss projections in Florida. *Reliability Engineering & System Safety, 93*(12), 1896-1905. doi: http://dx.doi.org/10.1016/j.ress.2008.03.017

Pita, G. L., Pinelli, J.-P., Gurley, K. R., & Hamid, S. (2013). Hurricane vulnerability modeling: Development and future trends. *Journal of Wind Engineering and Industrial Aerodynamics, 114*(0), 96-105. doi: http://dx.doi.org/10.1016/j.jweia.2012.12.004

Poulter, B., & Halpin, P. N. (2008). Raster modelling of coastal flooding from sea-level rise. *International Journal of Geographical Information Science, 22*(2), 167-182. doi: 10.1080/13658810701371858

Prakash, E., Brindle, G., Jones, K., Suiping, Z., Chaudhari, N. S., & Kok-Wai, W. (2009). Advances in Games Technology: Software, Models, and Intelligence. *Simulation & Gaming, 40*(6), 752-801. doi: 10.1177/1046878109335120

Programme, U. N. H. S. (2011). *Cities and Climate Change: Global Report on Human Settlements 2011*: Earthscan.

Reible, D. D., Haas, C. N., Pardue, J. H., & Walsh, W. J. (2006). Toxic and Contaminant Concerns Generated by Hurricane Katrina. *The Bridge, 36*(Spring 2006), 9.

Rowe, M. (2011). Dossier: Come hell OR HIGH WATER. *Geographical (Geographical Magazine Ltd.), 83*(4), 34-41.

Rua, H., & Alvito, P. (2011). Living the past: 3D models, virtual reality and game engines as tools for supporting archaeology and the reconstruction of cultural heritage – the case-study of the Roman villa of Casal de Freiria. *Journal of Archaeological Science, 38*(12), 3296-3308. doi: 10.1016/j.jas.2011.07.015

Rygel, L., O'sullivan, D., & Yarnal, B. (2006). A Method for Constructing a Social Vulnerability Index: An Application to Hurricane Storm Surges in a Developed Country. *Mitigation and Adaptation Strategies for Global Change, 11*(3), 741-764. doi: 10.1007/s11027-006-0265-6

Sandvik, B. (2008). *Using KML for Thematic Mapping.* (M. Sc.), University of Edinburgh. Retrieved from http://hdl.handle.net/1842/2464

Schaeffer, M., Hare, W., Rahmstorf, S., & Vermeer, M. (2012). Long-term sea-level rise implied by 1.5 C and 2 C warming levels. *Nature Clim. Change, advance online publication*. doi: http://www.nature.com/nclimate/journal/vaop/ncurrent/abs/nclimate1584.html#supplementary-information

Schmaltz, J. (Producer). (2010, 7-Mar-2014). Tropical Cyclone Ike 2008. Retrieved from http://www.nasa.gov/mission_pages/hurricanes/archives/2008/h2008_ike.html

Senkbeil, J. C., Brommer, D. M., & Comstock, I. J. (2011). Tropical Cyclone Hazards in the USA. *Geography Compass, 5*(8), 544-563. doi: 10.1111/j.1749-8198.2011.00439.x

SPSS, I. (2011). *IBM SPSS Forecasting 20* (pp. 124). Retrieved from ftp://public.dhe.ibm.com/software/analytics/spss/documentation/statistics/20.0/en/client/Manuals/IBM_SPSS_Forecasting.pdf

Statistics, B. B. o. (2001). *District wise Population as on Population Census 2001* [Statistics]. Spreadsheet. Retrieved from: http://www.bbs.gov.bd/DistrictWisePopulation.aspx?disName=All

Statistics, N. (2012). *Taiwan Population September 2012* [Statistics]. Spreadsheet. Retrieved from: http://eng.stat.gov.tw/mp.asp?mp=5

Steed, C. A., Swan, J. E., Jankun-Kelly, T. J., & Fitzpatrick, P. J. (2009, 12-13 Oct. 2009). *Guided analysis of hurricane trends using statistical processes integrated with interactive parallel coordinates.* Paper presented at the Visual Analytics Science and Technology, 2009. VAST 2009. IEEE Symposium on.

Stevens, J. P. (1984). Outliers and influential data points in regression analysis. *Psychological Bulletin, 95*(2), 334-344.

Tabachnick, B. G. F. L. S. (2007). *Using multivariate statistics*. Boston: Pearson/Allyn & Bacon.

Tachikawa, T., Hato, M., Kaku, M., & Iwasaki, A. (2011a). *ASTER GDEM* [Raster Digital Elevation Model]. Raster DEM. Retrieved from: http://gdem.ersdac.jspacesystems.or.jp/download.jsp

Tachikawa, T., Hato, M., Kaku, M., & Iwasaki, A. (2011b). *The Characteristics of ASTER GDEM Version 2.* Paper presented at the IGARSS 2011, Vancouver, BC. Canada.

Tactuk, P., Ureña, F. C., & Mejía, M. M. (2010). *IX CENSO NACIONAL DE POBLACIÓN Y VIVIENDA 2010* [Statistics]. PDF. Retrieved from: http://censo2010.one.gob.do/volumenes_censo_2010/vol1.pdf

Tang, B., & Emanuel, K. (2012). Sensitivity of Tropical Cyclone Intensity to Ventilation in an Axisymmetric Model. *Journal of the Atmospheric Sciences, 69*(8), 20p.

Thrane, S., Ojika, T., & Berry, R. (2002). Enhanced Environments: Large-Scale, Real-Time Ecosystems. *Presence: Teleoperators & Virtual Environments, 11*(3), 221.

Tracy, A., Trumbull, K., & Loh, C. (2007). Impact of Climate Change in Hong Kong and the Pearl River Delta. *China Perspectives, 2007*(1), 18-29.

Trenberth, K. E. (2010). Global change: The ocean is warming, isn't it? *Nature, 465*(7296), 304-304.

Trenberth, K. E., & Fasullo, J. T. (2010). CLIMATE CHANGE Tracking Earth's Energy. *Science, 328*(5976), 316-317. doi: 10.1126/science.1187272

Vafaee, F., Harati, S. A. N., & Sabbaghian, H. (2012). Investigation of Coastal Inundation Due to a Rise in Sea Level (Temporary and Permanent). *Polish Journal of Environmental Studies, 21*(1), 209-217.

Vickery, P. J., Masters, F. J., Powell, M. D., & Wadhera, D. (2009). Hurricane hazard modeling: The past, present, and future. *Journal of Wind Engineering and Industrial Aerodynamics, 97*(7–8), 392-405. doi: http://dx.doi.org/10.1016/j.jweia.2009.05.005

Vickery, P. J., & Wadhera, D. (2008). Statistical Models of Holland Pressure Profile Parameter and Radius to Maximum Winds of Hurricanes from Flight-Level Pressure and H*Wind Data. *Journal of Applied Meteorology and Climatology, 47*(10), 2497-2517. doi: 10.1175/2008jamc1837.1

Vigh, J. L., Knaff, J. A., & Schubert, W. H. (2012). A Climatology of Hurricane Eye Formation*. *Monthly Weather Review, 140*(5), 1405-1426. doi: 10.1175/mwr-d-11-00108.1

Vimont, D. J., & Kossin, J. P. (2007). The Atlantic meridional mode and hurricane activity. *Geophysical Research Letters, 34*(7), L07709.

Westerink, J. J., Luettich, R. A., Feyen, J. C., Atkinson, J. H., Dawson, C., Roberts, H. J., . . . Pourtaheri, H. (2008). A Basin- to Channel-Scale Unstructured Grid Hurricane Storm Surge Model Applied to Southern Louisiana. *Monthly Weather Review, 136*(3), 833-864. doi: 10.1175/2007MWR1946.1

Wolshon, B. (2006). Evacuation Planning and Engineering for Hurricanes. *The Bridge, 36*(Spring 2006), 8.

Yin, J., Yin, Z., Wang, J., & Xu, S. (2012). National assessment of coastal vulnerability to sea-level rise for the Chinese coast. *Journal of Coastal Conservation, 16*(1), 123-133. doi: 10.1007/s11852-012-0180-9

Yu, L., & Gong, P. (2011). Google Earth as a virtual globe tool for Earth science applications at the global scale: progress and perspectives. *International Journal of Remote Sensing, 33*(12), 3966-3986. doi: 10.1080/01431161.2011.636081

Yusuf, A. A., & Francisco, H. (2009). Climate Change Vulnerability Mapping for Southeast Asia: Economy and Environment Program for Southeast Asia (EEPSEA).

8 Appendix A: SSHWS Variable Program Blocks

```
x = x_end - x_start
If x < 0
        Then x_quad = -1
        Else x_quad = 1

y = y_end – y_start
If y < 0
        Then y_quad = -1
        Else y_quad = 1

If x_quad > 0 and y_quad > 0
    Then quad = 1
    Else if x_quad > 0 and y_quad < 0
        Then quad = 2
        Else if x_quad < 0 and y_quad < 0
            Then quad = 3
            Else quad = 4

If x = 0
    Then intm = 90
    Else intm = abs(degrees(atan(y/x)))

If quad = 1
Then NORTH_0_360 = 90 – intm
Else if quad = 2
    Then NORTH_0_360 = 90 + intm
    Elseif quad = 3
        Then NORTH_0_360 = 270 – intm
        Else if quad = 4
            Then NORTH_0_360 = 270 + intm
```

Program Block 1: NORTH_0_360

```
If quad = 4
Then right_dimension = atc_w64_r1
Else if quad = 1
    Then right_dimension = atc_w64_r2
    Elseif quad = 2
        Then right_dimension = atc_w64_r3
        Else if quad = 3
            Then right_dimension = atc_w64_r4
```

Program Block 2: RIGHT_DIMENSION

```
If quad = 4
Then left_dimension = atc_w64_r3
Else if quad = 1
     Then left_dimension = atc_w64_r4
     Else if quad = 2
          Then left_dimension = atc_w64_r1
          Else if quad = 3
               Then left_dimension = atc_w64_r2
```

Program Block 3: LEFT_DIMENSION

9 Appendix B: IBTrACS data Multiple Linear Regression Analysis (MLR)

9.1 Computed Hurricane Data Variables Required for MLR

To run the MLR analysis, hurricane data available directly from IBTrACS as well as several computed data variables were required. The calculated data were Max_64 (the maximum value of ATC_w64_r1, ATC_w64_r2, ATC_w64_r3, ATC_w64_r4 recorded to the nearest 5 kt), HR_VEL_KT_Fine (Hurricane forward velocity rounded to the nearest 5 kt; values below 5 rounded to the nearest 1 kt), and HURR_FCAT_OBSER (chronologically numbered starting at 1 for the first hurricane category 1 observation going to the last observation of the hurricane). NORTH_0_360 (hurricane 360 angular degree direction of travel described in the previous section) and Y_START_ROUND (latitude of the hurricane observation start point value rounded to the nearest 2 decimal places) is obtained from Y_START as described in the previous section. WMO_PRES (central pressure to nearest 1 mb) is recorded in the IBTrACS dataset.

The maximum wind radii distance (Max_64) was calculated in Excel using a built function to find the maximum value of the IBTrACS data variables ATC_w64_r1, ATC_w64_r2, ATC_w64_r3, and ATC_w64_r4. There are several cases where more than 1 of the 4 variables have the same maximum value. Since a hurricane's structure is typically asymmetrical with the maximum winds located to the right of the forward direction of travel (George & Gray, 1976; Jarvinen, Neuman, & Davis, 1988), the maximum wind radii distance should be located in the quadrant to the right of the hurricane trajectory.

Hurricane forward velocity (HR_VEL_KT_Fine) is calculated from the GIS vector line start and end points. The hurricane observation line segment distance (LINE_DISTANCE (km)) was calculated in ArcGIS using built-in functions. Hurricane Velocity in both metric (km/h) and knots were calculated in ArcGIS using the built-in equation editor based on readings being 6 hours apart. HR_VEL_KT_fine was rounded to the nearest 5 kt with the exception of values falling between 1-5 kt which are rounded to the nearest 1 kt to reduce the number of 0 kt velocity values in the data set.

The hurricane first observation (HURR_FCAT_OBSER) was used as a hurricane aging variable. IBTrACS contains 6 hour observation readings for the life of a hurricane. Each hurricane track segment was classified using the Saffir-Simpson Hurricane Wind Scale (SSHWS) classification into intensities of hurricane categories (SSHWS_CATEGORY – see Program Block 4) 0 through 5 using the wind speed variable (WMO_WIND).

```
If wmo_wind >= 137
Then SSHWS_CATEGORY = 5
Else if wmo_wind >= 113
     Then SSHWS_CATEGORY = 4
     Elseif wmo_wind >= 96
          Then SSHWS_CATEGORY = 3
          Else if wmo_wind >= 83
               Then SSHWS_CATEGORY = 2
               Else if wmo_wind >= 64
                    Then SSHWS_CATEGORY = 1
                    Else SSHWS_CATEGORY = 0
```

Program Block 4: SSHWS_CATEGORY

Since 64 kt wind radii data only exists at the point when the hurricane reaches SSHWS Category 1 intensity, all observations prior to this are discarded. Each record within each hurricane was chronologically numbered (HURR_FCAT_OBSER) starting at 1 for the first observation reaching SSHWS hurricane category 1 status and sequentially incremented to its last recorded observation including points when the storm went below SSHWS category 1.

9.2 Statistical Analysis of Hurricane Wind Radii using 2004 - 2011 data

Statistical analysis techniques are used to predict both hurricane path and wind radii size. Knaff et al discuss latitude, hurricane forward velocity and azimuth as factors determining hurricane size and path. Since hurricane path prediction is not required as this study uses historical hurricane tracks, only the wind radii right and left size dimensions are the required elements. Based on Knaff's study, the corresponding variable used for latitude is Y_START_ROUND; forward velocity is HR_VEL_KT_Fine; and azimuth is NORTH_0_360. Additional data input variables were also required to obtain the right and left width dimensions. Max_64, the maximum 64 kt wind radii typically found in the right side quadrant to the hurricane trajectory, is an intermediary variable. HURR_FCAT_OBSER is a time series variable representing the point where the observation exists in the hurricane's lifecycle. Hurricane wind speed (wmo_wind) was considered as a characteristic to be used in the linear regression analysis but was removed due to collinearity (Fattah, 2010) with central pressure (wmo_pres). These two variables are highly related to each other in that central pressure decreases as wind speed increases therefore only one of the variables can be used in the regression. The R^2 value obtained when using wind speed is not as high as that of central pressure. As a result, wind speed is not used in the linear regression analysis. There is a limitation with using central pressure. It is not consistently tracked in the NA IBTrACS dataset until 1979. This puts a lower boundary on the time frame used in the analysis.

A data filter was to be applied to remove all storms in the dataset not reaching a minimum SSHWS category 1 strength (SSHWS_Category > 0). Another filter was used to retain all data records beginning at the point where the first observation within each hurricane reached a status of SSHWS category 1 or greater (HURR_FCAT_OBSER > 0). The hurricane data was also limited to observations situated below 30° latitude (Y_START_ROUND <= 30) which is just above the study area. Data outlier observations containing values significantly outside of a normal bell curve were also removed by using a mahalanobis distance greater than 24.3 (Stevens, 1984; Tabachnick, 2007).

9.3 Statistical Analysis to obtain Right and Left Wind Radii Values for 1979 – 2003

The Linear Regression module from IBM SPSS Statistics version 21 release 21.0.0.1 was used to estimate the dependant variables Max_64, RIGHT_DIMENSION, and LEFT_DIMENSION. The "Simultaneous" method was selected where all variables were used in the calculation at the same time.

The 64 kt wind radii data collection started with the 2004 hurricane season. This data allowed for the creation of a width dimension to the hurricane track paths. Since only 8 years of records exist in the dataset, statistical linear regression was used to extend the 64 kt wind radii data. Two hurricane characteristics that influence the size of the wind radii are the circular wind speed (WMO_WIND), and central pressure (WMO_PRES). These two variables are highly correlated with a statistic of -0.93 (see Table 9.3.1) meaning as wind speed increases there is a corresponding decrease in central pressure. Collinearity exists when correlations or relationships between independent variables are strong (Fattah, 2010). The Variance Inflation Factor (VIF) statistic which measures multicollinearity in SPSS contained a value of 12. The method chosen to illuminate this issue was to remove one of the highly correlated variables. Statistical linear regression models produce an "R^2" or "goodness of fit" value to measure how well a resulting equation will represent the statistical model (SPSS, 2011). The hurricane characteristic "wmo_pres" produced a better R^2 value than "wmo_wind". As a result, the variable "wmo_wind" was removed from the statistical model. The drawback from using central pressure for all SSHWS category level hurricane observations is that it is not consistently recorded for the NA basin in IBTrACS until 1979. Consequently the 1979 hurricane season becomes the earliest year the 64 kt wind radii can be extended to.

Correlation	wmo_wind	wmo_pres
wmo_wind	1	-.930**
wmo_pres	-.930**	1

Table 9.3.1: Correlation WMO_WIND & WMO_PRES. Pearson Correlation; Sample Size: 4055; **. Correlation is significant at the 0.01 level (2-tailed).

Statistical linear regression techniques produce mathematical equations or models to best represent the data. In this study, three statistical linear regression models were successfully run using the 2004 – 2011 IBTrACS NA 64 kt wind radii to acquire the right and left width dimensions for the hurricane track line segments. The first regression was required to obtain the maximum 64 kt wind radii distance (Max_64) which was then used as an input to the linear regression for the right and left hurricane dimensions. A filter was applied to reduce the dataset to include only those hurricane observation points satisfying the following requirements:

a) hurricane tracks must be SSHWS category 1 strength or greater (SSHWS_MAX > 0)
b) the first data observations for each hurricane must start at the point where it becomes a SSHWS category 1 (HURR_FCAT_OBSER > 0)
c) the latitude is below 30° North (Y_START_ROUND <= 30)
d) the mahalanobis value is less than or equal to 24.3 (MAH_1 <= 24.3)

There are 895 hurricane observations meeting the above criteria. The models were run with a statistically significant confidence level of PIN(.10) and POUT(.15).

9.3.1 Dependant Variable: Max_64

The dependant variable "Max_64" is used as an intermediary input to derive the right and left width dimension for the GIS hurricane line segment. Using the SPSS linear regression module, Max_64 is calculated with all inputs NORTH_0_360, HURR_FCAT_OBSER, HR_VEL_KT_fine, wmo_pres, Y_START_ROUND contributing to the model (see Table 9.3.2 – Top). An "Adjusted R Square" value of 0.714 with standard error of 14.158 is acceptable given only 5 hurricane characteristics are being considered. The collinearity VIF values are also within a reasonable range at just above 1.0 (see Table 9.3.2 – Bottom).

Model	Variables Entered	Method
1	NORTH_0_360, HURR_FCAT_OBSER, HR_VEL_KT_fine, wmo_pres, Y_START_ROUND[b]	Enter

Model Summary[b]

Model	R	R Square	Adjusted R Square	Std. Error of the Estimate
1	.846[a]	.715	.714	14.158

a. Predictors: (Constant), NORTH_0_360, HURR_FCAT_OBSER, HR_VEL_KT_fine, wmo_pres, Y_START_ROUND
b. Dependent Variable: Max_64

Coefficients[a]

Model		Unstandardized Coefficients		Standardized Coefficients			Collinearity Statistics	
		B	Std. Error	Beta	t	Sig.	Tolerance	VIF
1	(Constant)	788.124	19.095		41.273	.000		
	wmo_pres	-.809	.019	-.790	-42.910	.000	.945	1.058
	Y_START_ROUND	.824	.128	.134	6.456	.000	.745	1.343
	HURR_FCAT_OBSER	.268	.047	.118	5.725	.000	.759	1.318
	HR_VEL_KT_fine	.385	.111	.062	3.453	.001	.980	1.021
	NORTH_0_360	.017	.005	.061	3.298	.001	.934	1.070

a. Dependent Variable: Max_64

Table 9.3.2: Max_64 Linear Regression Results. Top: Linear regression method uses all variables simultaneously. Middle: Model Summary results. Bottom: B – Equation coefficients for the linear regression model and Collinearity Statistics.

9.3.2 Dependant Variable: RIGHT_DIMENSION

The dependant variable "RIGHT_DIMENSION" is calculated for the hurricane line segment right width dimension used in the GIS overlay analysis. Linear regression is again used to calculate RIGHT_DIMENSION with all inputs Max_64, NORTH_0_360, HURR_FCAT_OBSER, HR_VEL_KT_fine, wmo_pres, Y_START_ROUND contributing to the model (see Table 9.3.3 – Top). An "Adjusted R Square" value of 0.984 with standard error of 3.406 (see Table 9.3.3 – Middle) was obtained from the model.

Model	Variables Entered	Method
1	Max_64, HR_VEL_KT_fine, HURR_FCAT_OBSER, NORTH_0_360, Y_START_ROUND, wmo_pres[b]	Enter

Model Summary

Model	R	R Square	Adjusted R Square	Std. Error of the Estimate
1	.992[a]	.984	.984	3.406

a. Predictors: (Constant), Max_64, HR_VEL_KT_fine, HURR_FCAT_OBSER, NORTH_0_360, Y_START_ROUND, wmo_pres

Coefficients[a]

Model		Unstandardized Coefficients		Standardized Coefficients	t	Sig.
		B	Std. Error	Beta		
1	(Constant)	16.506	7.844		2.104	.036
	HURR_FCAT_OBSER	.052	.011	.023	4.495	.000
	wmo_pres	-.016	.008	-.015	-1.968	.049
	HR_VEL_KT_fine	.024	.027	.004	.890	.374
	NORTH_0_360	.004	.001	.013	3.008	.003
	Y_START_ROUND	-.152	.031	-.025	-4.839	.000
	Max_64	.978	.008	.976	121.235	.000

a. Dependent Variable: RIGHT_DIMENSION

Table 9.3.3: RIGHT_DIMENSION Linear Regression Results. Top: Linear regression method uses all variables simultaneously. Middle: Model Summary results. Bottom: B – Equation coefficients for the linear regression model.

9.3.3 Dependant Variable: LEFT_DIMENSION

The dependant variable "LEFT_DIMENSION" is calculated for the hurricane line segment left width dimension used in the GIS overlay analysis. Linear regression is again used to calculate LEFT_DIMENSION with all inputs Max_64, NORTH_0_360, HURR_FCAT_OBSER, HR_VEL_KT_fine, wmo_pres, Y_START_ROUND contributing to the model (see Table 8 – Top). An "Adjusted R Square" value of 0.772 with standard error of 8.205 (see Table 8 – Middle) was obtained from the model.

Model	Variables Entered	Method
1	Max_64, HR_VEL_KT_fine, HURR_FCAT_OBSER, NORTH_0_360, Y_START_ROUND, wmo_pres[b]	Enter

Model Summary

Model	R	R Square	Adjusted R Square	Std. Error of the Estimate
1	.879[a]	.773	.772	8.205

a. Predictors: (Constant), Max_64, HR_VEL_KT_fine, HURR_FCAT_OBSER, NORTH_0_360, Y_START_ROUND, wmo_pres

Coefficients[a]

Model		Unstandardized Coefficients		Standardized Coefficients	t	Sig.
		B	Std. Error	Beta		
1	(Constant)	221.151	18.898		11.702	.000
	HURR_FCAT_OBSER	.092	.028	.062	3.344	.001
	wmo_pres	-.223	.019	-.336	-11.666	.000
	HR_VEL_KT_fine	-.370	.065	-.093	-5.695	.000
	NORTH_0_360	-.009	.003	-.049	-2.961	.003
	Y_START_ROUND	.252	.076	.063	3.329	.001
	Max_64	.372	.019	.574	19.163	.000

a. Dependent Variable: LEFT_DIMENSION

Table 9.3.4: LEFT_DIMENSION Linear Regression Results. Top: Linear regression method uses all variables simultaneously. Middle: Model Summary results. Bottom: B – Equation coefficients for the linear regression model.

10 Appendix C: 2004 – 2011 IBTrACS Data Analysis

10.1 2004 – 2011 Hurricane Impact Zones

The modified GIS overlay analysis technique was run using 64 kt wind radii data from the 2004 - 2011 IBTrACS NA basin dataset. A right and left width buffer was created for each storm track reaching a minimum of SSHWS category 1 intensity (see Table 10.1.1). Although 14 hurricane tracks made landfall within the study area, Hurricanes Rita and Tomas did not contribute significantly to the impacted area. The 2008 hurricane season had the largest impact in the study area affecting 61,818 km^2.

Hurricane 2004 - 2011	Season	Total Impact Area (km^2)
CHARLEY	2004	3,509
DEAN	2007	6,529
DENNIS	2005	32,358
FRANCES	2004	4,713
GUSTAV	2008	14,024
HANNA	2008	432
IKE	2008	44,720
IRENE	2011	5,323
IVAN	2004	10,956
JEANNE	2004	4,098
PALOMA	2008	2,642
RITA	2005	2
TOMAS	2010	1
WILMA	2005	1,919

Hurricane Season	Total Impact Area (km^2)
2004	23,276
2005	34,279
2007	6,529
2008	61,818
2010	1
2011	5,323
Total	**131,226**

Table 10.1.1: 2004 – 2011 Hurricanes Intersecting the Study Area. Table Left: Named hurricanes impacting the Caribbean Study Area of The Bahamas, Cuba, Dominican Republic, Haiti, Jamaica, and Puerto Rico from 2004 – 2011. Table Right: Yearly hurricane impact area totals in the study area.

Figure 10.2.1 contains a map illustrating regions in the study area during the 2004 – 2011 time period categorized into hurricane impact zone frequency counts. The maximum frequency any given location was hit by multiple hurricanes was 4 occurrences. Cuba experienced the largest impacted land area in each of the 4 classifications (see Table 10.1.2) totaling 70% of its country land size. The Bahamas experienced a frequency hit count of 4 hurricanes impacting 7,519 km^2 or 56% of its land area. Jamaica was also significantly affected as 5,450 km^2 was hit by a frequency of 2 hurricanes with a total land area of 64% being hit over the 2004 – 2011 time period.

Location 2004 - 2011	Country Area (km^2)	Area (km^2) 1	Area (km^2) 2	Area (km^2) 3	Area (km^2) 4	Area (km^2) Total	
Bahamas	13,418	2,731	2,340	2,435	13	7,519	56%
Cuba	111,025	59,633	14,127	3,666	321	77,747	70%
Dom. Rep.	48,254	1,831	0	0	0	1,831	4%
Haiti	27,158	1,154	0	0	0	1,154	4%
Jamaica	11,035	1,566	5,450	0	0	7,016	64%
Puerto Rico	8,999	837	0	0	0	837	9%

Table 10.1.2: 2004 - 2011 Total Impact Zone Area. The total area per country and per impact occurrence of hurricanes hitting the same location measured in square kilometers. The Total percentage is based on how much of the country's land area was hit by hurricanes from all 4 frequency classes.

10.2 Hurricane Strength Storm Impact Zones on Land Cover 2004 – 2011

An overlay of the reclassified 2008 FAO urban, agriculture & grazing, and other raster was combined with the 2004 – 2011 GIS hurricane impact zone shapefile (see Figure 10.2.2). This overlay provided information to identify the frequency of hurricane hit counts on population and food production locations within the study area. Table 10.2.1 shows a breakdown for each country based on land classification and total area impacted by all hurricanes in the 2004 – 2011 timeframe. In the urban land class, 7,246 km^2 comprising 75% of Cuba, 1,836 km^2 (73%), in Jamaica and 661

km^2 (11%) in Puerto Rico were most significantly hit by one or more hurricanes. Although the urban land class in the Bahamas is a smaller land area than the other countries in the study area, 278/285 km^2 (98%) was hit affecting almost the entire class. In the agriculture & grazing category, Cuba (56,539 km^2) was most affected then Jamaica (4,051 km^2), and the Bahamas (1,100 km^2).

Location 2004 - 2011	Country Area (km^2)	Area (km^2) Urban		Area (km^2) Agriculture & Grazing		Area (km^2) Other		Area (km^2) Total Impact Zones	
Bahamas	13,418	278	98%	1,100	44%	6,141	58%	7,519	56%
Cuba	111,025	7,246	75%	56,539	71%	13,962	63%	77,747	70%
Dom. Rep.	48,254	1	0%	1,586	5%	244	3%	1,831	4%
Haiti	27,158	20	4%	861	4%	273	4%	1,154	4%
Jamaica	11,035	1,836	73%	4,051	61%	1,129	60%	7,016	64%
Puerto Rico	8,999	661	11%	0	0%	176	16%	837	9%

Table 10.2.1: 2004 - 2011 Hurricane Impact Zones based on Land Classification. Country size and land reclassification are expressed in km^2. Percentage values of each land classification are based on land area for that class. Total impact zone percentage is based on country size.

A breakdown of each land class based on the number of hurricane impact frequencies hitting the same location is shown in Table 10.2.2. The Bahamas and Cuba experienced minor impacts in locations hit by 4 occurrences in each land type. Jamaica had 70% of urban and 45% of agriculture & grazing land hit twice by hurricanes. Dominican Republic, Haiti, and Puerto Rico were hit once by hurricanes.

2004 – 2011 Land Use	Area (km^2) Country	Area (km^2) 1		Area (km^2) 2		Area (km^2) 3		Area (km^2) 4	
Bahamas	13,418								
Urban	285	124	44%	0	0%	154	54%	0	0%
Agriculture & Grazing	2,511	54	2%	401	16%	645	26%	0	0%
Other	10,622	2,553	24%	1,939	18%	1,636	15%	13	0%
Cuba	111,025								
Urban	9,654	4,656	48%	1,496	15%	1,011	10%	83	1%
Agriculture & Grazing	79,262	46,750	59%	7,661	10%	1,896	2%	232	0%
Other	22,109	8,227	37%	4,970	22%	758	3%	7	0%
Dom. Rep.	48,254								
Urban	4,902	1	0%	0	0%	0	0%	0	0%
Agriculture & Grazing	34,141	1,586	5%	0	0%	0	0%	0	0%
Other	9,210	244	3%	0	0%	0	0%	0	0%
Haiti	27,158								
Urban	538	20	4%	0	0%	0	0%	0	0%
Agriculture & Grazing	19,907	861	4%	0	0%	0	0%	0	0%
Other	6,713	273	4%	0	0%	0	0%	0	0%
Jamaica	11,035								
Urban	2,521	64	3%	1,772	70%	0	0%	0	0%
Agriculture & Grazing	6,619	1,090	16%	2,961	45%	0	0%	0	0%
Other	1,895	412	22%	717	38%	0	0%	0	0%
Puerto Rico	8,999								
Urban	6,040	661	11%	0	0%	0	0%	0	0%
Agriculture & Grazing	1,833	0	0%	0	0%	0	0%	0	0%
Other	1,125	176	16%	0	0%	0	0%	0	0%

Table 10.2.2: 2004 - 2011 Hurricane Impact Zone Frequency and Land Classification Breakdown. Country size and land Classification totals are expressed in km^2. Percentage values of each land classification are based on land area for that class.

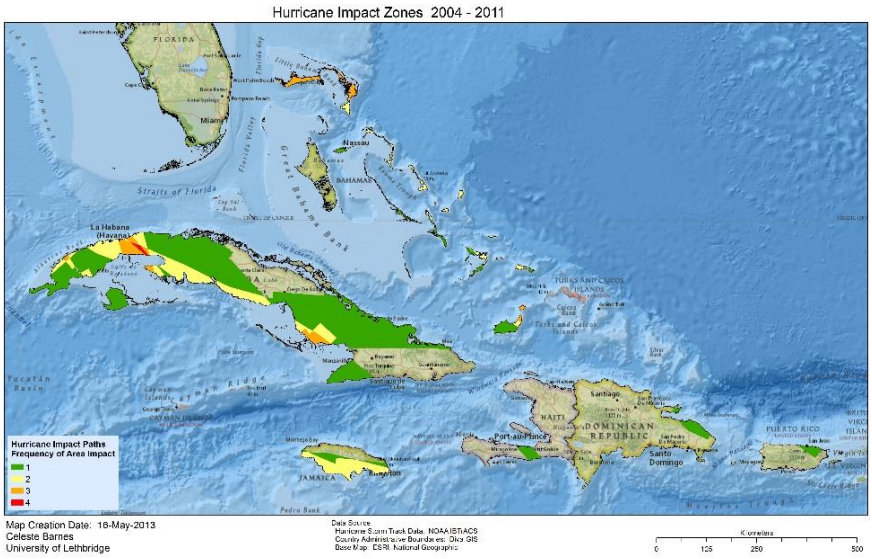

Figure 10.2.1: 2004 - 2011 64 kt Hurricane Impact Zones. Frequency of impact is a maximum of 4 occurrences in the same location.

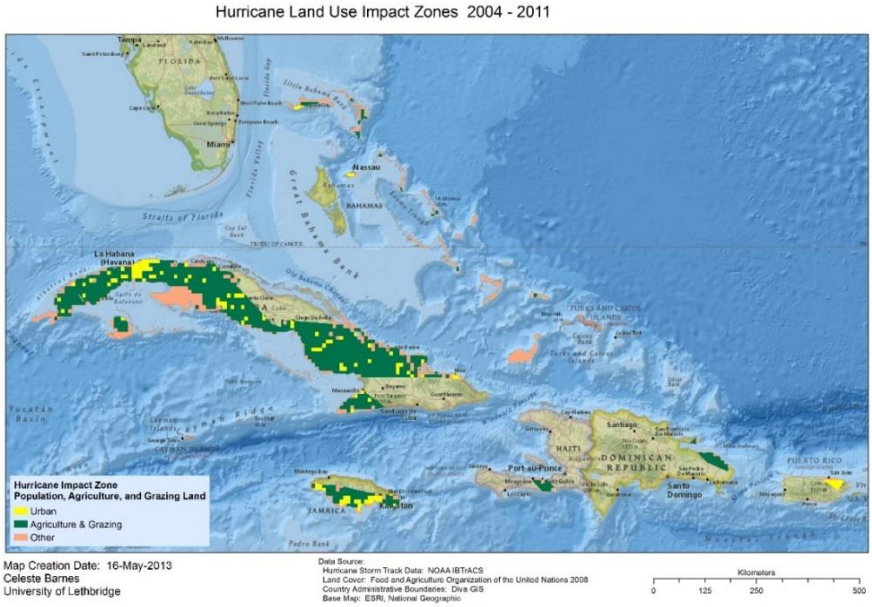

Figure 10.2.2: 2004 - 2011 Land Classification Impact Zone. Hurricane impact zones based on land cover/land use reclassification.

11 Appendix D: 2008 FAO Land Cover/Land Use

11.1 Data Reclassification

Land Class	Description	ID Code
1	Urban land	22
2	Agriculture - large scale Irrigation	20
2	Agriculture - protected	21
2	Crops and high livestock density	18
2	Crops and mod. intensive livestock density	17
2	Crops, large-scale irrigation, moderate or higher livestock density	19
2	Forest - with agricultural activities	4
2	Forest - with moderate or higher livestock density	5
2	Grasslands - high livestock density	10
2	Grasslands - low livestock density	8
2	Grasslands - moderate livestock density	9
2	Open Water - inland Fisheries	37
2	Rain fed crops (Subsistence/Commercial)	16
2	Sparsely vegetated areas – moderate or high livestock density	30
2	Sparsely vegetated areas - with low livestock density	29
3	Bare areas - unmanaged	31
3	Forest - protected	3
3	Forest - virgin	2
3	Grasslands - protected	7
3	Grasslands - unmanaged	6
3	No data	1
3	Open Water - protected	36
3	Open Water - unmanaged	35
3	Shrubs - unmanaged	11
3	Sparsely vegetated areas - protected	28
3	Sparsely vegetated areas - unmanaged	27
3	Wetlands - protected	24
3	Wetlands - unmanaged	23

Table 11.1.1: Land Cover/Land Use Reclassification. Breakdown of the Land Classification used for Impact Zones for Urban, Agriculture & Grazing, and Other